Resources

Remote sensing of land-use-specific actual evapotranspiration of entire catchments containing plantations

Project number: PNC286-1112 May 2017

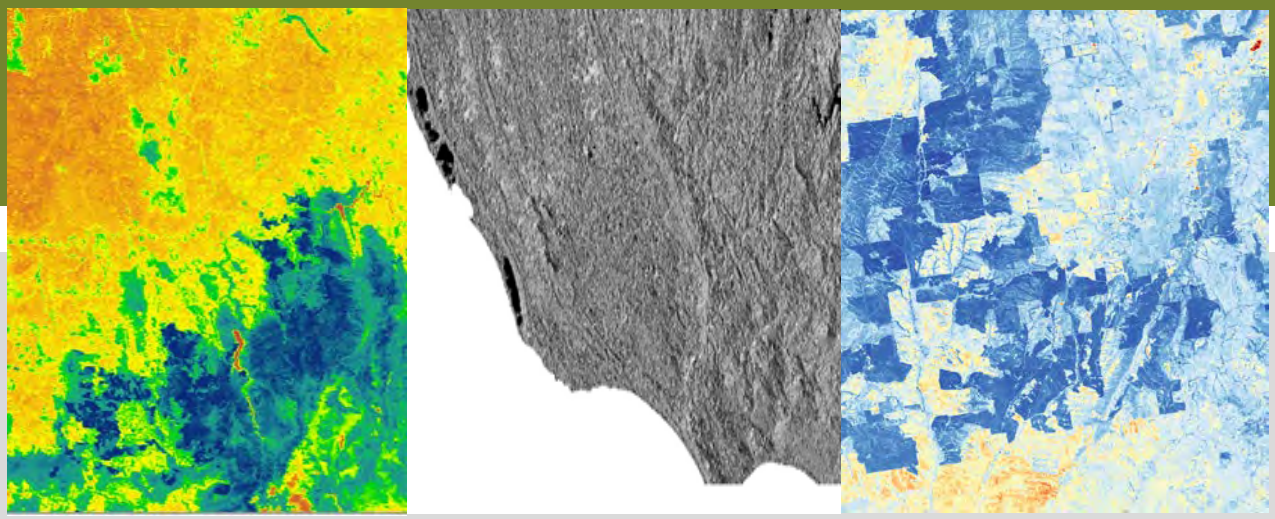

Level 11, 10-16 Queen Street
Melbourne VIC 3000, Australia
T +61 (0)3 9927 3200 E info@fwpa.com.au
W www.fwpa.com.au

Forest & Wood Products Australia

Remote sensing of land-use-specific actual evapotranspiration of entire catchments containing plantations

Prepared for

Forest & Wood Products Australia

by

Tim R McVicar, Thomas G Van Niel and LingTao Li

Publication: Remote sensing of land-use-specific actual evapotranspiration of entire catchments containing plantations

Project No: PNC286-1112

This work is supported by funding provided to FWPA by the Department of Agriculture, Fisheries and Forestry (DAFF).

ISBN: 978-1-925213-60-7

Researchers:
Tim R McVicar and LingTao Li
CSIRO Land and Water, GPO Box 1700, Canberra ACT 2601, Australia

Thomas G Van Niel
CSIRO Land and Water, Private Bag No. 5, Wembley WA 6913, Australia

Final report received by FWPA in June 2016

Forest & Wood Products Australia Limited
Level 11, 10-16 Queen St, Melbourne, Victoria, 3000
T +61 3 9927 3200 F +61 3 9927 3288
E info@fwpa.com.au
W www.fwpa.com.au

Executive Summary

How forest actual evapotranspiration (AET) rates compare to those of other land-uses in catchments containing plantations is highly contested. This project aimed to develop a time series of remotely sensed AET grids with suitable spatial resolution and temporal frequency characteristics to adequately determine the relative and volumetric water-usage across two study sites that include forestry-managed plantations. We develop this dataset by 'blending' information from high-spatial resolution (yet low temporal repeat, especially when considering clouds) Landsat imagery with the high-temporal frequency (yet low-spatial resolution) MODIS imagery. The output series has high-spatial resolution and high-temporal frequency (i.e., the 'best of both worlds'). This series is then input to a remote sensing AET algorithm that allows AET to be estimated across the entire study sites at high-spatial resolution and high-temporal frequency. The study sites are: (i) the Tumut region in NSW (27,170 km^2); and (ii) the Green Triangle straddling the SA-Vic border (25,184 km^2). Validation against all available in situ AET observations and stream-flow data demonstrated that the resultant Landsat-MODIS blended AET grids were highly accurate. Evaluation with forestry management and 'environmental variability' datasets revealed that the blended AET grids were fit-for-purpose to extract land-use-specific water-usage time series from.

Results showed that, volumetrically (GL/d), both agricultural and native vegetation areas used more water than forestry plantation at both study sites. We found that the main forestry plantation land-use classes had the highest relative rates of AET (mm/d) at both sites, but that this assessment was biased due to the plantations being planted in high precipitation (P) areas. When land-uses were summarised by AET/P, the forestry plantation land-uses were found to be low water users at the NSW site (6^{th} and 8^{th} out of 9), which indicated that forestry plantation water use needs to be considered on a site-by-site basis and within hydrological context. Further, we found that there was high variability of AET/P across the forestry plantations, so forestry water use should not be treated uniformly even over a single study site.

These findings allow the forest industry to lead an 'evidence-based' informed debate regarding the role of forestry activity on water-usage at two key sites. Having access to this information will allow the forestry industry to proactively work with Federal and State regulators to produce well-reasoned and quantitatively informed policy and management outcomes. This will require well-targeted messages being developed as some regulators may have pre-conceived perceptions about forestry water-use. Thus, highly transparent, scientifically-based evidence should help to move the discussions to a quantitative 'evidence-based' footing. Additionally, integrating the resultant Landsat-MODIS blended AET time series with forestry management and planning information should allow the forest industry to better understand: (i) water use efficiency; (ii) surface water and groundwater usage; (iii) the AET contribution from ephemeral water bodies; and (iv) the water-usage from a variety of forest management actions.

To gain benefit from this research the forest industry could implement a range of activities. Firstly, to influence policy, the outcomes of this research need to be effectively communicated with relevant Federal and State regulators to ensure they understand the nuances of the output, especially with respect to normalised water-use and volumetric water-use. Secondly, the data can be used internally by the industry to develop water-accounts for forestry management practices, among others. Thirdly, if the industry wishes to cross-check the regional AET estimates for these two sites then thermal-based surface energy balance methods could be implemented. Fourthly, the method developed here could be applied to other forestry regions.

Table of Contents

1 Introduction

Evaporation is the phase change from liquid to gas. Evaporation of water may occur from the Earth's surface (*e.g.*, the soil or a water body), through plant leaves (termed transpiration) or from rainfall intercepted by objects above ground (primarily vegetation in natural environments). The combined term evapotranspiration (ET) covers these three components, though interception is not explicitly used in the compound word. ET, like precipitation, has the dimensions of depth per time, and common units of mm/d. When spatially integrated over an area (m^2, such as a paddock, catchment, basin or country), the dimensions of ET become volume per time, and common units are m^3/d or GL/d.

The distinction between different forms of ET is important (McMahon et al., 2013). Potential ET (PET) and pan evaporation are estimates and measurements, respectively, of atmospheric evaporative demand under environmental conditions having limitless access to water. This means they are not representative of the actual ET (AET) when and where the surface is not saturated and/or when transfer from the surface limits AET rates. PET can be readily calculated using commonly measured meteorological variables (Donohue et al., 2010), and pan evaporation can be readily measured (Roderick et al., 2009a, 2009b).

AET, on the other hand, is time consuming to measure at a single location (Leuning et al., 2012), with flux tower energy-balance closure being in the order of 30%. It is challenging to accurately estimate AET both spatially and temporally over large areas. AET can be conceptualised as a two-stage process (Budyko, 1974; Donohue et al., 2007; Philip, 1957; Ritchie, 1972). In the first stage, water is freely available (*e.g.*, following sufficient precipitation or irrigation) and AET is limited largely by energy. Energy-limited AET is primarily determined by meteorology, specifically the four principal meteorological drivers: (i) net radiation, (ii) air temperature; (iii) relative humidity and (iv) wind (McVicar et al., 2012a; McVicar et al., 2012b; Penman, 1948). In the second stage, water is the limiting factor. As the soil dries and plants possibly close their stomata, AET de-couples from available energy. The water-limited AET process is complex, depending more on biology and soil water content than energy-limited AET. For most places and most times in Australia, AET is in the more complex water-limited stage. The concept of water-limited and energy-limited evaporation has long been used to understand the role of evaporation in the water balance at both hydroclimatologic (Budyko, 1974; Donohue et al., 2007) and agronomic (Philip, 1957; Ritchie, 1972) space and time scales. Herein the hydroclimatological terms 'energy-limited' and 'water-limited' are used in preference to the equivalent agronomic terms of 'constant rate stage (stage 1)' and 'falling rate stage (stage 2)', respectively. This is, because the energy-limit – akin to the concept of PET – is not constant as it is both temporally variable (influenced by both seasonal variability and climate-change related trends: e.g., Donohue et al., 2010) and spatially variable (related to topographic position: e.g., McVicar et al., 2007b).

AET is the largest consumptive term of the catchment water balance in Australia (Zhang et al., 2016), so characterising its spatial and temporal variation is important for improved understanding of the catchment water balance. This is especially the case for high water yielding catchments containing a variety of land-uses, like those containing forestry plantations. Fully understanding multiple land-use's water-use, especially when land-use is changing, is important in Australia (e.g., Webb, 2012 and the references therein) and is a key issue in many other regions / countries with limited water resources including: (i) India (Calder, 1986; Calder et al., 1993); (ii) South Africa (Dye, 2013; Dye & Versfeld, 2007;

Everson et al., 2011); (iii) Brazil (Ferraz et al., 2013; Rodriguez-Suarez et al., 2011); and (iv) China (McVicar et al., 2007a; Zhang et al., 2008).

van Dijk and Keenan (2007) reviewed the scientific basis for estimating plantation water use and its influence on the water balance, especially for catchments containing multiple land-uses, and they concluded that the perceived negative impacts tend to be overstated. To sensibly inform policy and management decisions (and public perception) of the hydrological impact of different land-uses on the catchment water balance (e.g., McVicar et al., 2007a; van Dijk & Keenan, 2007) land-use-specific AET estimates at a suitable spatial and temporal scale are required over catchments containing plantations. Considering the size of catchments containing plantations and the long time series required to adequately characterise land-use-specific AET dynamics, remote sensing analyses are needed (Everson et al., 2011). Noting it is best if remotely sensed estimates, of any variable, are validated using independent good-quality field data, the errors of which also have been characterised.

There are three general remote sensing approaches to estimate catchment AET, including: (*i*) vegetation-index based methods (Glenn et al., 2010); (*ii*) thermal approaches (Kalma et al., 2008); and (*iii*) hybrid approaches that combine information about vegetation vigour and environmental moisture to scale PET to AET (Guerschman et al., 2009). In an Australia-wide intercomparison of eight AET products against two independent evaluation datasets (*i.e.*, catchment water balance and flux tower measurements), with representative products from each of the three groups identified above, the hybrid approach was objectively determined to provide the optimal accuracy against the independent evaluation datasets (Glenn et al., 2011; King et al., 2011).

Previously, the hybrid AET algorithm has only been implemented using a single-sensor satellite monitoring system, like Landsat (containing the TM or ETM+ sensors) or Terra (containing the MODIS sensor). All single-sensor monitoring systems have inherent 'domain-characteristics' in the spectral, radiometric, spatial and temporal domains. The remotely sensed data are defined by the extent, resolution and density in each domain, resulting in a high level data summary (Table 1). The high-level relevant 'domain-characteristics' for both Landsat and MODIS are illustrated in Figure 1. Landsat and MODIS sensor specific details for the bands relevant for the AET algorithm used here are provided in the Methods section (see Table 4 of Emelyanova et al., 2012 for reflective 'domain-characteristic' information for both Landsat and MODIS).

Table 1. Domain-characteristic elements of remote sensing data arrays; from Emelyanova et al. (2013), modified from McVicar et al. (2002).

Domain	**Characteristic**		
	Extent	Resolution	Density
Spectral	Portion(s) of the EMS being sampled	Bandwidth(s) [a]	Number of bands in a particular portion of the EMS [b]
Radiometric	Dynamic range of radiances (min and max radiance per band)	Change in radiance due to change by one digital number	Number of bits used across the dynamic range of radiances
Spatial	Area covered by the image	Pixel size acquired [c]	Complete [d]
Temporal	Recording period over which the data are available [e]	Period of data acquisition [f]	Satellite repeat characteristics [g]

[a] The narrower bandwidth the higher the spectral resolution

[b] For example, hyperspectral sensors (*e.g.*, Hyperion) have higher spectral density than broadband instruments (*e.g.*, Landsat TM/ETM+) though they sample similar EMS extents.
[c] The smaller the pixel size the higher spatial resolution.
[d] This contrasts with the low spatial density of ground-based sampling, for example, meteorological stations.
[e] For some remotely sensed systems (*e.g.*, AVHRR and Landsat TM) data have been recorded near-continuously for ~30 years.
[f] For remotely sensed images this is a matter of seconds, which contrasts with meteorological data such as daily rainfall totals.
[g] For some applications using optical (*i.e.*, reflective and thermal) data the availability of cloud-free images is an important consideration. Whereas the satellite repeat characteristics do not change, cloud cover will change the effective temporal density of a site over time.

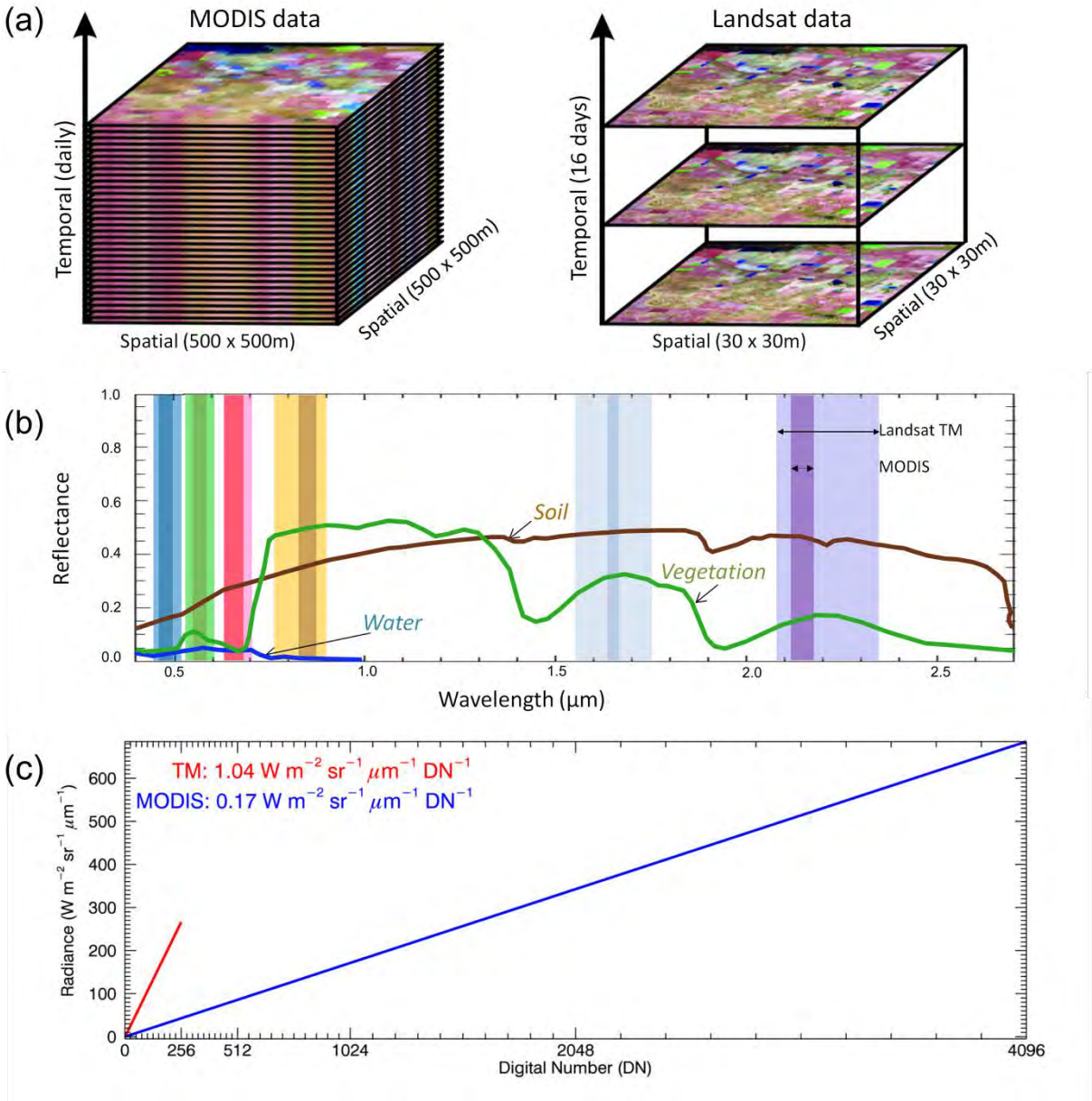

Figure 1. MODIS vs. Landsat TM data domain-characteristic elements: (a) temporal density and spatial resolution; (b) spectral extent, resolution and density (darker colours represent the MODIS bands and lighter colours the Landsat TM bands); (c) radiometric extent, resolution and density for the TM and MODIS red bands.

Ultimately all single-sensor monitoring systems are constrained by the 'domain characteristics' expressed in Table 1 (e.g., Ludwig et al., 2007; Phinn, 1998). To overcome this constraint, two or more remotely sensed data sources with complementary data frameworks can be combined. This process is often called data 'blending' or data 'fusion'. When the data are remote sensing images, the word 'data' is often replaced with the word 'image'.

A number of image blending algorithms have recently been developed that exploit multi-sensor remote sensing data to better capture changes of surface reflectance. Some examples include: (*i*) Spatial and Temporal Adaptive Reflectance Fusion Model (STARFM; Gao et al., 2006); and (*ii*) the Enhanced version of STARFM (ESTARFM; Zhu et al., 2010). These algorithms blend high spatial resolution imagery (*e.g.*, Landsat TM/ETM+) with high temporal density imagery (*e.g.*, MODIS or AVHRR) resulting in a simulated image with high spatial resolution and high temporal density characteristics to better capture spatial and temporal dynamics (i.e., the blending algorithms seek to gain the "best of both worlds"). The blending algorithms assume that any spectral and radiometric differences between sensors introduce negligible differences, and this assumption is extended to all algorithms used herein. A high level overview of the interactions between the Landsat and MODIS imagery to blend or simulate a Landsat-like image is provided in Figure 2.

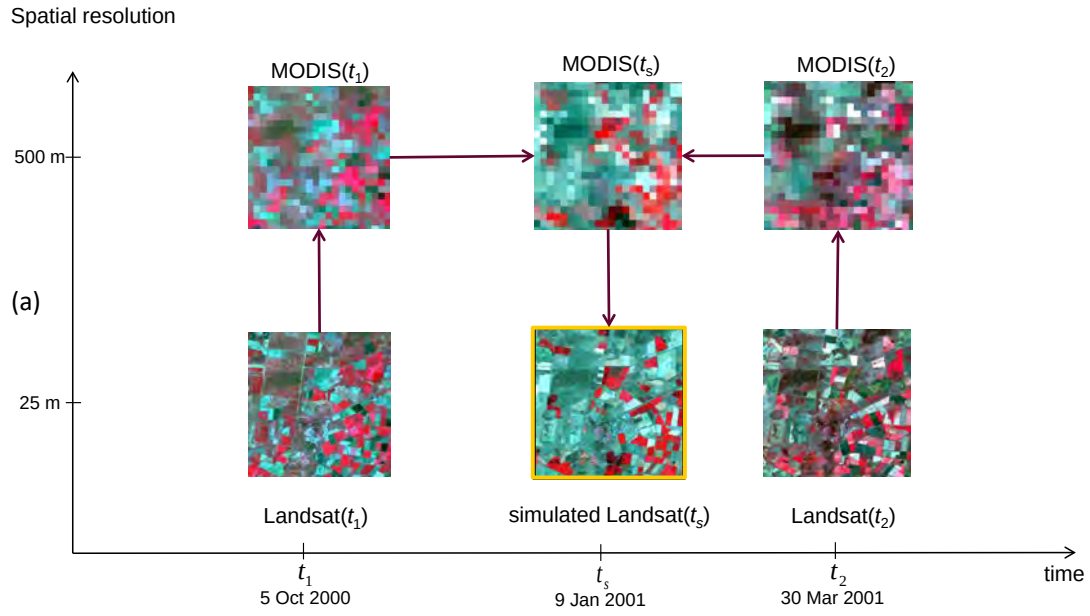

Figure 2. Generic overview of Landsat-MODIS blending. Simulation of a Landsat-like image is performed from two Landsat-MODIS pairs (t_1 and t_2) and one MODIS image observed at t_s: $t_1 < t_s < t_2$. The simulated image is indicated by the yellow border. The direction of information flow is represented by the arrows.

When the blending algorithms are run multiple times this allows the generation of a temporally dense time-series of Landsat-like simulated images that can be used to in-fill gaps present in the Landsat data time-series. These gaps are due to both the: (i) 16-day revisit characteristics of the Landsat series of satellites; and (ii) more relevant for most areas where (non-irrigated) forestry activity is conducted is the high likelihood of optical remote sensing being corrupted by cloud.

The two-fold objective of the project was to develop a Landsat-MODIS (LM) blended AET 8-day time-step dataset from February 2000 through December 2011, validated and evaluated against available field data to assess: (*i*) the magnitudes and dynamics of land-use-specific water use for entire catchments containing plantations; and (*ii*) whether there are other high-water use activities in the selected catchments/regions that use as much, or possibly even more, water as plantation forestry but are yet not explicitly considered under the National Water Initiative (Sinclair Knight Merz et al., 2010). Blending Landsat and MODIS data will result in optimal domain characteristics, (i.e., high spatial resolution and temporal density).

Inherent in the above objective statements is that these improved domain characteristics should be obtained without decreasing AET accuracy. To assess any potential accuracy loss, the blended AET model, the Landsat-only AET model, and the MODIS-only AET model will be assessed against validation and evaluation datasets. It is important to note, that the domain characteristics of Table 1 and Figure 1 are not the same as accuracy. Accuracy is calculated by comparing model output to some reference, or validation datasets. Given our AET focus, here, we define validation data as measurements that are representative of AET to first-order and in the same physical units, like flux tower observations, for example (discussed in detail below). We define evaluation data as measurements that are not acquired in the same physical units as AET yet are related to the process of AET and provide a means of assessing AET from a catchment management and/or forestry perspective.

To date, most blending research using STARFM or ESTARFM, has focused on: (i) the performance of blending algorithms in typical remote sensing units (e.g., surface reflectance); or (ii) generating simulated images to better characterise vegetation dynamics (Emelyanova et al., 2013; their Table 8). Only nine papers used either the STARFM or ESTARFM algorithms to generate high temporal-frequency and high spatial-resolution AET grids (Table X). All these papers use daily AET grids at the high and low spatial resolutions as input to the blending algorithm, these AET grids are generated from thermal-based remotely sensing AET models, including the DisALEXI model (Anderson et al., 2012; Anderson et al., 2007; Norman et al., 2003), or for ETWatch SEBS (Surface Energy Balance System, Su, 2002, to generate the AET grids using MODIS and AVHRR data) or SEBAL (Surface Energy Balance Algorithm for Land, Bastiaanssen et al., 1998, to generate the AET grids using Landsat and ASTER data) algorithms. The review presented in Table 2 highlights three novel aspects of our research. Firstly, ours is the first research to use simulated reflective data, in this case indices, as input into an AET algorithm (all other applications blended thermal-based AET grids). Secondly, ours is the first research to use ESTARFM when producing high temporal-frequency and high spatial-resolution AET grids (others have used ESTARFM for input to heavy-duty biophysical modelling). While no other papers have used ESTARFM in AET modelling, it has been used to generate input for several other papers modelling complex biophysical processes including: (i) gross primary productivity (GPP; Chen et al., 2010); (ii) net ecosystem exchange (NEE; Fu et al., 2014); and (iii) Leaf Area Index (LAI) and above-ground biomass (Dong et al., 2016). Additionally, when compared with four other blending algorithms (including STARFM) in a study site with complex terrain ESTARFM generated the most accurate results (Wu et al., 2014); though this finding is not universal as blending algorithm performance depends on the relative amounts of spatial and temporal variance (Emelyanova et al., 2013; Jarihani et al., 2014). Thirdly, our study sites cover a much larger-longer spatial-temporal domain than all previous studies. In that, our study sites are larger than all previous studies and we cover a longer temporal extent than all previous studies and we use a greater number of high-resolution input grids than all previous studies (see Table 2 for full details).

Table 2. Review of studies that have used STARFM or ESTARM when generating high temporal-frequency and high spatial-resolution AET grids. Records are sorted chronologically then alphabetically. When there are two study sites reported in a single paper these are identified with an (A) and (B) in the relevant columns as required.

N	Reference / Blending Algorithm	Region / Landscape specifics	Remote Sensing input / Study period / study area (km^2)	RSing Approach to estimate / AET Model	Key results for AET accuracy
1	Anderson et al. (2011 / STARFM, their Figure 4)	Orlando, Florida, USA / Irrigated fields, urban and wetland areas	Thermal-based AET estimates from 2 Landsat-MODIS pairs, 9 daily MODIS images / Nov–Dec 2002 / 8432	Thermal / ALEXI-DisALEXI	Visual comparison with MODIS based DisALEXI output
2	Liu et al. (2011 / STARFM, their Section 2.3.4)	Miyun county, Beijing, China / Forest, Reservoir and farmland	Thermal-based AET estimates from 9 MODIS images and 1 Landsat image / May 2007 / 2229	Thermal / ETWatch	30 m monthly AET estimates had $r^2 = 0.91$ when compared to 1km MODIS monthly AET estimates (their Figure 4). STARFM better captures both 30m AET spatial range when compared to 3 other blending approaches (their Table 2).
3	Jia et al. (2012 / STARFM, their Figure 2)	Hai River Basin, China / Farmland, forest and grassland	Thermal-based AET estimates from MODIS and AVHRR Penman Re-scaled daily AET (cloudy days) and TM and ASTER daily AET (clear days) / 2002 to 2009 / 15,619 *	Thermal / ETWatch	Three flux towers, 30 m monthly AET estimates $r^2 = 0.88$ (their Figure 7d)
4	Wu et al. (2012 / STARFM, their Section 2.2.3)	Hai River Basin, China / Farmland, forest and grassland	Thermal-based AET estimates from MODIS and AVHRR Penman Re-scaled daily AET (cloudy days) and TM and ASTER daily AET (clear days) / 2002 to 2009 / 100 #	Thermal / ETWatch	Five flux towers, the daily and monthly absolute deviations between field measurements and ETWatch calculations were -3.8% and -2.8%, respectively. Using three large aperture scintillometers the daily and monthly absolute deviations between field measurements and ETWatch calculations were -1.9% and 8.2%, respectively (their Table 8).
5	Cammalleri et al. (2013 / STARFM, their Figure 2)	Walnut Creek catchment, central Iowa, USA / Farmland (corn and soybean)	Thermal-based AET estimates from MODIS AET 1km daily and 5 cloud-free Landsat 30m / May–Sep 2002 / 51	Thermal / ALEXI-DisALEXI	At 8-sites Landsat only AET estimates had a relative error and seasonal cumulative AET of 14.2% and -20.2 mm, respectively. For Landsat-MODIS AET estimates these reduced to 11.0% and -7.5 mm. Landsat-MODIS blended AET estimates (bias 2%) outperformed Landsat only AET estimates (bias -10%) of cumulative AET at 8 sites (their Figure 7 and paragraph 40)

N	Reference / Blending Algorithm	Region / Landscape specifics	Remote Sensing input / Study period / study area (km^2)	RSing Approach to estimate / AET Model	Key results for AET accuracy
6	Cammalleri et al. (2014 / STARFM, their Figure 1)	(A) Bushland, Texas, USA / Farmland (irrigated and rainfed cotton) (B) Mead, Nebraska, USA / Farmland (corn)	(A) Thermal-based AET estimates from MODIS 1km daily and 5 cloud-free Landsat 30m / Jun-Aug 2008 / 0.047 (B) Thermal-based AET estimates from MODIS 1km daily and 6 cloud-free Landsat 30m / May-Sep 2003 / 1.67	Thermal / ALEXI-DisALEXI	(A) Relative error (RMSE / Mean of observations) of daily AET from 5 dates for 3 flux towers = 10.1% (their Table 1) (B) Relative error (RMSE / Mean of observations) of daily AET from 5 dates for 3 flux towers = 12.3% (their Table 1)
7	Ring (2014 / STARFM, their page 25)	(A) Tonzi Ranch, California, USA / Oak savannah, farmland and urban (B) Metolius Intermediate Pine Forest, Oregon, USA / Ponderosa pine forest, dwarf shrub, farmland and urban	(A) Thermal-based AET estimates from 12 Landsat scenes and numerous MODIS scenes / 28 Jun to 2 Oct 2013 / 1600 (B) Thermal-based AET estimates from 4 Landsat scenes numerous MODIS scenes / 10 Jun to 13 Aug 2013 / 1240	Thermal / ALEXI-DisALEXI	(A) Daily AET bias compared at two flux towers was -2.6 mm/day (their Tables 3.1 and 3.2). (B) Daily AET bias compared at one flux tower was -2.4 mm/day (their Table 3.3).
8	Semmens et al. (2016 / STARFM, their Figure 1)	Central Valley, California, USA / Wine grapes	Thermal-based AET estimates from 22 Landsat-8 scenes and MODIS imagery / Apr-Oct 2013 / 16	Thermal / ALEXI-DisALEXI	Compared with flux tower AET, the fusion estimates had r^2 values of 0.67 (daily) and 0.76 (weekly) for Site 1 and r^2 values of 0.46 (monthly) and 0.49 (weekly) for Site 2 (their Table 2).
9	Yang et al. (2016 / STARFM, their Section 2.2.2 and their Figure 2)	Parker Tract, lower coastal plain, North Carolina, USA / Commercially managed loblolly pine (*Pinus Taeda*) plantation and AET compared with other land-uses	Thermal-based AET estimates from 8 Landsat scenes (1 Landsat-7 and 7 Landsat-8) and numerous MODIS scenes / Feb-Nov 2013 / 822 (their Figure 3 and 11)	Thermal / ALEXI-DisALEXI	Two sites with flux towers. NC1 (established in 1991 and thinned in 2010) provided relative errors of AET over the study period of 0.9%, 1.3%, 2.7% and 3.2%, respectively for STARFM, Landsat only, MODIS smoothed and ALEXI. For NC2 (harvested in 2012 and established in 2013) these statistics were 5.8%, 9.7%, 84.8% and 58.0%. Their Table 3.

* While the Hai River Basin covers 318,000 km^2, using STARFM the high resolution AET grids were only developed for 16 counties (their paragraph 15) covering 15,618.85 km^2 (pers. comm. Shaomin Liu, Beijing Normal University, 26 June 2016).

While the Hai River Basin covers 318,000 km^2, in their Table 1 the largest spatial extent reporting both resolutions of imagery is the watershed with cover 10,000 m, so assuming this direction is covered in both directions the largest area STARFM was used to generate high resolution AET grids is 100 km^2.

2 Methodology

A general overview of the major steps of the study is shown in Figure 3. These steps also provide a general outline of the current report. We aim to keep the details of this report at a higher level, providing the scientific details. A companion report provides the technical details required to implement the study (Van Niel et al., 2016).

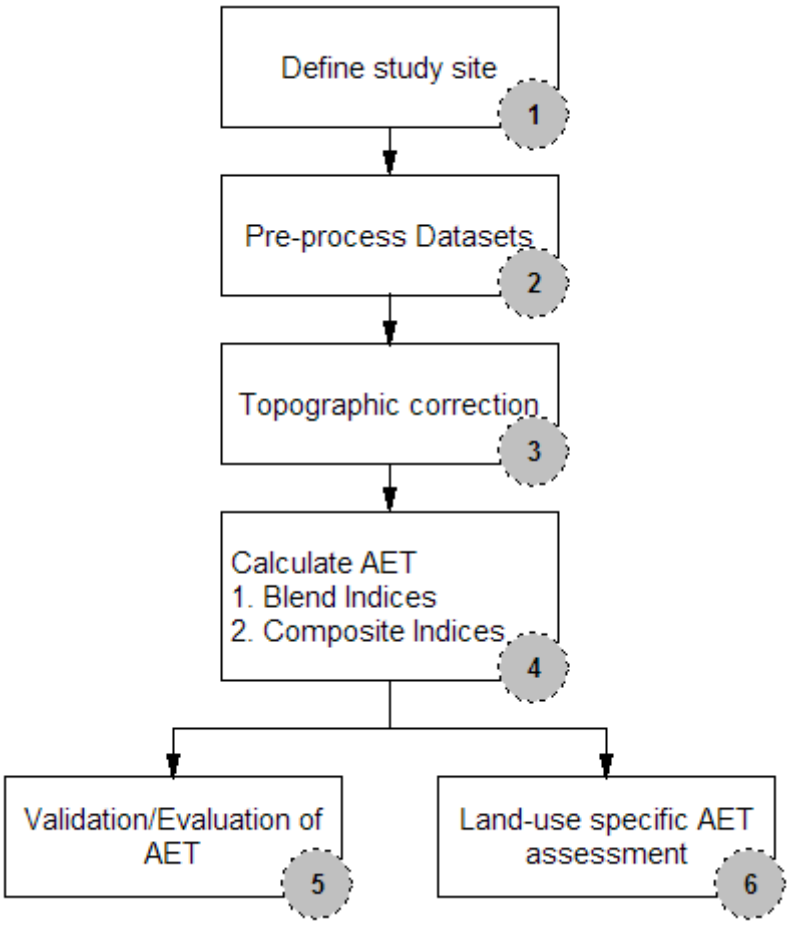

Figure 3. The general overview of the major steps of this study are shown.

There were six main steps conducted to complete this study; they are briefly outlined below.

1. Select the study sites which given the objectives of the study means selecting catchments that contain plantations and other land-uses allowing for land-use-specific rates of AET to be calculated. To reflect the range of plantation activity in Australia, and to maximise the range of environments where the project was performed, two contrasting study sites where identified. Briefly they are: (i) in the vicinity of Tumut, NSW; and (ii) the Green Triangle area straddling the South Australia and Victoria border.

2. Pre-process the datasets. The main data sets involved in the project were: (i) remotely sensed data (comprised of Landsat and MODIS); and (ii) field data (comprised of validation data and evaluation data). The validation datasets included a flux tower located in the Tumut study site, stream gauge data located in both study sites, and in situ measurements of AET in the Green Triangle site. Evaluation datasets included fire scars, forestry management and age class datasets. More emphasis is placed on

validation than evaluation in this report.

3. Topographic correction needed to be performed on the high resolution Landsat data that was obtained from Geoscience Australia. Without performing this topographic correction the resulting AET were heavily impacted by artefacts due to topography, whereas once performed the AET results were not driven by topography.

4. The topographically corrected Landsat imagery and MODIS imagery were used to calculate two remotely sensed indices needed in the AET algorithm and these were then blended to provide high-spatial-resolution and high-temporal-frequency indices that were input to the AET algorithm. If there is cloud present in any of the five input images used to simulate the Landsat-like indices then data-gaps are present in the resultant blended output. To overcome this problem we developed a 'hierarchical blending approach' using input imagery with minimal amounts of cloud cover (yet recorded with a long gap between them) as input to the blending to infill the imagery which had more substantiative amounts of cloud cover (yet with as short a period between images as possible). The output from this step were 8-day AET estimates covering both study sites.

5. Next the 8-day 25-m AET grids were validated (assessed against field observations with the same units) and evaluated (compared with field observations with related units). The validation provides a means of assessing the accuracy of the 8-day 25-m AET grids. The evaluation provides examples of how these grids can be used to monitor forestry practices and to inform forestry management decisions.

6. Finally, land-use-specific AET rates were determined for the two study sites. These are presented relatively (normalised for the different areas of different land-use) and are also volumetrically (taking into account the different areas of different land-use).

More detail about these major steps is provided below.

2.1 Study sites

This project has two study sites purposefully chosen (in consultation with the project steering committee) to have different terrain and catchment characteristics to test the blending-AET algorithms over the wide range of environmental conditions that plantations are grown in Australia. Their locations are shown Figure 4. To ensure that we had a wide-range of land-covers, each site comprised parts of two Landsat scenes (Figure 4), and as MODIS imagery is Australia-wide there was no need to consider MODIS imagery when defining the geographical extent of the two study sites. These study sites are generally much larger than sites used to test AET-blending algorithms, as pointed out previously (Table 2), and hence required some 'industrial-strength' near-operational computing solutions to be implemented to process the large numbers and to store the large volumes of imagery used and generated in the project.

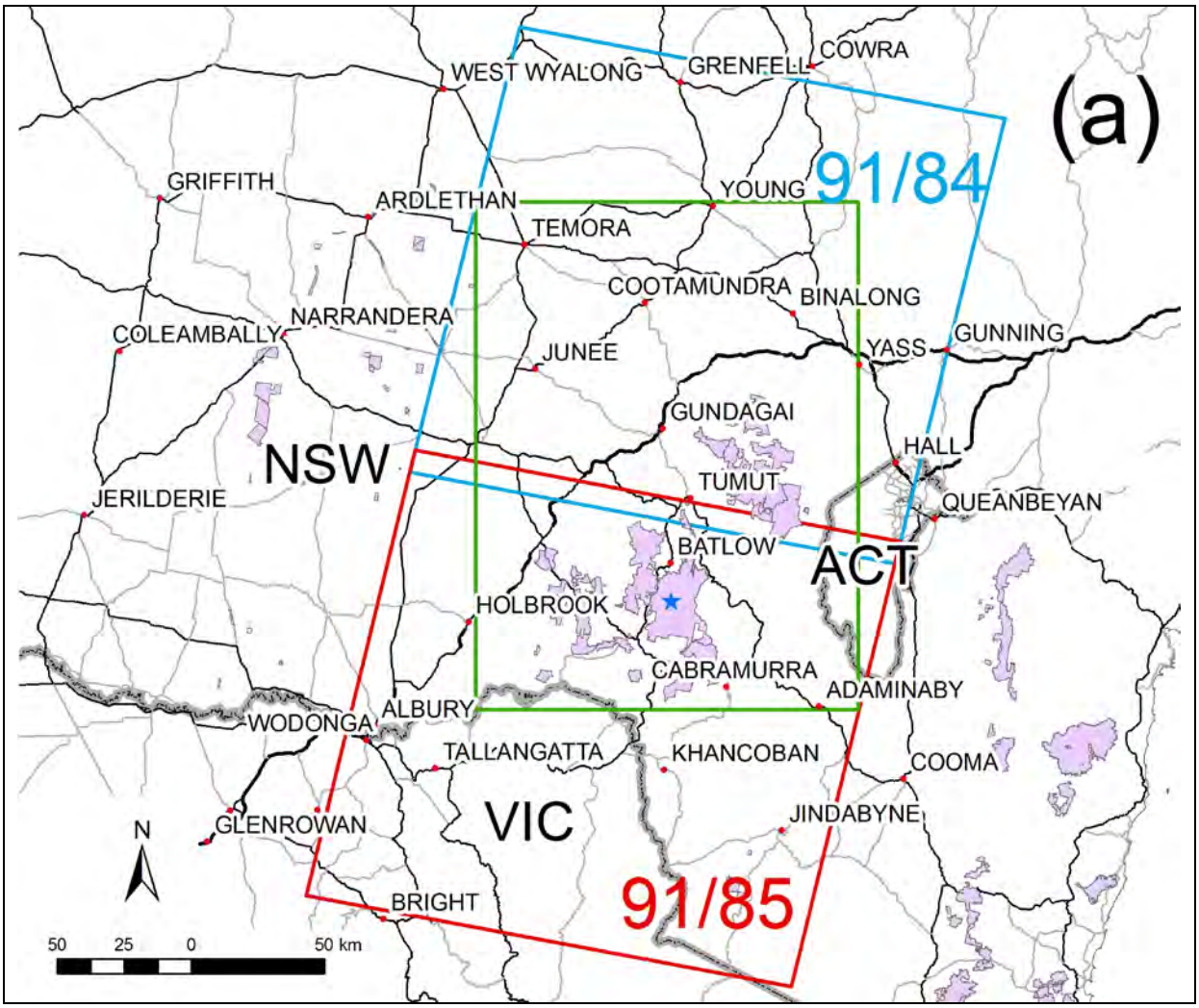
(a)
WEST WYALONG
GRENFELL
COWRA
91/84
GRIFFITH
ARDLETHAN
YOUNG
TEMORA
COOTAMUNDRA
BINALONG
NARRANDERA
COLEAMBALLY
JUNEE
YASS
GUNNING
GUNDAGAI
HALL
NSW
TUMUT
JERILDERIE
QUEANBEYAN
BATLOW
ACT
HOLBROOK
CABRAMURRA
ADAMINABY
ALBURY
WODONGA
TALLANGATTA
KHANCOBAN
COOMA
VIC
JINDABYNE
GLENROWAN
N
BRIGHT
91/85
50 25 0 50 km

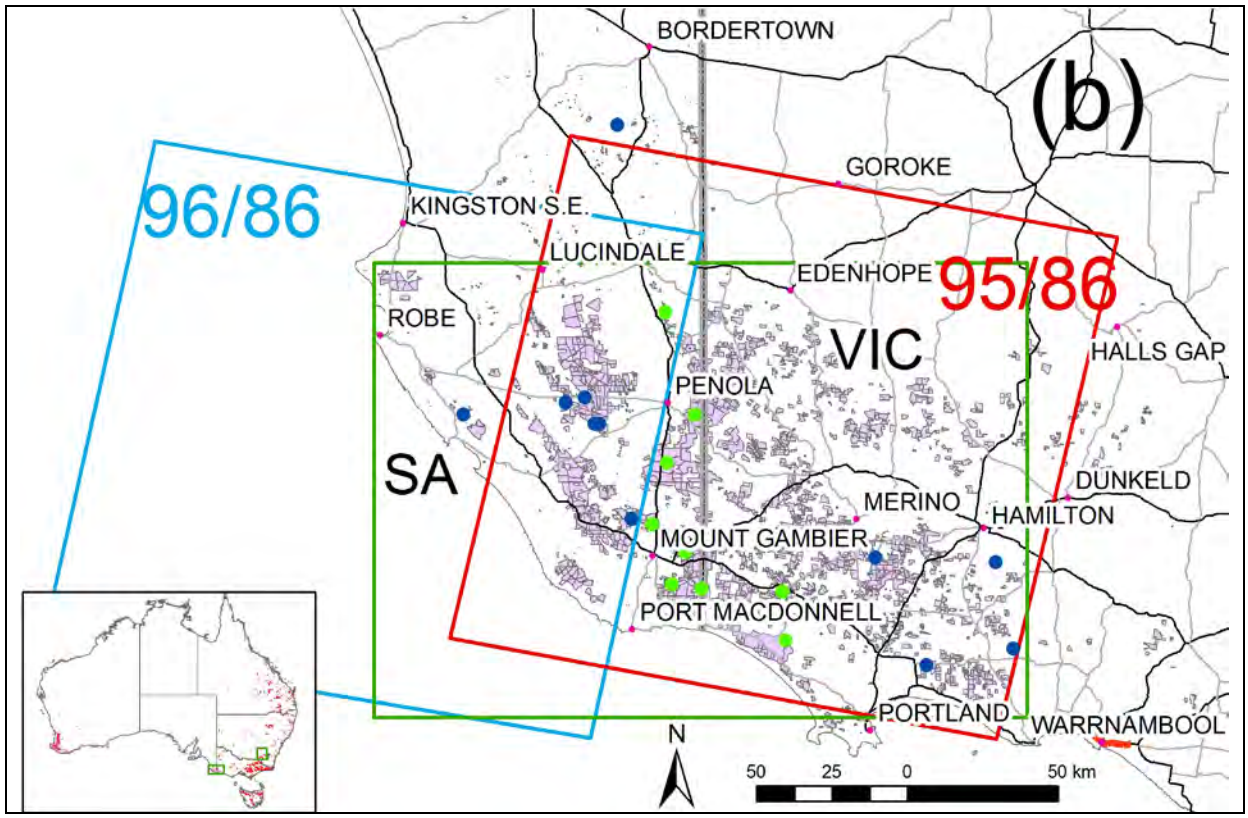

Figure 4. Study site locations for the: (a) NSW site and (b) SA site. The green rectangles define each study site, whereas the numbered blue and red rectangles are the images Landsat with the 'Path/Row' coordinates provided. For both sites forestry land-use areas (State Forest for NSW and gross plantations for SA) are shaded pink. In (a) the location of the Tumbarumba flux tower is indicated by the blue star. In (b) the locations of the site water use studies are indicated by green dots (for those studies performed in Pine plantations) and blue dots (studies performed in Blue Gum plantations). The inset map shows the locations of the two study sites (the green rectangles) relative to Australia with plantations coloured red.

The first site (Figure 4(a)) is centred on the plantation forestry catchments in the vicinity of Tumut, NSW. In this report it is called 'Tumut' or 'NSW' interchangeably. This site is 190 km north-south and 143 km east-west, covering 27,170 km^2. The majority (26,252 km^2) is located in NSW, with minor parts being located in the Australian Capital Territory (641 km^2) and Victoria (277 km^2). This study site is located in upland catchments that form the eastern edge of the Murray-Darling Basin, the majority of the study site is located in the Murrumbidgee catchment, with rivers predominately draining west. The study site extends from Temora in the north-west to Adaminaby in the south-east. The elevation of the NSW site ranges from 171 to 1,896 m, the mean elevation is 574 m, with a standard deviation of 334 m; see Figure 5(a). Aspects are primarily east and west given the primarily north-south linear geological features contained in the NSW site (Figure 5(b)). The mean slope is 7.03°, with a standard deviation of 6.94°, the maximum slope is almost 70° located in the mountainous south-east of the NSW site (Figure 5(c)).

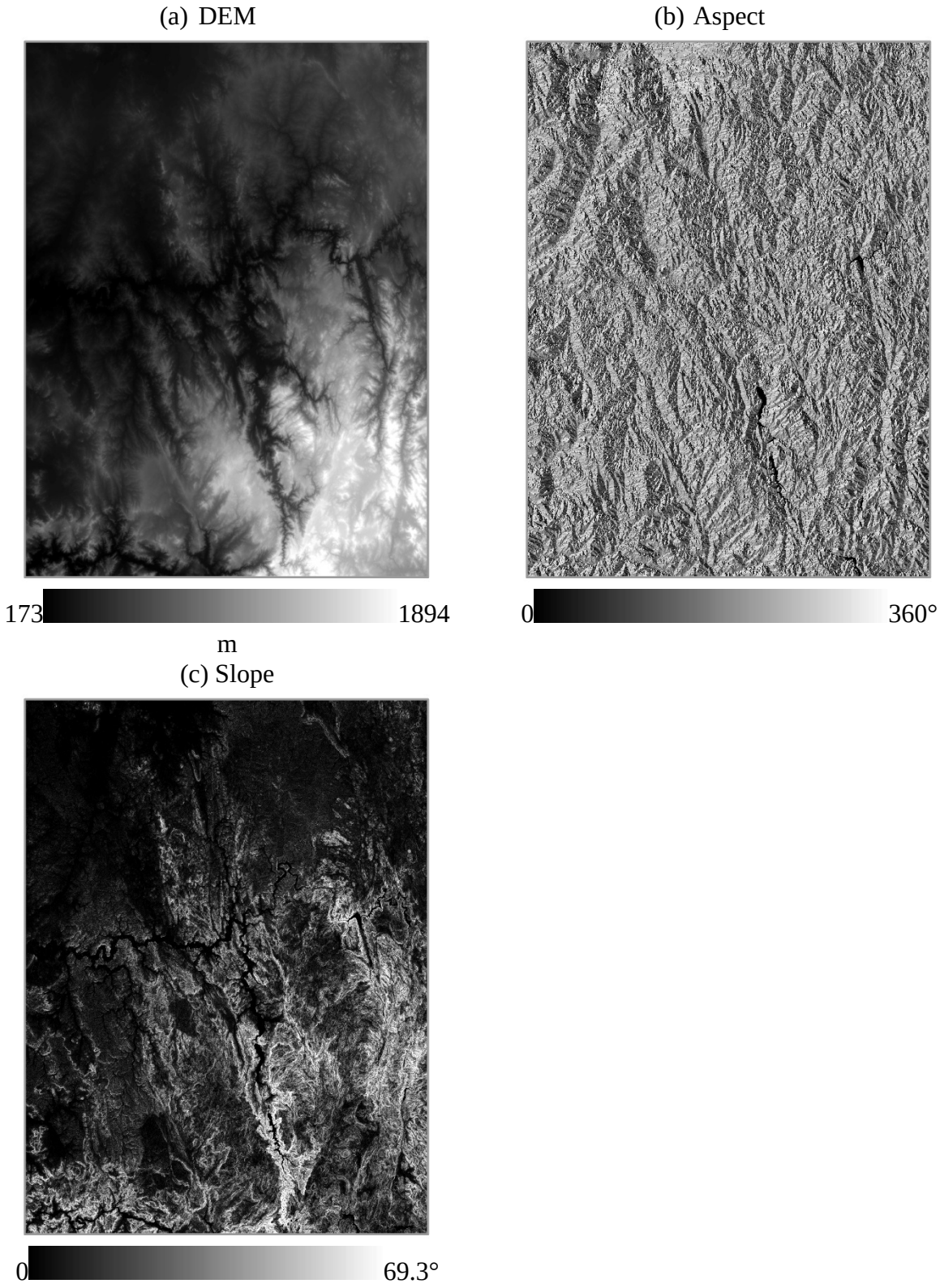

Figure 5. Topographic characteristics for the NSW site. Part (a) shows the elevation (m above mean sea level), (b) is the aspect (° from north) and (c) is the slope (° from horizontal). The elevation data are the Shuttle Radar Topographic Mission (SRTM) Digital Elevation Model (DEM-S) as processed by Gallant et al. (2011).

Using all-Australian climatic grids, which are subject to observational errors and geostatistical uncertainty (Jones et al., 2009), from 2000 to 2011, Figure 6 shows the mean annual site precipitation (P) ranges from 430 to 1500 mm/year. There is a strong P gradient across the site; the maximum P is associated with the Great Dividing Range and minimum P is around Temora. The mean annual Priestley-Taylor PET (Donohue et al., 2010) for the study site ranges from about 1250 to 1700 mm/year. The Aridity Index (AI), calculated as PET/P, ranges from 0.83 to 3.66 (Figure 6). If an area has an AI value greater than 1.0, then the AET from this place is deemed to be 'water-limited' (as P < PET). In contrast when AI is below 1.0, then the AET is said to be 'energy-limited' (as P > PET); see Donohue et al. (2007) and McVicar et al. (2012b) for an introduction to the Budyko framework which is built on the premise of limits to AET. Seasonally, the climate for the NSW site is relatively drier in summer and autumn with wettest conditions experienced in winter and early spring (especially in the higher elevation areas in the study site), with PET again increasing by late spring. This is clearly shown in Figure 7 and the long-term seasonal study site ranges for P, PET and AI are provided in Table 3.

Table 3. Mean seasonal climate data ranges for the NSW site; for images see Figure 7.

Season	P Range (mm / season)	PET Range (mm / season)	AI Range (PET/P)
DJF	117 – 334	561 – 726	1.693 – 5.558
MAM	69 – 258	239 – 329	0.929 – 4.561
JJA	111 – 478	82 – 153	0.180 – 1.162
SON	110 – 452	352 - 495	0.789 – 4.147

Next we briefly characterise the vegetation dynamics of the NSW site. This is performed by temporally decomposing (Donohue et al., 2009) the time-series of monthly MODIS 250 m Collection 5 imagery. This decomposition splits the monthly time-step vegetation coverage signal (derived from the Normalised Difference Vegetation Index (NDVI); Donohue et al., 2008) into the persistent and recurrent components. Respectively, these components generally represent trees and grasses, though perennial pastures will be identified as persistent and they don't have a strong seasonal signal like other grasses such as rain-fed crops and pastures. In Figure 8(a) the forested areas (both native and plantations) are clearly shown by the high vegetation cover in the annual persistent signal, and it also shows the pasture and cropping land-use classes which have a low annual persistent component (Figure 8(a)) and moderate coverage in the annual recurrent signal (Figure 8(b)). The seasonal dynamics are also shown for the recurrent component. The annual cycle of low recurrent coverage in summer (Figure 8(c)), slightly increasing in autumn (Figure 8(d)), with more growth occurring in winter (Figure 8(e)) and most growth in spring (Figure 8(f)) are clearly visible. Note: similar seasonal dynamics are not shown for the persistent component, which by definition, is persistent throughout the year, so there is negligible (essentially none) temporal variability to illustrate.

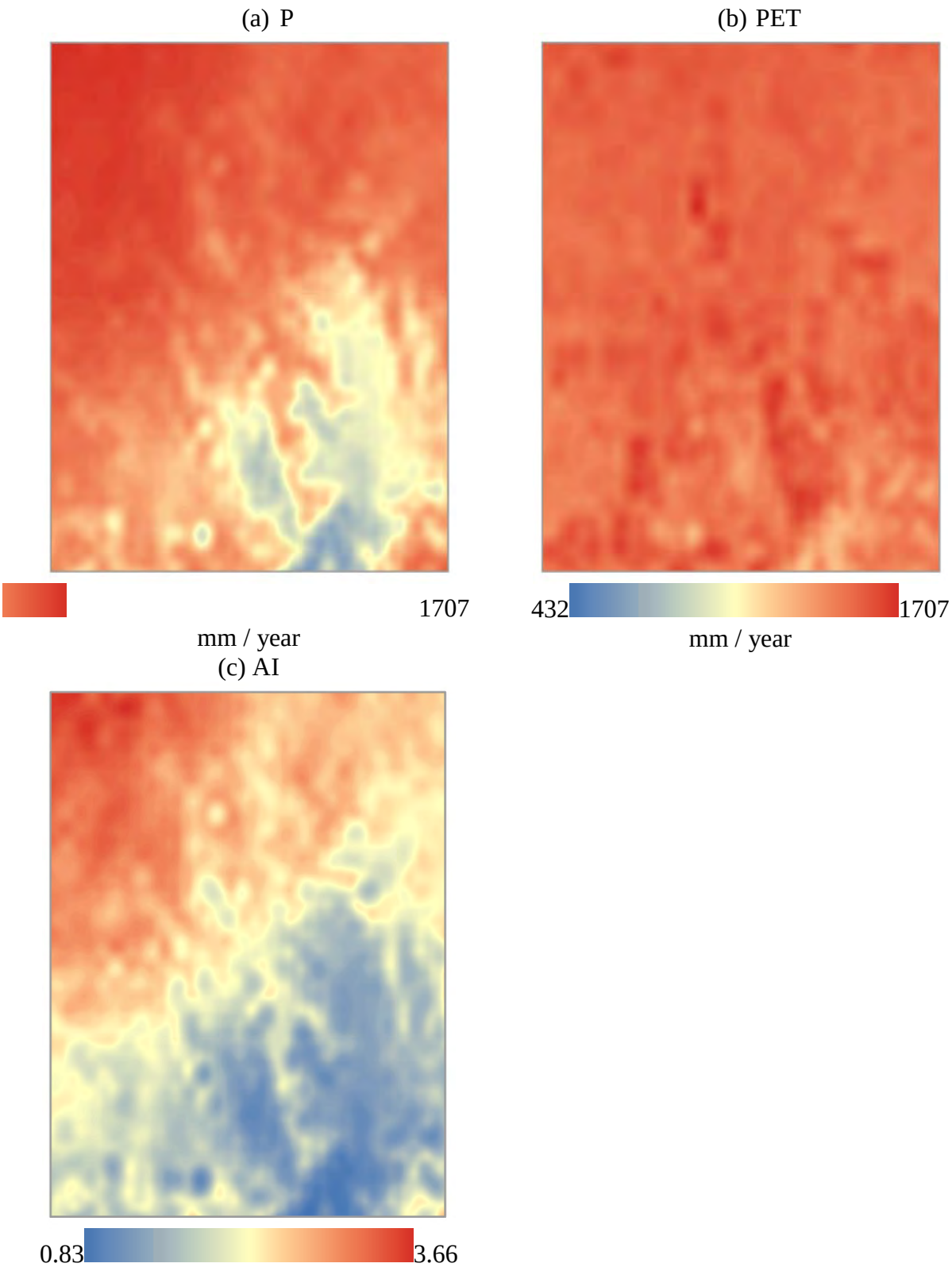

Figure 6. Mean annual climate data for the NSW site. Part (a) shows the 2000 to 2011 mean annual site precipitation (P), (b) is the mean annual Priestley-Taylor PET, and (c) is the mean annual Aridity Index (AI=PET/P). To enable direct comparison P and PET have the same stretch.

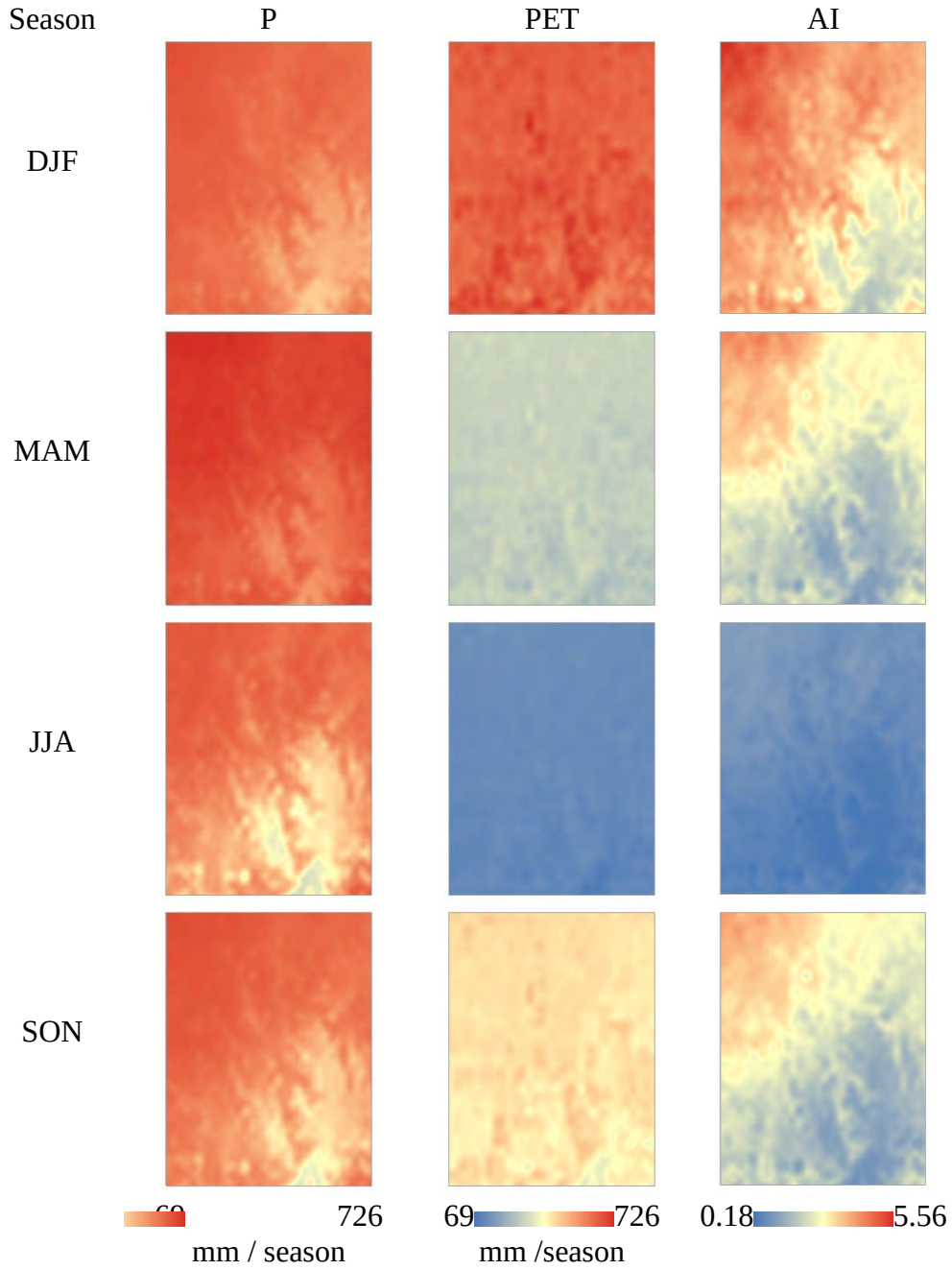

Figure 7. Mean seasonal climate data for the NSW site. Part (a) shows the 2000 to 2011 mean seasonal site precipitation (P), (b) is the mean seasonal Priestley-Taylor PET, and (c) is the mean seasonal Aridity Index (AI=PET/P). To enable direct comparison P and PET have the same stretch.

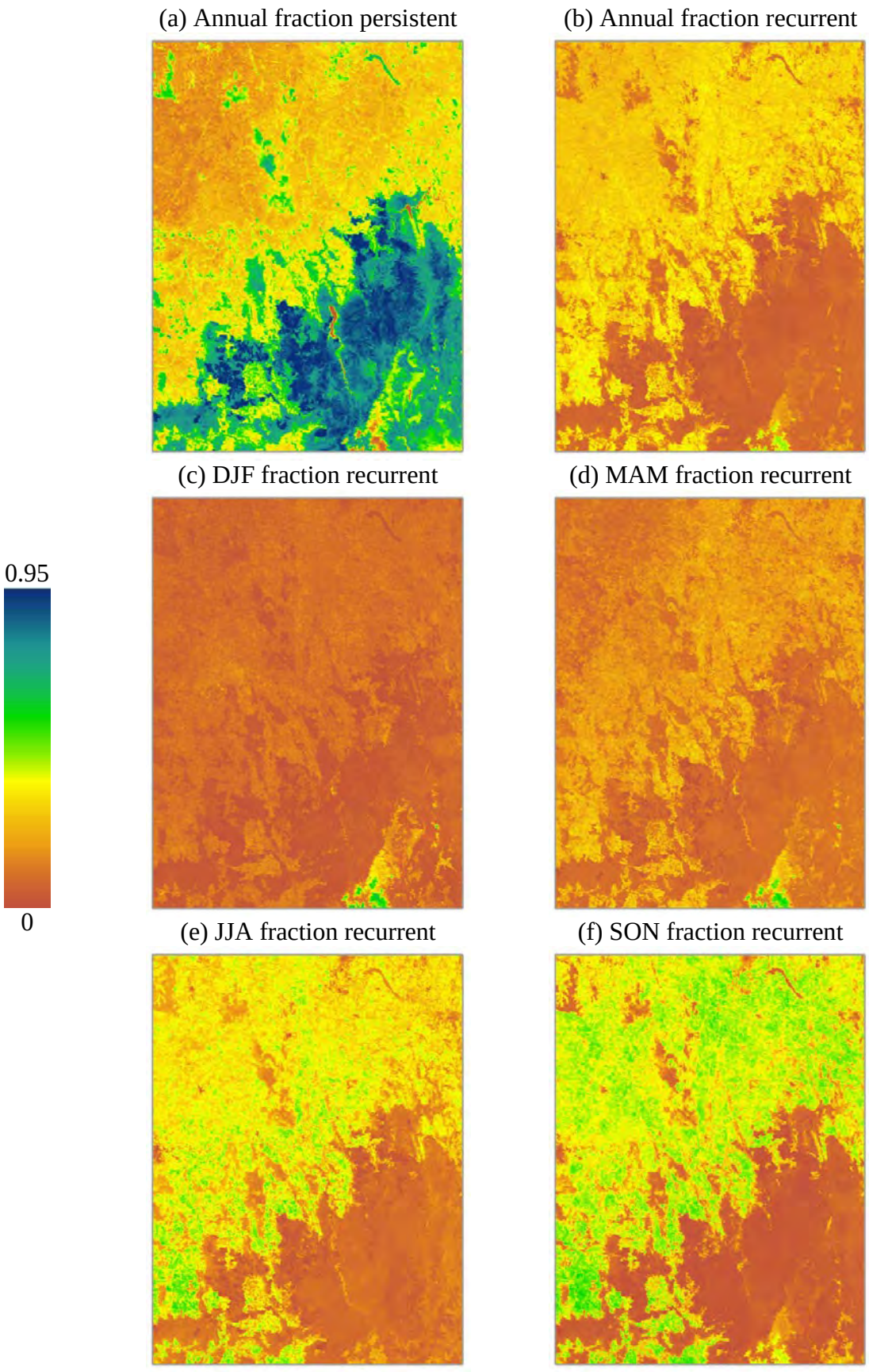

Figure 8. MODIS-based vegetation dynamics of the NSW site. Parts (a) and (b) show the annual persistent and recurrent components, respectively. Parts (c) to (e) are the seasonal recurrent components, for summer, autumn, winter and spring, respectively.

The second site is the Green Triangle area that straddles the South Australia and Victoria border; with Mount Gambier being a major regional centre located in the study site. In this report it is called 'Green Triangle' or 'SA' interchangeably. This site is 151 km north-south and 217 km east-west covering 32,767 km^2. There is 7,583 km^2 of ocean in the site (which is masked out in all processing), and the remaining land area (i.e., 25,184 km^2) is split across South Australia (9,732 km^2) and Victoria (15,452 km^2). This study site is located in lowland catchments with a relative flat topography; there are exceptions in both SA and Victoria with 'The Grampians' (located in western Victoria the eastern part of our study site) having the highest local relative relief in this study site. The study site extends from Robe in the north-west to Warrnambool in the south-east. The elevation of the SA site ranges from sea-level to 540 m, the mean elevation is 103 m, with a standard deviation of 75 m; see Figure 9(a). Aspects are well distributed, primarily controlled by the north-west to south-east linear geological features (both mountainous and due to the receding coastline in the Quaternary geological period) contained in the SA site (Figure 9(b)). The mean slope is 2.57°, with a standard deviation of 3.52°, the maximum slope is almost 90° located in the mountainous north-east of the SA site (in other words western Victoria; Figure 9(c)).

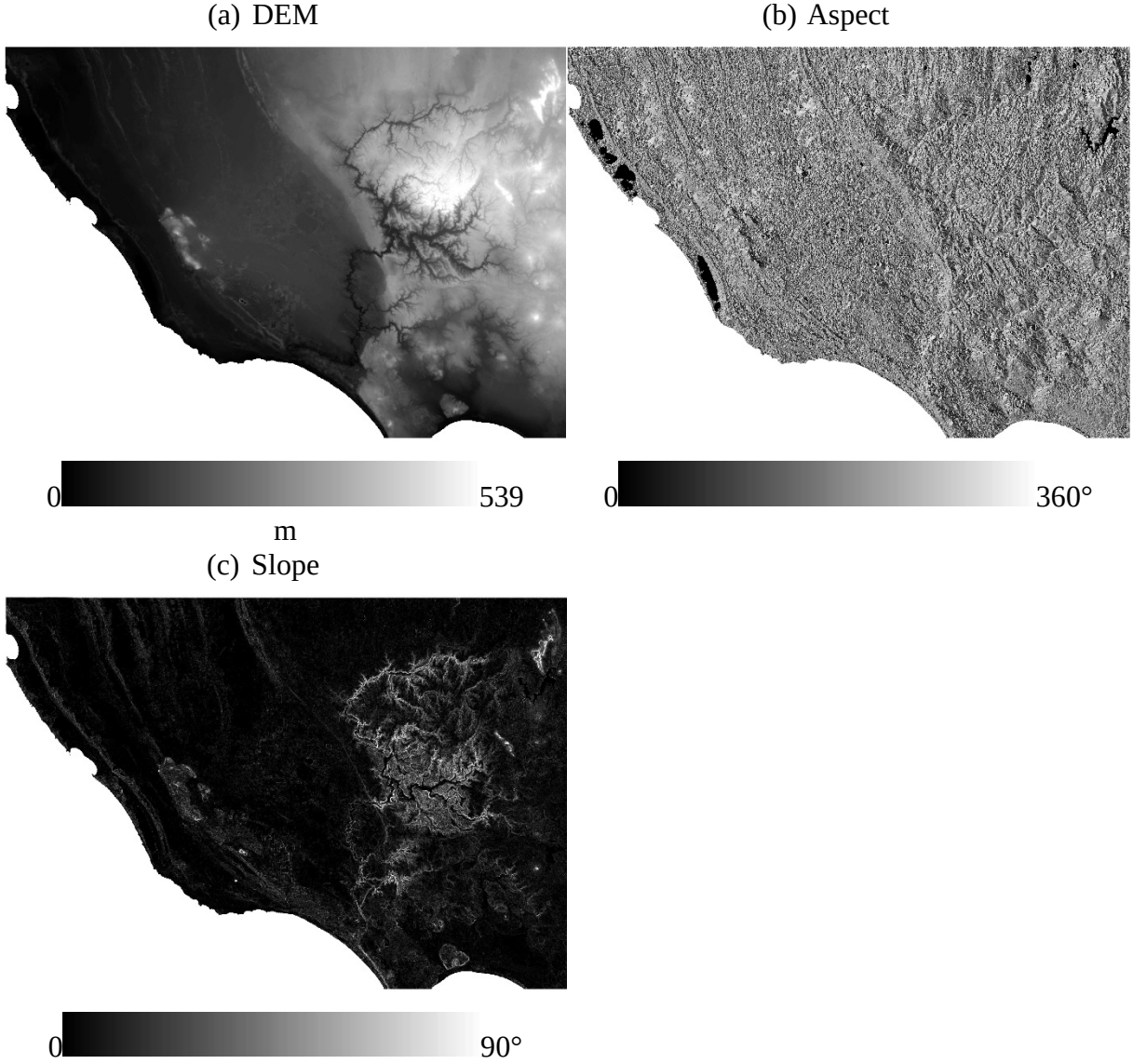

Figure 9. Topographic characteristics for the SA site. Part (a) shows the elevation (m above mean sea level), (b) is the aspect (° from north) and (c) is the slope (° from horizontal). The elevation data are the Shuttle Radar Topographic Mission (SRTM) Digital Elevation Model (DEM-S) as processed by Gallant et al. (2011).

Summarising the all-Australian climatic grids (Jones et al., 2009) from 2000 to 2011, Figure 10 shows the mean annual site P ranges from 450 to 850 mm/year. There is an influential P gradient across the site, with higher P received near the coast and declining inland to the north-east of the site. The mean annual Priestley-Taylor PET (Donohue et al., 2010) for the study site ranges from about 1100 to 1600 mm/year. The Aridity Index (AI; introduced above in the NSW site introduction), calculated as PET/P, ranges from 1.24 to 3.43 (Figure 10). Seasonally, the climate for the SA site is, climatological, much drier in summer and autumn with wettest conditions experienced in winter and early spring, with PET again increasing by late spring. This is clearly shown in Figure 11 and the long-term seasonal study site ranges for P, PET and AI are provided in Table 4.

Table 4. Mean seasonal climate data ranges for the SA site; for images see Figure 11.

Season	P Range (mm / season)	PET Range (mm / season)	AI Range (PET/P)
DJF	74 - 148	440 – 699	3.663 – 7.900
MAM	76 – 178	197 - 316	1.211 – 3.817
JJA	152 – 341	89 - 180	0.268 – 0.820
SON	113 - 211	320 - 477	1.597 – 3.954

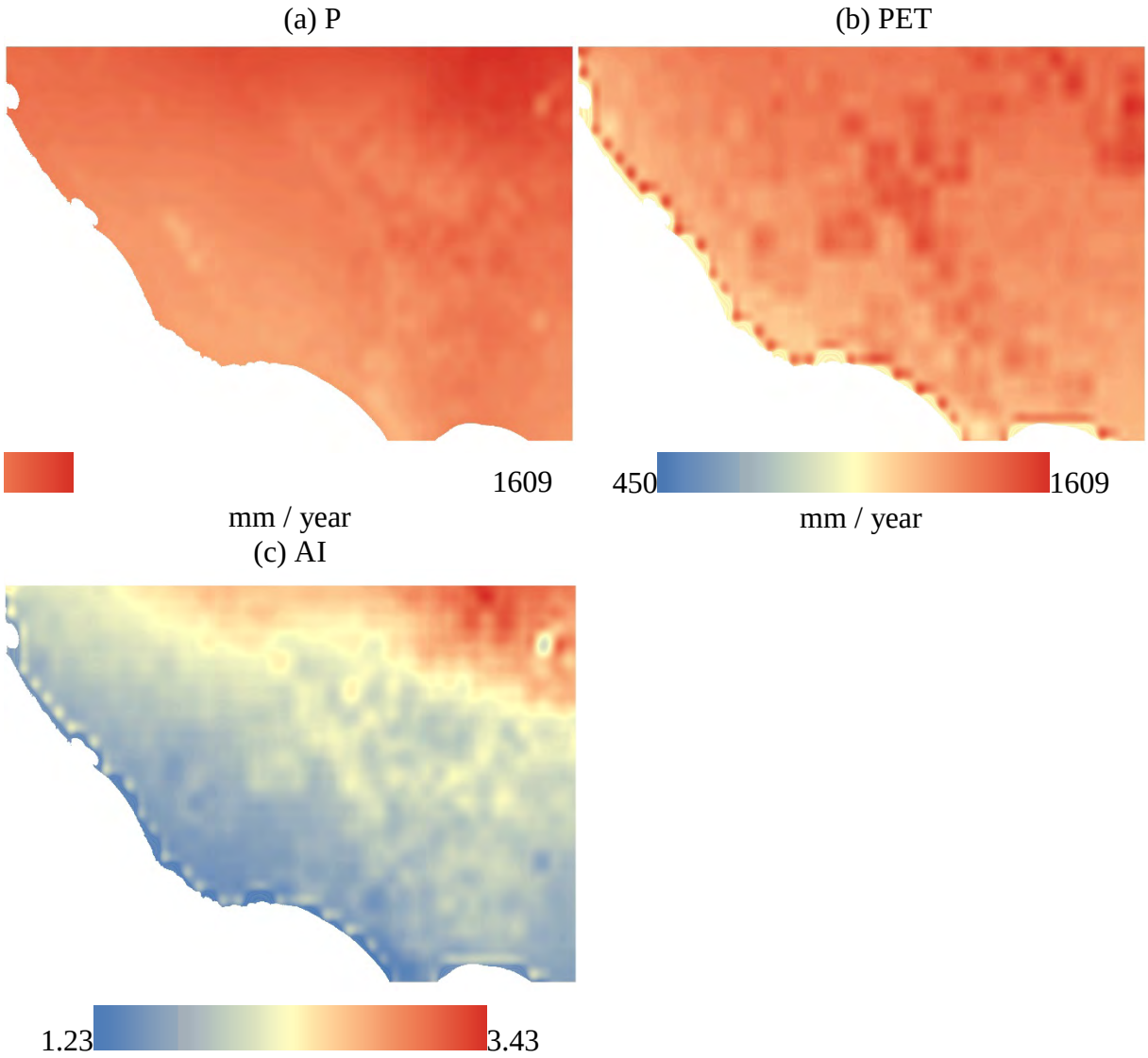

Figure 10. Mean annual climate data for the SA site. Part (a) shows the 2000 to 2011 mean annual site precipitation (P), (b) is the mean annual Priestley-Taylor PET, and (c) is the mean annual Aridity Index (AI=PET/P). To enable direct comparison P and PET have the same stretch.

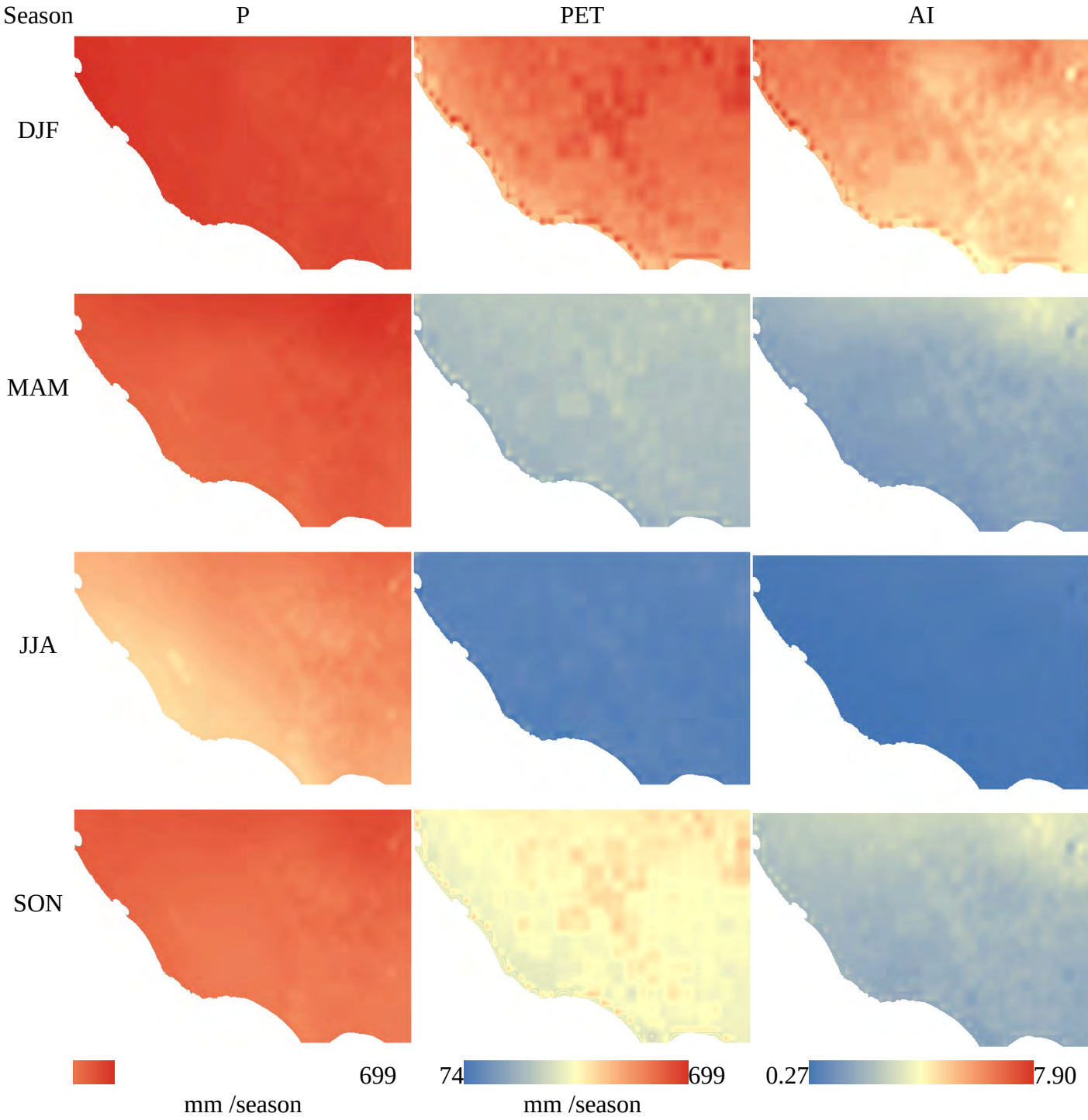

Figure 11. Mean seasonal climate data for the SA site. Part (a) shows the 2000 to 2011 mean seasonal site precipitation (P), (b) is the mean seasonal Priestley-Taylor PET, and (c) is the mean seasonal Aridity Index (AI=PET/P). To enable direct comparison P and PET have the same stretch.

Next we briefly characterise the vegetation dynamics of the SA site. Again, this is performed by temporally decomposing (Donohue et al., 2009) the time-series of monthly MODIS 250 m Collection 5 imagery. This decomposition splits the monthly time-step vegetation coverage signal (derived from the Normalised Difference Vegetation Index (NDVI); Donohue et al., 2008) into the persistent and recurrent components. In Figure 12(a) the forested areas (both

native and plantations) are clearly shown by the high vegetation cover in the annual persistent signal, and it also shows the pasture and cropping land-uses which have a low annual persistent component (Figure 12(a)) and moderate coverage in the annual recurrent signal (Figure 12(b)). The seasonal dynamics are also shown for the recurrent component. The annual cycle of low recurrent coverage in summer (Figure 12(c)), slightly increasing in autumn (Figure 12(d)), with more growth occurring in winter (Figure 12(e)) and most growth in spring (Figure 12(f)) are clearly visible. Again, the seasonal dynamics are not shown for the persistent component, which is persistent throughout the year.

(a) Annual fraction persistent

(b) Annual fraction recurrent

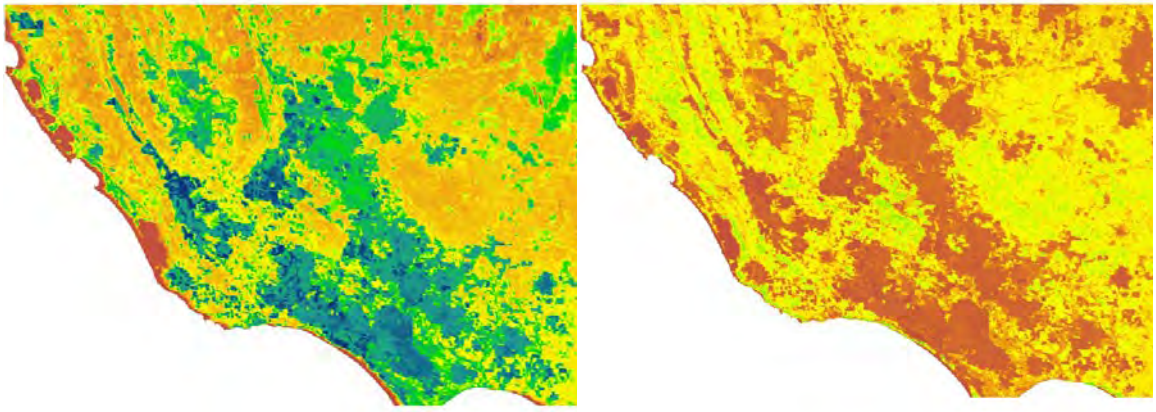

(c) DJF fraction recurrent

(d) MAM fraction recurrent

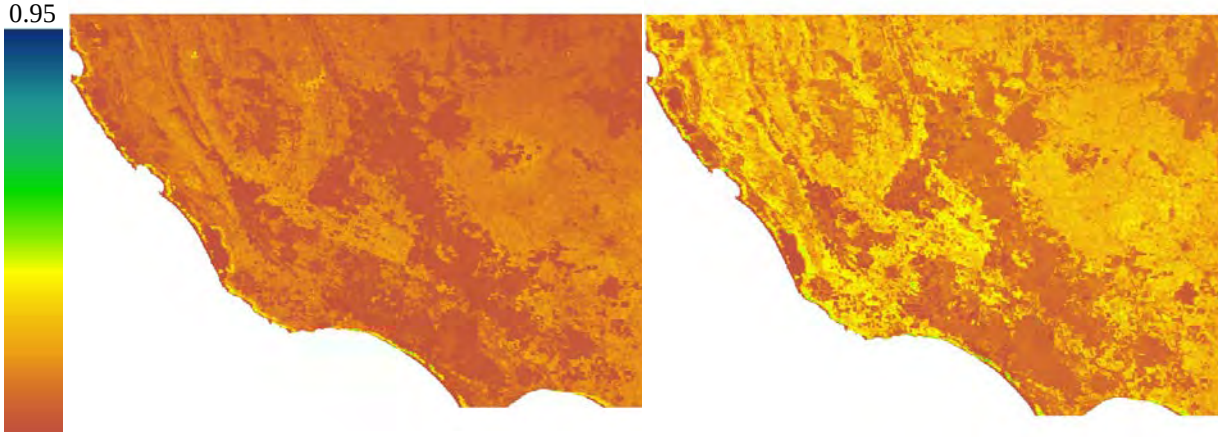

(e) JJA fraction recurrent

(f) SON fraction recurrent

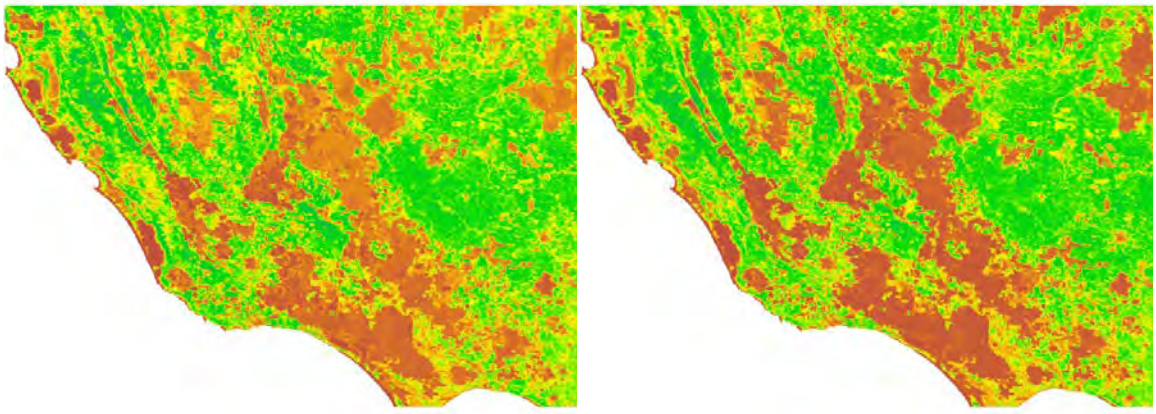

Figure 12. MODIS-based vegetation dynamics of the SA site. Parts (a) and (b) show the annual persistent and recurrent components, respectively. Parts (c) to (e) are the seasonal recurrent components, for summer, autumn, winter and spring, respectively.

2.2 Datasets

The three characteristics of remote sensing data of most relevance to this report are: (i) temporal density; (ii) spatial resolution; and (iii) spectral density, see Table 1 and Figure 1 for details. Remote sensing datasets are available at regular time intervals, which define their temporal density (e.g., 16-day repeat cycle for Landsat). They are also made available on a regular spatial interval at some nominal spatial resolution (e.g., 25 m by 25 m for Landsat data available within Australia). For optical sensors, multiple spectral wavebands of data are also usually collected from three sensors observing the visible (VIS) and near infrared (NIR), the shortwave infrared (SWIR) and the thermal infrared (TIR) regions, respectively, thus defining the spectral density (the number of bands over a particular portion of the electro-magnetic spectrum) and spectral resolution (the width of each of the bands). Here, we adapt the general nomenclature of Sun et al. (2010), where a multi-spectral spatio-temporal remote sensing dataset of surface reflectance is expressed as a three-dimensional array:

$$\boldsymbol{\rho} = \left[\rho_{ijw} \right]_{m \times n \times q}, \tag{1}$$

where i=1,m time intervals, j=1,n spatial cells, and w=1,q spectral wavebands. The bolded variable denotes an array, and the symbol ρ expresses surface reflectance (proportion). Eq. (1) results in a data array useful for describing any given remote sensing platform, having various specifications of m, n, and q. That is, having specific temporal density, spatial resolution, and spectral density. Different sensors also have specific radiometric characteristics (extent, resolution, and density) and spectral resolution, but these characteristics are not expressed in the equation. Spatial extent is defined by the study site boundary and temporal extent is limited by the lifespan of the sensor. For ease of interpretation, the indexes (i, j, and w) will be left off of symbolic notation whenever possible, except where they are explicitly required to improve communication. Herein, bolded variables represent some form of data array whereas variables that are unbolded represent a scalar value, which allows better interpretation of the equations used in this report. Not all data arrays expressed in this report contain the spectral dimension. For example, the spatio-temporal array of precipitation has only the spatial and temporal dimensions and would be expressed by $\mathbf{P} = \left[P_{ij} \right]_{m \times n}$. In these cases, the representation of such an array will also simply be presented as a bolded variable. It was deemed a suitable level of discrimination to allow immediate discrimination of arrays from scalar values. Specifics of the arrays will be noted in the appropriate place as the variables are presented.

2.2.1 Remote sensing data

The Landsat data used were from the Australian Reflectance Grid 25 (ARG25) product v1 (http://www.ga.gov.au/corporate_data/75062/Australian_Reflectance_Grid_ARG25_Product_Description_V1-0.pdf, accessed 31-July-2015). ARG25 v1 provides a standardised surface reflectance of Landsat TM/ETM+/OLI data over the entire Australian landmass. The data are atmospherically and bi-directional reflectance distribution function (BRDF) corrected using the physics-based algorithm described in Li et al. (2012). These type of data are commonly termed view angle corrected Nadir BRDF-Adjusted Reflectance (NBAR, proportion). Importantly (as shown later) ARG25 v1 was not topographically corrected. Figure 13 shows the percentage of valid pixels for each Landsat scene comprising the NSW site. For the northern image the largest data gap is 64 days and for the southern image the largest data gap is 48 days. These gap calculations only take into account an image if it was present, they do not consider the number of valid pixels within an image, which would increase the gap length.

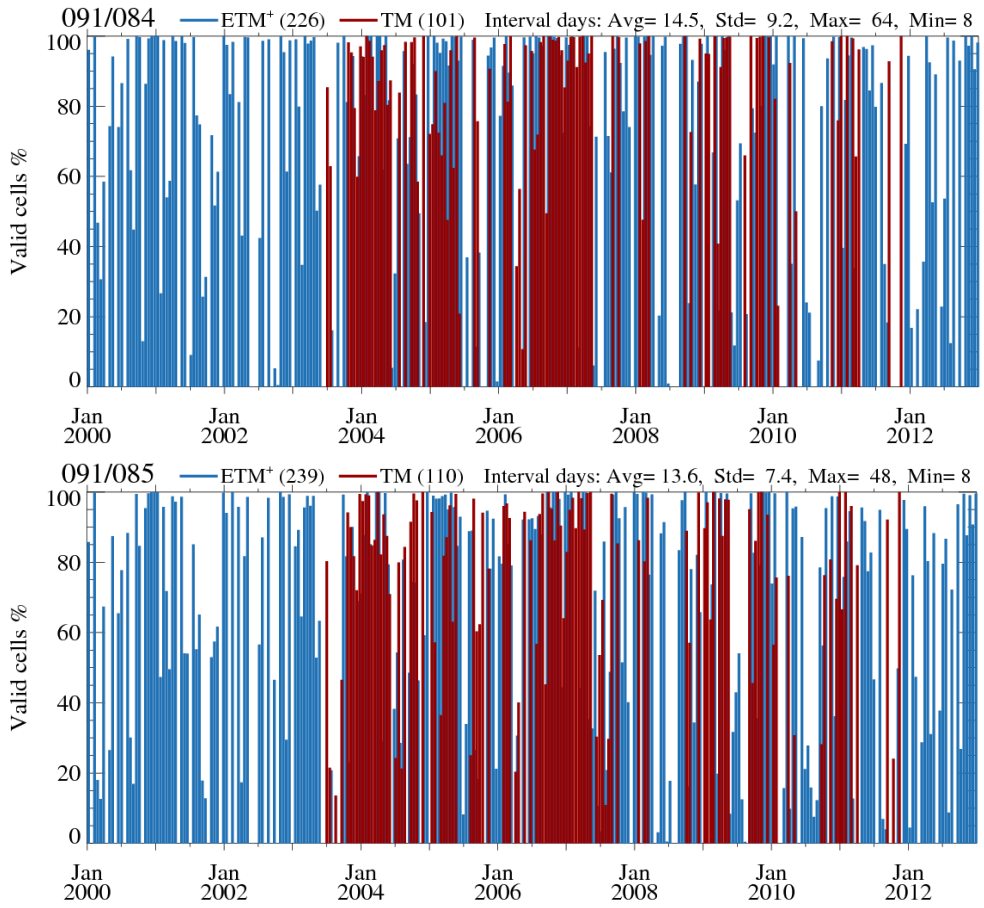

Figure 13. Time series of percentage valid Landsat data for the NSW site. The top plot represent the northern Landsat scene (i.e., 91/84 see Figure 4(a)) and the bottom plot is the southern Landsat scene (i.e., 91/85). The valid cells calculation is only performed for the part of the Landsat scene that comprises the NSW site. The number of Landsat-7 ETM+ and Landsat-5 TM scenes are provided in parenthesis on the top of each sub-plot. Basic descriptive statistics of the intervals (or gap length) between are provided in units of days.

Figure 14show the percentage of valid pixels for each Landsat scene comprising the SA site. For the eastern image the largest data gap is 128 days and for the western image the largest data gap is 144 days. These gap calculations only take into account an image if it was present, they do not consider the number of valid pixels within an image, which would increase the gap length. Obviously the SA site is considerably cloudier than the NSW site and being able to reduce a gap of missing data from approximately 130 days to 8 days while maintaining 25 m resolution AET estimates highlights the utility of Landsat-MODIS blending.

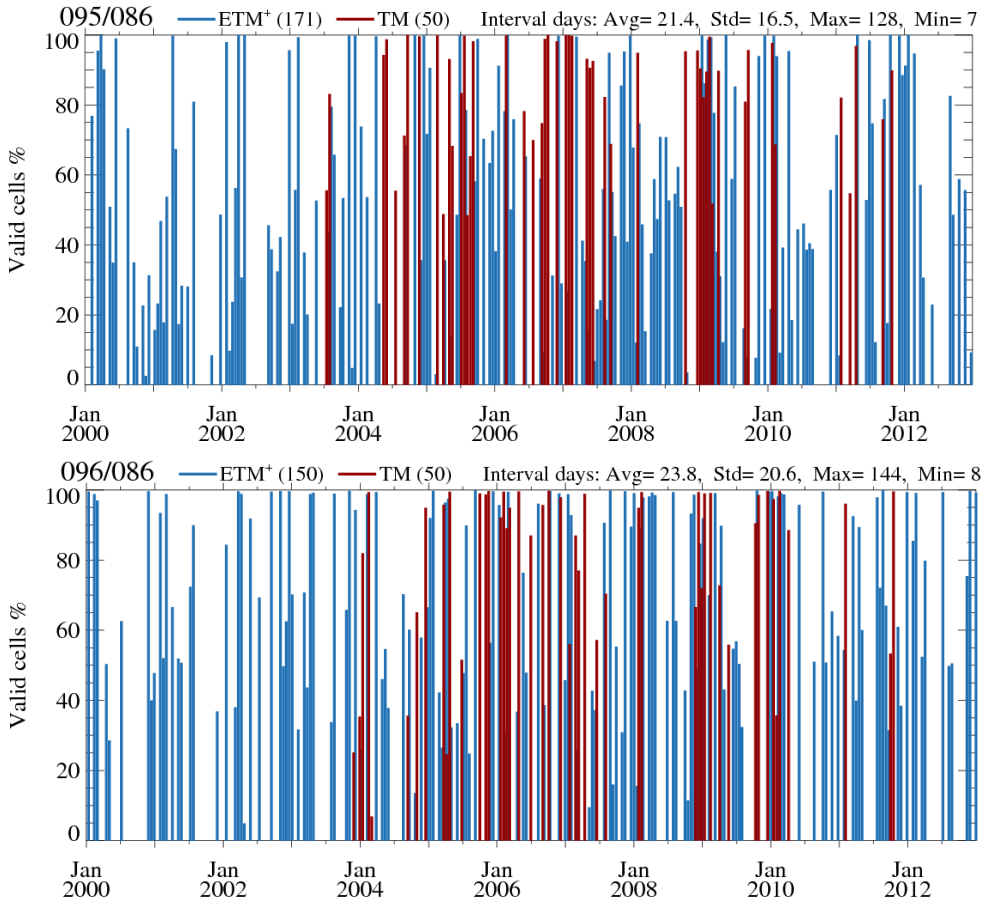

Figure 14. Time series of percentage valid Landsat data for the SA site. The top plot represent the eastern Landsat scene (i.e., 95/86 see Figure 4(b)) and the bottom plot is the western Landsat scene (i.e., 96/86). The valid cells calculation is only performed for the part of the Landsat scene that comprises the SA site. The number of Landsat-7 ETM+ and Landsat-5 TM scenes are provided in parenthesis on the top of each sub-plot. Basic descriptive statistics of the intervals (or gap length) between are provided in units of days.

The MODIS data used were the MCD43A4 product, which is also view angle corrected nadir BRDF-adjusted surface reflectance (https://www.umb.edu/spectralmass/terra_aqua_modis/v006/mcd34a4_nbar_product, accessed 31-July-2015). As provided, the MCD43A4 data are composited to 8-day time step and represent the reflectance at solar noon. MCD43A4 are also not topographically corrected.

As will be described below, topographic correction was applied to both the Landsat and MODIS data. This correction required the terrain slope and aspect at both study sites. We used the Shuttle Radar Topographic Mission (SRTM) Digital Elevation Model (DEM-S) as processed by Gallant et al. (2011). The DEM-S data were clipped to the study site extents, reprojected from geographic to UTM projection, and the spatial resolution was resampled from 27 m to 25 m using the Geospatial Data Abstraction Library (GDAL, www.gdal.org). The terrain slope and aspect were calculated as per Wilson and Gallant (2001) using the Interactive Data Language (IDL) software. The 25 m data were used to topographically correct both the Landsat and MODIS data. For MODIS, bilinearly re-sampled NBAR reflectances were used.

2.2.2 Land use data

The original land-use data was from the Australian Land Use and Management Classification (version 7), provided in (ABARES, 2011). We used the catchment scale land use data, which vary in scale from 1:25,000 to 1:250,000. The source of these data are varied, coming from state, public land, satellite, and field data (ABARES, 2011). The Australian Land Use and Management Classification (version 7) data offers the benefit of avoiding classification artefacts due to State boundaries and is the land-use data used in many national summaries.

The original classes were adapted, resulting in 9 land-use classes utilised in the current study (see Figure 16). The 9 classes relate to the original classification from as follows:

1. Native vegetation: comprised of all classes in "1 Conservation and Natural Environments" as well as "2.1.0 Grazing native vegetation";
2. Plantation unknown: all classes in "2 Production from Relatively Natural Environments" except "2.1.0 Grazing native vegetation";
3. Plantation hardwood: "3.1.1 Hardwood plantation";
4. Plantation softwood: "3.1.2 Softwood plantation";
5. Dryland Cropping: all classes in "3 Production from Dryland Agriculture and Plantations" except 3.1.1, 3.1.2 and 3.2.0 – 3.2.5;
6. Irrigation: all classes in "4 Production from Irrigated Agriculture and Plantations"
7. Urban: all classes in "5 Intensive Uses";
8. Water: all classes in "6 Water"; and
9. Grazing Modified Pasture: classes 3.2.0 – 3.2.5 in "3 Production from Dryland Agriculture and Plantations".

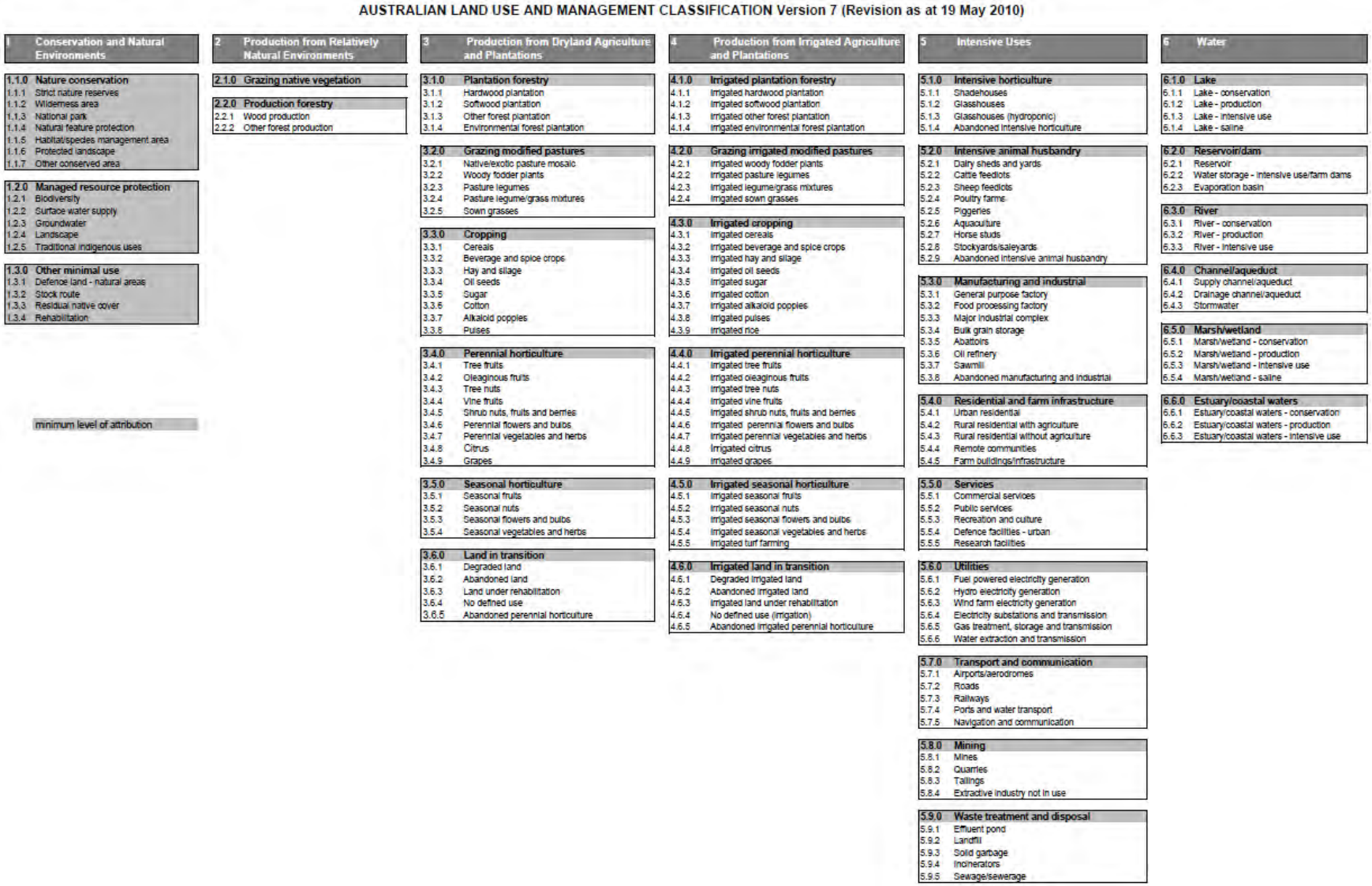

Figure 15. The Australian Land Use and Management Classification (version 7) criteria are shown.

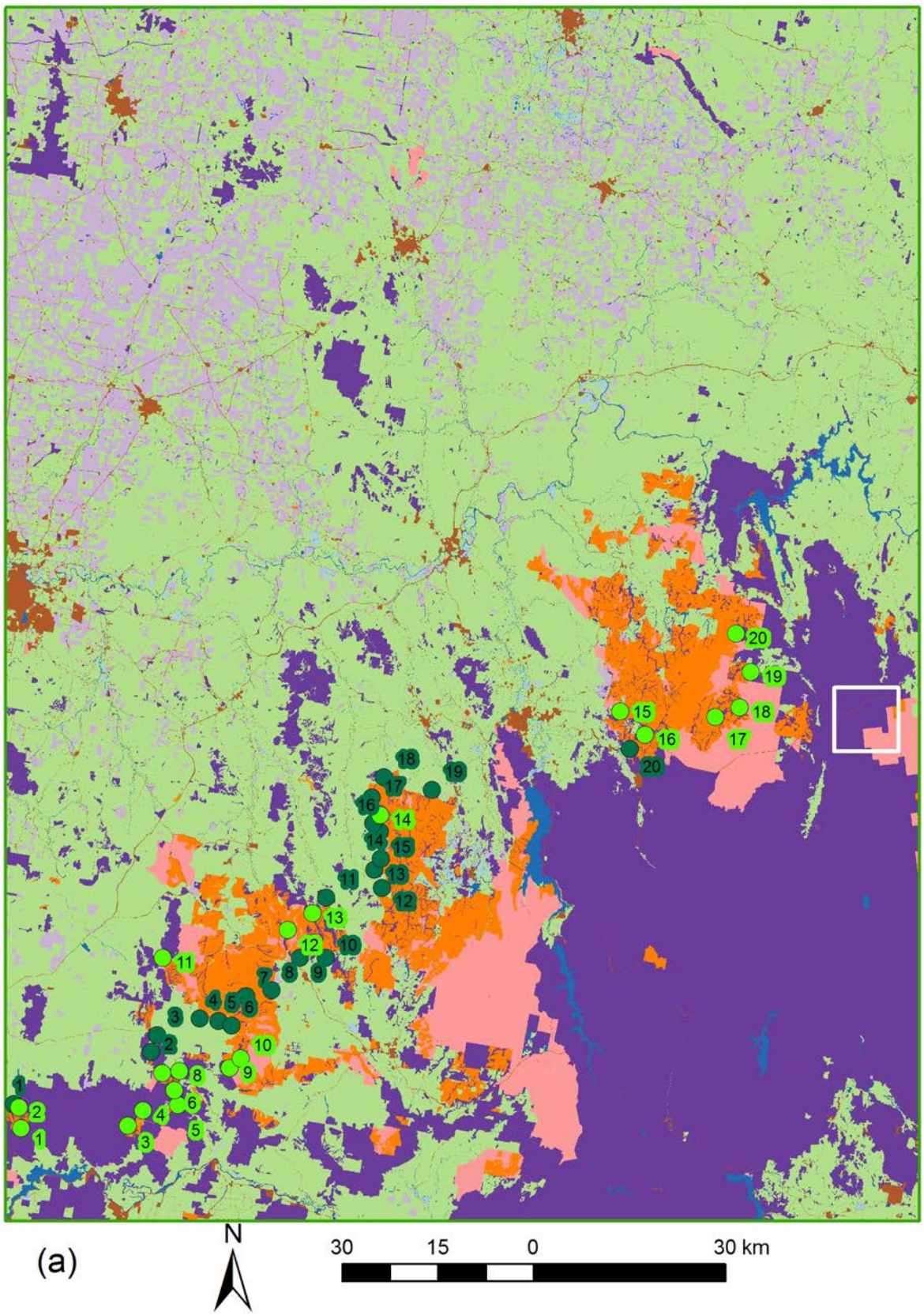
(a)
N
30
15
0
30 km

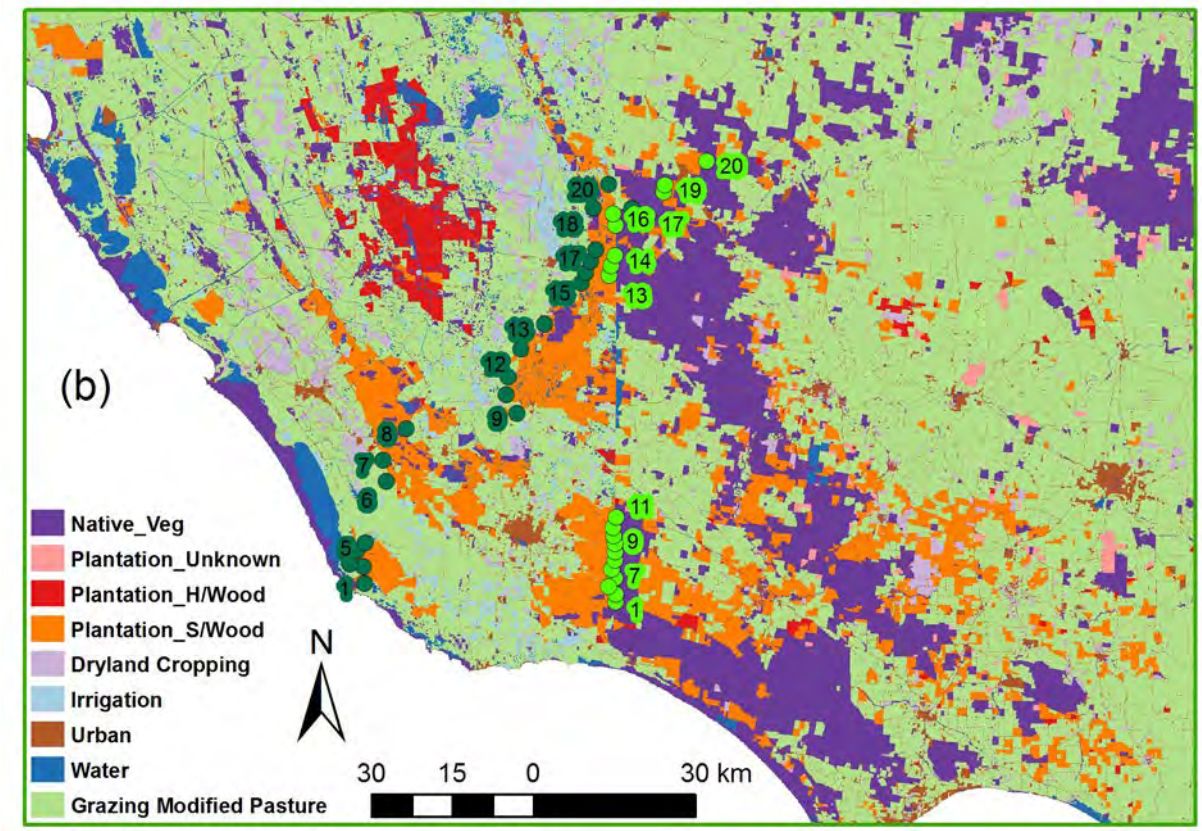

Figure 16. Land-use data for the (a) NSW site and (b) SA site. The green rectangles are the study sites and the white rectangle in (a) describes an assessment area of the topographic correction, discussed in detail below. The legend in (b) also applies to (a). The light green points show the average locations of the paired analysis between the Softwood Plantation and Native Vegetation land-use classes, described in detail later. The dark green points show the average locations of the paired analysis between the Softwood Plantation and Grazing Modified Pasture land-use classes, described in detail later.

2.2.3 Validation data

We define validation as the comparison between modelled AET and measurements that are representative of AET to first-order and in the same physical units. There were three types of validation datasets available across our two study sites: (*i*) water balance in catchments (reaches) where precipitation and stream flow were measured (calibrated); (*ii*) observations of actual evaporation at an eddy covariance flux tower; and, (*iii*) site water use from sap-flow and site water balance measurements. Here, the validation and evaluation datasets are described, along with the description of processing that was performed prior to our obtaining the data. The processing we performed on these data is described in the methods section, below.

At both sites, precipitation from the Bureau of Meteorology (BoM) as described in (Jones et al., 2009) was available. Stream flow data (Q, mm) for the Forestry Corporation NSW (FCNSW) unimpaired catchments and 16 additional gauges from the BoM all-Australia unimpaired Q dataset (Zhang et al., 2013) were available within the NSW study area and time period, see Table 5 and Figure 17a. Precipitation and stream flow values were adjusted for nested catchments (Table 5). Streamflow data were also available as calibrated output from the AWRA-R model for 5 river reaches (as opposed to catchments) where stream gauges could be used along with the contributing areas to perform water balance, see Figure 17a and

Table 6 below. In AWRA-R, river reach streamflow was calibrated independently in each reach from upstream to downstream reaches following the order dictated by the node-link network defined for the AWRA-R model (Lerat et al., 2013). During calibration, the upstream inflows were set to the observed stream flow data. Outside of this period, or during periods with no stream flow data, upstream simulated inflows were used instead (Lerat et al., 2013). Model parameters for every reach were optimised at the downstream main gauge of the reach using the Nelder-Mead optimiser (Nelder & Mead, 1965). Observed daily stream flow data at the downstream gauge corresponding to the main stem outflow of the reach was used for parameter optimisation (Dutta et al., 2015). The reach contributing area was defined from flow accumulation and direction rasters and pour points from DEM analysis (Dutta et al., 2015). The purpose for which AWRA-R was originally developed was to provide retrospective information on fluxes (e.g., streamflow, diversions) and stores (e.g., in-stream volumes, lakes, reservoirs) in both regulated and unregulated systems and in order to support the production of national water accounts by the Bureau of Meteorology (Dutta et al., 2015). Here we use it as a form of validation as it is based on observed river streamflow. Unimpaired catchment water balance data were also available at the SA site and time period for 9 catchments from the BoM dataset (Zhang et al., 2013), see Table 7 and Figure 17c.

Table 5. Catchments within the NSW site where nearly complete precipitation and stream flow data were available. Some catchments have nested contributing areas, and completeness is based on daily data. Start date is the later of the stream flow data start date or our modelled AET data start date. End date is the earliest of the stream flow record end date and the end date of modelled AET data. Nested catchment areas that include another catchments' contributing area are denoted with an asterisk. An (F) in brackets in the Gauge name column means that the data were provided by Forestry Corporation NSW (FCNSW).

Count	Station ID	Gauge Name	Start Date	End Date	Complete (%)	Area (km^2)
1	410997	Kiley's Run (F)	1/12/2000	31/10/2011	88	1
2	410998	Red Hill (F)	1/03/2000	31/10/2011	90	2
3	410999	Sawmill Ck (F)	1/12/2000	31/10/2011	88	12*
4	—	BagoG3 (F)	1/03/2000	26/11/2007	100	53*
5	—	BagoG4 (F)	1/03/2000	26/11/2007	100	1
6	—	BagoG5 (F)	1/03/2000	26/11/2007	100	1
7	401008	Tooma	1/03/2000	17/06/2011	94	512*
8	401009	Maragle	1/03/2000	18/04/2011	97	216
9	401013	Jingellic	1/03/2000	21/06/2011	99	395
10	401017	Yarramundi	1/03/2000	18/04/2011	95	194
11	410024	Wee Jasper	1/03/2000	13/04/2011	100	990*
12	410038	Darbalara*	1/03/2000	29/04/2011	100	391
13	410044	Coolac	1/03/2000	29/04/2011	100	1072
14	410047	Old Borambola	1/03/2000	1/04/2011	100	1653
15	410048	Ladysmith	1/03/2000	5/05/2011	93	548*
16	410057	Lacmalac	1/03/2000	4/05/2011	100	668
17	410061	Batlow Rd	1/03/2000	8/12/2010	100	148
18	410088	Brindabella	1/03/2000	17/05/2011	100	432
19	410097	Aberfeldy	1/03/2000	20/04/2011	94	351
20	410107	Mountain Ck	1/03/2000	24/02/2011	95	185
21	410156	Book Book	1/03/2000	23/02/2011	100	145

(a)

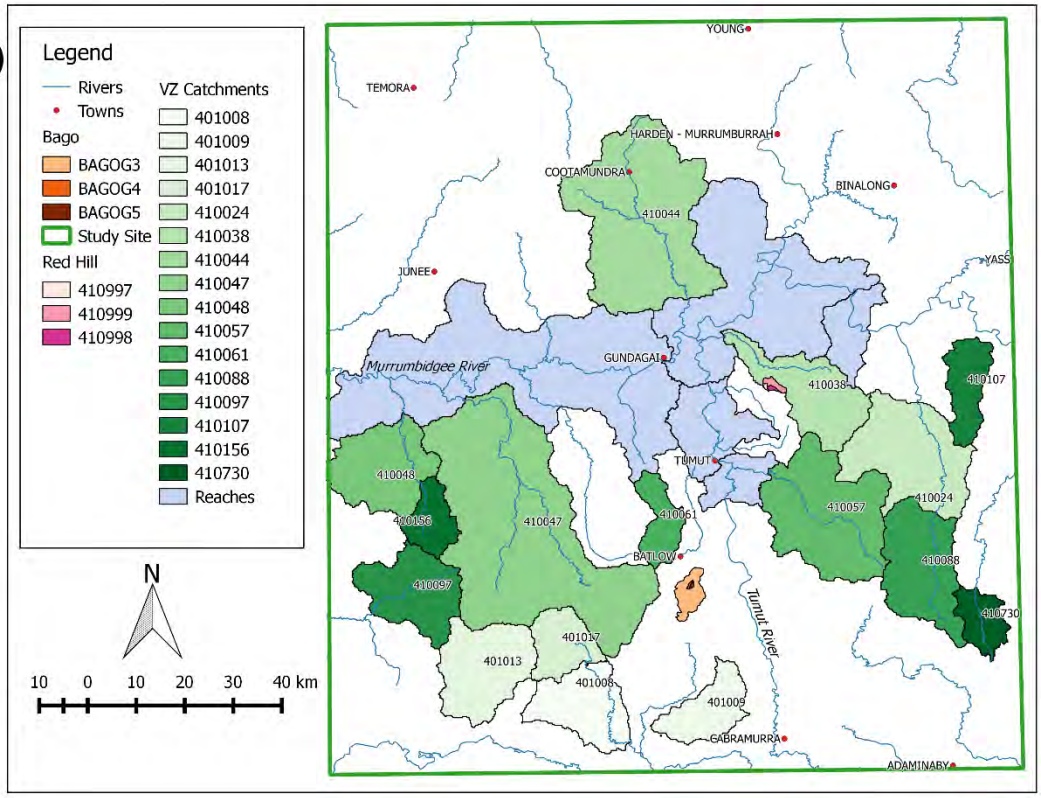
Legend
Rivers
Towns
Bago
BAGOG3
BAGOG4
BAGOG5
Study Site
Red Hill
410997
410999
410998
VZ Catchments
401008
401009
401013
401017
410024
410038
410044
410047
410048
410057
410061
410088
410097
410107
410156
410730
Reaches
N
10 0 10 20 30 40 km
YOUNG
TEMORA
HARDEN - MURRUMBURRAH
COOTAMUNDRA
BINALONG
JUNEE
YASS
Murrumbidgee River
GUNDAGAI
TUMUT
BATLOW
Tumut River
GABRAMURRA
ADAMINABY

(b)

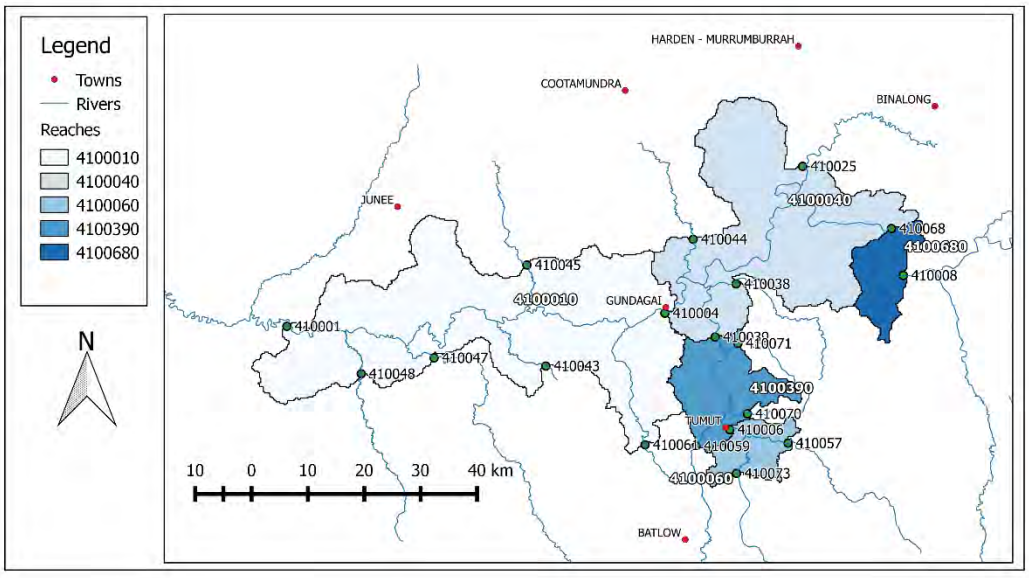
Legend
Towns
Rivers
Reaches
4100010
4100040
4100060
4100390
4100680
N
10 0 10 20 30 40 km
HARDEN - MURRUMBURRAH
COOTAMUNDRA
BINALONG
JUNEE
GUNDAGAI
TUMUT
BATLOW

(c)

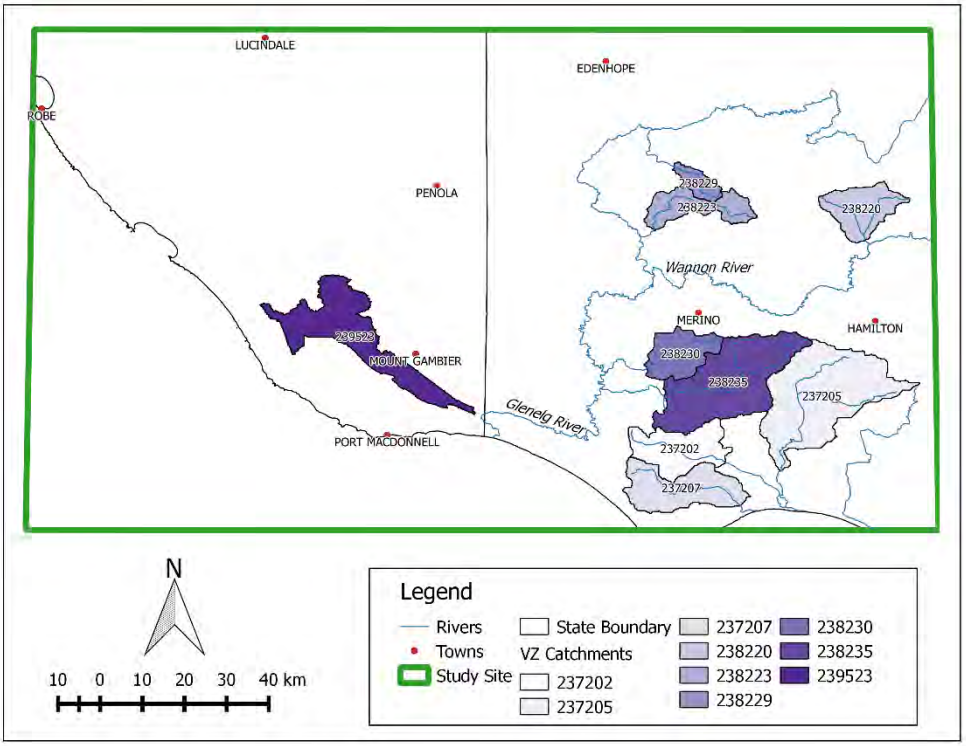

Figure 17. The water balance validation datasets are shown. In (a) are the NSW catchment boundaries for the Viney-Zhang BoM dataset and the FCNSW Bago and Redhill catchments; in (b) the five reaches used in this study and the stream flow gauges used to define them are shown; and in (c) the SA Viney-Zhang BoM dataset is shown. The location of the reaches within the NSW study site are also shown in (a) for completeness.

Table 6. Reach and streamflow gauge associations are shown. The outlet gauge is bolded while the upstream gauges are in normal font. The reach mass balance was determined by subtracting the sum of all upstream gauge streamflow from the downstream (outlet) gauge's streamflow. See for spatial distribution of gauges around each reach.

Number	Name of outlet gauge	Reach ID	Gauge ID
1	Murrumbidgee@Wagga Wagga	4100010	**410001**
			410004
			410043
			410045
			410047
			410048
			410061
2	Murrumbidgee@Gundagai	4100040	**410004**
			410025
			410038
			410039
			410044
			410068
3	Tumut@Tumut	4100060	**410006**
			410057

			410073
4	Tumut@Brungle Br	4100390	**410039**
			410006
			410059
			410070
			410071
5	Murrumbidgee@Glendale	4100680	**410068**
			410008

Table 7. Catchments within the SA/VIC site where nearly complete precipitation and stream flow data were available are shown. Completeness is based on daily data. Start date is the later of the stream flow data start date or our modelled AET data start date. End date is the earliest of the stream flow record end date and the end date of modelled AET data.

Count	Station ID	Gauge Name	Start Date	End Date	Complete (%)	Area (km^2)
1	237202	Heywood	1/03/2000	18/02/2009	100	268
2	237205	Homerton Br	1/03/2000	12/03/2009	100	714
3	237207	Heathmere	1/03/2000	17/02/2009	100	312
4	238220	Cavendish	1/03/2000	13/02/2009	99	214
5	238223	Wando Vale	1/03/2000	23/03/2009	100	180
6	238229	Chetwynd	1/03/2000	16/03/2009	100	69
7	238230	Teakettle	1/03/2000	25/02/2009	100	197
8	238235	Lower Crawford	1/03/2000	18/02/2009	100	601
9	239523	Woakwine Range	1/03/2000	18/03/2011	100	485

Hourly actual evapotranspiration data were measured at the long-term eddy covariance flux tower site at Tumbarumba, New South Wales (35.650°S, 148.151°E), see the blue star in Figure 4a. Hourly measurements were made at Tumbarumba over 3965 days between February 2001 and December 2011, see Table 8 for seasonal and overall average flux summaries. Tumbarumba is located in a native wet sclerophyll forest with no distinct seasonality in precipitation. Instrumentation, data quality, and data processing of the flux tower data have been described in detail previously (Guerschman et al., 2009; Leuning et al., 2005; Van Gorsel et al., 2007). Energy balance closure is a frequently used diagnostic at eddy covariance flux sites. The daily averaged hourly energy balance closure is within 10% at Tumbarumba (Leuning et al., 2005), which indicates the data are of high quality.

Table 8. Overall and seasonal mean fluxes are shown for the Tumbarumba flux site, expressed as hydrological equivalent units of mm d^{-1}. Flux densities were averaged over seasons of December, January, and February (DJF); March, April, and May (MAM); June, July, and August (JJA); September, October, and November (SON); and January – December (Annual).

	Tumbarumba (mm d^{-1})		
Time	Actual ET	Available Energy	Precipitation
DJF	3.9	6.2	3.0
MAM	2.1	3.0	2.3
JJA	1.1	1.5	4.7
SON	2.6	4.9	3.9
Annual	2.5	4.1	3.5

Site water balance data were available over the SA area, described in detail in (Benyon & Doody, 2015; Benyon et al., 2006). Briefly, forestry plantation water balance components were measured in 20 by 20 m experimental plots, 18 of which had valid data during our project temporal extent when intersected with valid remotely sensed data (Table 9 and Figure 18). The experimental design of the site water balance collection assumed surface water flow and subsurface lateral flow within the vadose zone were negligible, estimating the site water balance from measured evapotranspiration, rainfall, and changes in root-zone soil water (Benyon et al., 2006). Sites varied by species, age, depth to watertable, slope, soils, and stocking rates (see Benyon et al., 2006 for details) as well as by distance from edge of the stand. Interception was measured by 8 collection troughs per site, soil evaporation was measured with 5-9 mini-lysimeters per site, and transpiration was measured by heat-pulse with sapflow sensors (Benyon et al., 2006). Observed soil evaporation data from the lysimeters were used when soil water content in the top 0.3 m of soil outside the lysimeters was greater than 50% of the maximum water content. When the soil water content was lower than 50% of the maximum, soil evaporation was estimated from average soil water conditions and a linear model between daily evaporation rate and soil water content in the top 0.3 m of the soil profile (Benyon et al., 2006). This relationship was used in an attempt to account for potentially underestimating the site soil water depletion due to exclusion of live roots in the lysimeters. The impact of applying this adjustment factor was not formally assessed. The site water balance data were collected, roughly, on a fortnightly basis. In our study, these data and the modelled AET data were aggregated to monthly values, so they could be compared (Table 9).

Table 9. The site water balance dataset points are summarised. The Identification (ID) code is that of Benyon et al. (2006). The valid number of months for each site (N) are shown when these field data were intersected with the remote sensing data. Two sites (EG4 and PR18) had 0 months intersecting both field and remote sensing data. There were a total of 591 months (398 months from 11 *E. globulus* (EG) sites and 193 months from 7 *P. radiata* (PR) sites) available.

ID	Name	Plant Year	Species	N (Months)
EG1	Will	1998	*E. globulus*	26
EG2	MtView	1996	*E. globulus*	65
EG3	McRoos	1996	*E. globulus*	43
EG4	WoakWine	1994	*E. globulus*	0
EG5	Jack	1998	*E. globulus*	32

EG6	Jill	1998	*E. globulus*	36
EG7	Gummy	1996	*E. globulus*	55
EG9	Vicki	1998	*E. globulus*	37
EG10	DPI	1996	*E. globulus*	28
EG11	Jasper	1998	*E. globulus*	23
EG12	Bessie	1998	*E. globulus*	36
EG13	Wanda	1992	*E. globulus*	17
PR10	Rainy	1996	*P. radiata*	27
PR11	Piney	1996	*P. radiata*	61
PR12	Julia	1970	*P. radiata*	7
PR13	Nangwarry_South	1986	*P. radiata*	22
PR14	Miles	1978	*P. radiata*	37
PR15	Caroline	1971	*P. radiata*	8
PR17	Dart	1994	*P. radiata*	31
PR18	Hurdle	1996	*P. radiata*	0

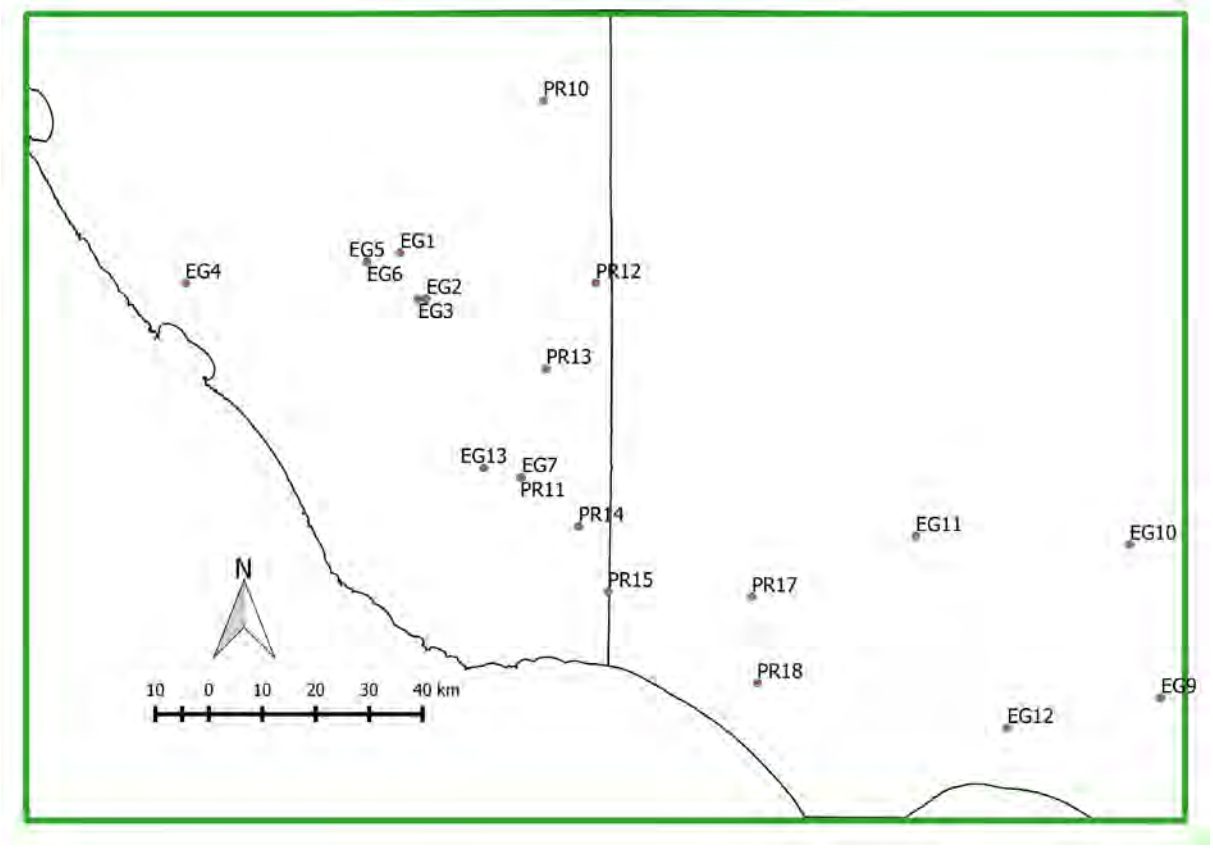

Figure 18. The site water balance locations are shown. The labels are those of Benyon et al. (2006) as given in Table 9. The green rectangle is the SA study site extent and the black lines are the state boundaries.

2.2.4 Evaluation data

Evaluation is the comparison between modelled AET and some dataset that allows for more confidence in the model to be established, but where a more formal error/uncertainty analysis is not possible. Evaluation allows for 'multiple-lines-of-evidence' to be built, which bolsters the user's confidence in the estimates. Three types of evaluation datasets have been

categorised over our two study sites: (i) vegetation plot data; (ii) history & management; and (iii) environmental variability data.

At the NSW site, ten 800 m^2 circular forest growth plots measuring diameter at breast height over bark (DBHOB, or herein, simply DBH) were available within the Red Hill catchment (Major et al., 1998; Webb & Kathuria, 2012). The plots were all in 1989 age-class stands of *P. radiata* and DBH measurements were made on all stems > 5cm (Webb & Kathuria, 2012). DBH measurements were made at four times within the temporal extent of our study: on 30/Sep/2009, 07/Sep/2010, 05/Jul/2011, and 03/Aug/2011 (Table 10). Plot locations were provided in Australian Map Grid (AMG) coordinates and were converted to Map Grid of Australia (MGA, zone 55) coordinates to match the projection of the remote sensing datasets. The plots are rather close together with respect to assessment of 25 m remote sensing pixels: maximum spread of the 10 plots is 21 pixels in the x-direction and 29 pixels in the y-direction (for 25 by 25 m pixels). Thinning occurred at various times over the plots, sometimes reducing the number of trees available for measurement at the later dates (Table 10). DBH was converted to stand basal area (m^2/ha) over the plots, which were converted to stand timber volume (m^3/ha) by making use of average plot tree height and assuming a conical trunk shape.

Table 10. Details of the 10 forest growth plots are shown. The X and Y locations are provided as MGA coordinates. The number of trees sampled is shown for the earliest and latest sampling dates within the temporal extent of our study.

Plot No.	Previous Cover Type pre-1989	X	Y	No. Trees 30/Sep/2009	No. Trees 03/Aug/2011
1	Improved Pasture	623358	6111314	27	27
2	Improved Pasture	623335	6111262	27	27
3	Improved Pasture	623438	6111297	32	17
4	Improved Pasture	623369	6111219	29	29
5	Improved Pasture	623502	6111278	30	21
6	Scattered Timber	623188	6111894	30	20
7	Scattered Timber	623264	6111932	29	18
8	Scattered Timber	623366	6111904	28	20
9	Scattered Timber	623705	6111803	24	14
10	Scattered Timber	623676	6111656	26	15

At the SA site, GIS data on species, age, and thinning management of the forestry plantations were available. We performed 3 evaluations, to summarise: (1) AET growth curves for two species (*E. globulus* and unthinned *P. radiata*); (2) the influence of thinning on AET of a single species (*P. radiata*); and (3) the ability to detect compartment-level harvest in AET. As stated above, evaluations are not intended to be as definitive as validation. The purpose of evaluations was to allow users to determine their level of confidence in the AET model output by assessing whether the model outputs pass several forms of 'reality-check'. First, evaluation of the average modelled output of unthinned *E. globulus* and unthinned *P. radiata* were summarised by age (years) using all available data. This summary evaluated whether there was a noticeable difference in growth pattern between the two species. The summary was performed irrespective of which year the compartment was planted. For example, an unthinned *P. radiata* compartment that was one year old in 2000 and a different unthinned compartment that was one year old in 2011 would both be used in the calculation of the mean AET for age class of 1 year for that species. This summary did not account for the variability in climate and/or site growing conditions. The overall mean AET by age would be less influenced by not accounting for temporal and spatial variability as the sample size becomes

larger. There was less *E. globulus* compartments than *P. radiata*, so this should be kept in mind when interpreting the *E. globulus* results in particular. The number of 25-m resolution cells (each covering 625 m^2) in the AET grids and the number of management compartments that were used to determine the average AET values varied by age and species. There was a median of 29 compartments (45,627 cells) per yearly age class used to determine the unthinned *E. globulus* values, whereas there was a median of 740 compartments (2,412,801 cells) per yearly age class used to determine the unthinned *P. radiata*. The forestry management data also included information on timing of multiple thinning operations. Secondly, we evaluated the average AET of *P. radiata* of those stands that had been first thinned in 2000, the initial year of our study period. These thinned stands had an average age of about 15 years old. We compared them to non-thinned *P. radiata* stands that had an age of 15 in the year 2000. This evaluation described the influence of thinning on AET. Again, the number of cells and compartments varied for thinned versus non-thinned classes, where *P. radiata* first thinned in 2000 had a median number of compartments of 287 (464,453 cells) per year and unthinned *P. radiata* having age 15 years in 2000 had a median number of compartments of 129 (2,746 cells) per year making of the average AET values. This comparison did account for temporal variability as each year after first thinning would be the same year (sequential from 2000). Thirdly and finally, we evaluated the ability of the LM blended AET output to detect forestry harvest operations in compartments in the vicinity of Burrungule in the SA site, which were harvested in 2004. For this evaluation, the MODIS-only AET and the LM blended AET average January AET maps for 2003, 2006, and 2009 were plotted to highlight the spatial representation of the AET 1 year before harvest, 2 years after harvest, and 5 years after harvest.

2.3 Topographic correction

Topographic correction was performed for each waveband using the so-called Minnaert correction model, given by Lu et al. (2008):

$$\boldsymbol{\rho}_{iw(H)} = \boldsymbol{\rho}_{iw(T)} \cdot \cos\left(\boldsymbol{\theta}_{(T)}\right) \Big/ \left[\cos\left(\boldsymbol{\theta}_{(T)}\right) \cdot \cos\left(\boldsymbol{\theta}_{i(I)}\right)\right]^{k_{iw}}, \tag{2}$$

where solar, terrain, and incident angles or reflectances are denoted with subscripts of (S), (T) and (I) respectively. $\boldsymbol{\rho}_{iw(T)}$ is the spatial array of view angle corrected nadir BRDF-adjusted surface reflectance (NBAR, proportion) of waveband *w* at time *i* at the terrain surface. $\boldsymbol{\rho}_{iw(H)}$ is the equivalent NBAR (proportion) on a horizontal surface (i.e., topographically corrected to the reflectance of a flat surface with incident angle zero). The spatial arrays (i.e., maps) of zenith angles (radians) are given in general form by $\boldsymbol{\theta} = \left[\theta_j\right]_n$. $\boldsymbol{\theta}_{(T)}$ is the map of slope facet zenith angle (for practical purposes, not a function of time), which is most often referred to as 'slope' in terrain analysis. $\boldsymbol{\theta}_{i(I)}$ is the map of incident zenith angle (radians) at time *i*, also known as the illumination angle, which is the angle between the solar beam and the normal to $\boldsymbol{\theta}_{(T)}$. For any particular day-of-year (DOY) and specific time-of-day (STOD), the map of $\boldsymbol{\theta}_{i(I)}$ is given by:

$$\cos\left(\boldsymbol{\theta}_{i(I)}\right) = \cos\left(\boldsymbol{\theta}_{i(S)}\right) \cdot \cos\left(\boldsymbol{\theta}_{(T)}\right) + \sin\left(\boldsymbol{\theta}_{i(S)}\right) \cdot \sin\left(\boldsymbol{\theta}_{(T)}\right) \cdot \cos\left(\boldsymbol{\varphi}_{i(S)} - \boldsymbol{\varphi}_{(T)}\right); \tag{3}$$

where the spatial arrays (maps) of azimuth angles (radians) are given by the general form $\boldsymbol{\varphi} = \left[\varphi_j\right]_n$. $\boldsymbol{\varphi}_{i(S)}$ is the solar azimuth angle at time *i*, while $\boldsymbol{\varphi}_{(T)}$ is the terrain azimuth angle (for practical purposes, not dependent upon time). $\boldsymbol{\varphi}_{(T)}$ is normally just referred to as

'aspect' in terrain analysis. After re-arrangement and transformation, Eq. (2) can be expressed in the general form of the linear regression, $y = a + b \cdot x$, by (Lu et al., 2008):

$$\log\left(\boldsymbol{\rho}_{iw(T)} \cdot \cos\left(\boldsymbol{\theta}_{(T)}\right)\right) = \log\left(\boldsymbol{\rho}_{iw(H)}\right) + k_{iw} \cdot \log\left(\cos\left(\boldsymbol{\theta}_{(T)}\right) \cdot \cos\left(\boldsymbol{\theta}_{i(I)}\right)\right). \quad (4)$$

The scalar value k_{iw} was estimated for each of the 46 climatological 8-day time periods, *i*, and each waveband, *w*, by minimisation of the ordinary least squares (OLS) of Eq. (4).

Lu et al. (2008) that the k_{iw} parameter changes as a function of terrain slope, but that the response asymptotes for slopes greater than 15 degrees. We tested this at our NSW site, and found the same result, so we defined k_{iw} based on Eq. (4) using only the portion of the study site having a terrain slope greater than 15 degrees. These estimates of k_{iw} were then used in Eq. (2) to topographically correct the Landsat and MODIS reflectances. For the MODIS data, the STOD of solar noon on that 4th day of the 8-day composite was used to calculate solar zenith and azimuth angles (as MCD43A4 data are modelled to represent solar noon of the 8-day period). For Landsat data the average of all STOD's of acquisition was used to calculate solar angles. If the empirical topographic correction method described above were calculated for every individual 8-day period, it could normalise the data, thus reducing its usefulness for time series analysis. To help reduce this deleterious effect, we calculated *k* from the climatological 8-day temporal average reflectances per band (i.e., the temporal average reflectance map for the first 8 days of the year, then of the second 8 days of the year, and so on until reaching the 46th 8-day period). The MODIS data resulted in smooth functions of *k* values. For SA, the original climatologies of *k* values were used. For NSW, there were a few slight anomalies present in the two visible bands in the second and third compositing periods. To avoid artefacts due to these anomalies, the NSW MODIS 8-day composite climatological *k* values were smoothed using a box-car smoothing algorithm using a window size of 2 composite periods either side of centre (5 8-day composite periods used in the full window). For both sites, the original 8-day climatological *k* values for Landsat were noisy due to the added influence of solar azimuth angle, Landsat's lower temporal density, and the increased sensitivity to terrain influences because of its higher spatial resolution. So, the Landsat *k* values were also box-car smoothed using the same window size. The topographic correction was then implemented by using the band and site specific *k* value for each individual epoch based on which 8-day period it fell within, using the original 8-day *k* value climatology for MODIS data at SA and the smoothed *k* value climatologies for MODIS at NSW and Landsat at both sites. Using the 8-day *k* climatologies prevented the parameter from containing trend, thus making the resultant terrain-corrected data suitable for time-series analysis. For example, if there was a vegetative greening trend at one of our study sites over the 11 years, and if the *k* parameter was estimated for each epoch individually, then the output model might be de-trended and the trend might reside in the time series of parameter values instead. On the other hand, since we use the climatological parameter value for each of the possible 46 8-day periods through the year, then the output model would retain trend due to land cover change. In this way k_{iw} was calculated for each of the 4 bands required to calculate EVI and GVMI (explained below) for both Landsat and the MODIS data at both sites. The influence of topographic correction on the AET algorithm was first qualitatively checked on observed Landsat imagery to assess how the illumination influence compared to major land cover change, namely a major fire event in 2003 at the NSW site. Modelled AET within the 2003 fire from the blended data without topographic correction and with topographic correction were also summarised over the entire fire boundary as defined from the NSWFC fire boundary data.

2.4 Actual evapotranspiration (AET) model

The model of actual evapotranspiration used was from Guerschman et al. (2009). It uses a vegetation greenness index and a vegetation moisture index from reflective remote sensing data to scale both potential evapotranspiration (PET) and precipitation (P) data. The remote sensing based indices require two wavebands in the VIS (blue and red), a NIR band, and a SWIR band, which are observed on both Landsat and MODIS platforms, Table 11). The bolded variables below represent the spatio-temporal array (time series of maps). To facilitate communication, the temporal and spatial indexes, *i* and *j*, respectively, are left off of the following equations.

Table 11. Landsat and MODIS spatial resolution, temporal density, spectral density and spectral resolution are shown.

Domain	**Satellite/sensor**	
	Landsat 5/TM	Terra/MODIS
Spatial resolution	25 m	250 m/ 500 m /1000 m
Temporal density	16 days	1 day
Spectral density	6 bands across a 1897 nm range including VIS, NIR, and SWIR	19 bands across a 1750 nm range including VIS, NIR, and SWIR
Spectral resolution	ρ_{blue} : 452–518 nm	ρ_{blue} : 459–479 nm
	ρ_{red} : 626–693 nm	ρ_{red} : 620–670 nm
	ρ_{NIR} : 776–904 nm	ρ_{NIR} : 841–876 nm
	ρ_{SWIR} : 1567–1784 nm	ρ_{SWIR} : 1628–1652 nm

The spatio-temporal array of enhanced vegetation index (EVI) was calculated for both Landsat and MODIS as (Huete et al., 2002):

$$\mathbf{EVI} = G \cdot \frac{\boldsymbol{\rho}_{NIR} - \boldsymbol{\rho}_{red}}{\boldsymbol{\rho}_{NIR} + C_1 \cdot \boldsymbol{\rho}_{red} - C_2 \cdot \boldsymbol{\rho}_{blue} + L}, \quad (5)$$

where $G = 2.5$, $C_1 = 6$, $C_2 = 7.5$, and $L = 1$, which are parameters accounting for aerosol scattering and absorption, and the spatio-temporal arrays of reflectance are those described in Table 11 for Landsat or MODIS. The spatio-temporal global vegetation moisture index (GVMI) was calculated by (Ceccato et al., 2002a; Ceccato et al., 2002b) as:

$$\mathbf{GVMI} = \frac{\left(\boldsymbol{\rho}_{NIR} + 0.1\right) - \left(\boldsymbol{\rho}_{SWIR} + 0.02\right)}{\left(\boldsymbol{\rho}_{NIR} + 0.1\right) + \left(\boldsymbol{\rho}_{SWIR} + 0.02\right)}. \quad (6)$$

The spatio-temporal array of AET was then calculated by partitioning the total evaporation into components as a function of PET and P (Guerschman et al., 2009) by:

$$\mathbf{AET} = \boldsymbol{\kappa}_C \cdot \mathbf{PET} + \boldsymbol{\kappa}_E \cdot \mathbf{P}, \quad (7)$$

where $\mathbf{AET}$ (mm) is the spatio-temporal array of modelled actual evapotranspiration (mm), $\mathbf{PET}$ (mm) is the spatio-temporal array of monthly Priestly-Taylor potential ET, and $\mathbf{P}$ (mm) is the spatio-temporal array of monthly precipitation. $\mathbf{P}$ was from the Bureau of Meteorology (BoM) as described in (Jones et al., 2009) and the Priestley-Taylor $\mathbf{PET}$ dataset was from (Donohue et al., 2010). These datasets were reprojected, bilinearly resampled from 5000 m to

25 m, and clipped to the study site extent using GDAL. $\boldsymbol{\kappa}_C$ and $\boldsymbol{\kappa}_E$ are the evaporative fraction of PET (called a 'crop' coefficient in Guerschman et al., 2009) and a term to represent interception of P, respectively. The term accounting for interception of P is given by (Guerschman et al., 2009):

$$\boldsymbol{\kappa}_E = \kappa_{E\_\max} \cdot \mathbf{EVI}_r , \tag{8}$$

where the scalar parameter $\kappa_{E\_\max} = 0.229$, and the spatio-temporal array of 're-scaled' EVI is (Guerschman et al., 2009):

$$\mathbf{EVI}_r = \frac{\mathbf{EVI} - EVI_{\min}}{EVI_{\max} - EVI_{\min}} , \tag{9}$$

where $EVI_{\min} = 0$ and $EVI_{\max} = 0.90$. The spatio-temporal array of evaporative fraction of PET was calculated by (Guerschman et al., 2009):

$$\boldsymbol{\kappa}_C = \kappa_{C\_\max} \cdot \left(1 - e^{-a \cdot \mathbf{EVI}_r^{\alpha} - b \cdot \mathbf{RMI}^{\beta}}\right). \tag{10}$$

The scalar parameters $\kappa_{C\_\max} = 0.680$, $a = 14.12$, $\alpha = 2.482$, $b = 7.991$, $\beta = 0.890$, and the spatio-temporal array of the residual moisture index (RMI) is (Guerschman et al., 2009):

$$\mathbf{RMI} = \left[\max\left(0, K_{RMI} \cdot EVI_{ij} + C_{RMI}\right) \right]_{m \times n} , \tag{11}$$

where $K_{RMI} = 0.775$, and $C_{RMI} = -0.076$. Note, in Eq. (11), the bracketed notation for a spatio-temporal array was used as it was more communicative. In this case, the temporal index of i=0,m and the spatial index of j=0,n is used.

Because the physical meaning of the parameters of the model, and the repercussions of any subsequent adjustment to them may not be clear to a user, a simple linear bias correction was later included (Van Dijk et al., 2015), yielding:

$$\mathbf{AET} = a_0 \left(\boldsymbol{\kappa}_C \cdot \mathbf{PET} + \boldsymbol{\kappa}_E \cdot \mathbf{P}\right) + a_1 . \tag{12}$$

The original bias correction parameters were defined using flux tower, water drainage division, and satellite gravity data (Rodell et al., 2009; Tapley et al., 2004a; Tapley et al., 2004b) using MODIS-only data as input. From that analysis, the MODIS-only bias correction parameters were defined as $a_0 = 0.853$ and $a_1 = 0.293$. As the blending work performed here also uses Landsat data and is performed only over two specific regions, we will determine whether these original bias correction parameters are ideal for our study, or whether regionally optimal parameters exist. Eq. (7) and (12) were used to estimate actual evapotranspiration after the Landsat and MODIS EVI and GVMI indices were blended, as described next.

2.5 Blending algorithm

The Enhanced Spatial and Temporal Adaptive Reflectance Fusion Model (ESTARFM, Zhu et al., 2010) was used. The detailed workflow for blending is given in Van Niel et al. (2016), including specifics for parallel processing on the National Computing Infrastructure (NCI). The authors of ESTARFM provided us with the IDL code to run the algorithm. We translated

the code to the open-source version of IDL called the GNU Data Language (GDL), and tested the code to ensure the same results were obtained for the IDL and GDL versions. Transferring the code to GDL allowed for running the blending on a supercomputer on the NCI. A general pictorial overview of the ESTARFM algorithm is provided in Figure 19 below. Five input images, two Landsat-MODIS (LM) pairs at time t_1 and time t_2 and a single MODIS image at time t_s (time of simulation) are required. The result of each blending instance is a single simulated image at time t_s that has the spatial resolution of Landsat, depicted by the yellow highlighted image in Figure 19. Jarihani et al. (2014) found that calculating the indices first, then blending was, overall, a better approach than blending first, then calculating the indices due to error propagation. Because of that recommendation, our blending was run on the two indices, EVI and GVMI. The added benefit was that only half as many operations were required compared to blending the four reflectance bands needed to generate the indices, so it was also computationally more efficient.

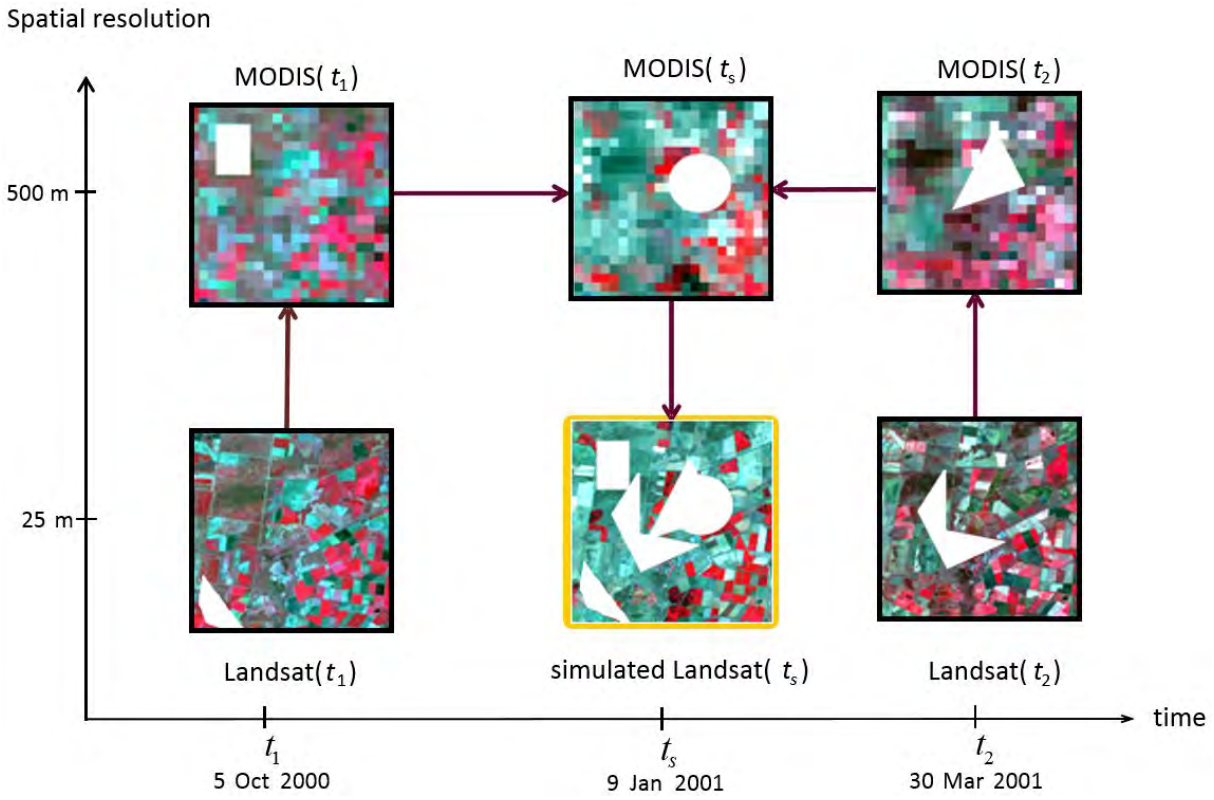

Figure 19. Influence of null data propagation from any of the input images to the output image. If cloud, cloud shadow or null data due to any other reason is present in any of the input images then the simulated image contains null data in those locations. In the above image 'cloud' is represented by white areas of different shapes in the input images which are combined in the simulated image.

To overcome persistent data gaps, three individual blending instances were performed. In all cases, all MODIS data were used. In the first case, all Landsat data were used, despite the amount of cloud (colloquially called 'bronze', herein). For this first case, the simulated data could have very large areas of missing values due to cloud masking, but the temporal proximity of the LM pairs would be as close as possible to the simulation date. In the second case, only Landsat images having 80% of their area being cloud-free ('silver') were used; the Landsat images input to the 'silver' processing had longer gaps than those used as input for the 'bronze' series. In the third case, only Landsat images having 98% of their area being cloud-free ('gold') were used; the Landsat images input to the 'gold' processing had longer

gaps than those used in the 'silver' processing. The second (i.e., 'silver') and especially the third (i.e., 'gold') case would have very low missing data, but may not be using LM pairs that were temporally proximate to the simulation date. This longer gaps between input Landsat imagery may impact the ability of the blending algorithms to accurately simulate the Landsat-like imagery (Fu et al., 2015); though the level of impact depends on magnitude of spatial and temporal variance captured in the input imagery (Emelyanova et al., 2013; Jarihani et al., 2014).

2.6 Index compositing

The result of the blending process was three high spatial resolution, 8-day composite EVI and GVMI index data cubes. A fourth low spatial resolution, 8-day composite EVI and GVMI index data cube was also available from the input MODIS dataset. Due to the blending procedure, clouds in either the fine or coarse spatial resolution dataset persist for all simulated images in between LM pairs. To help overcome this, we combined the three blending outputs, described above, and the input MODIS indices in a hierarchical fashion (see Figure 20). The data using the most temporally proximal LM pairs (*i.e.*, 'bronze') were given priority. Any gaps from that dataset were filled with data determined using LM pairs from the 80% cloud-free 'silver' dataset. Any data gaps still remaining were filled with the 98% cloud-free 'gold' dataset. Finally, any gaps that still remained were filled by the input MODIS indices. A spatio-temporal dataset keeping track of the origin of each pixel was kept for the composited 8-day dataset. These 8-day composited EVI and GVMI datasets were converted to estimates of AET using Eq. (12). The hierarchical compositing scheme attempts to model AET with Landsat data most temporally proximate to the simulation date, while minimising the amount of data gaps due to clouds.

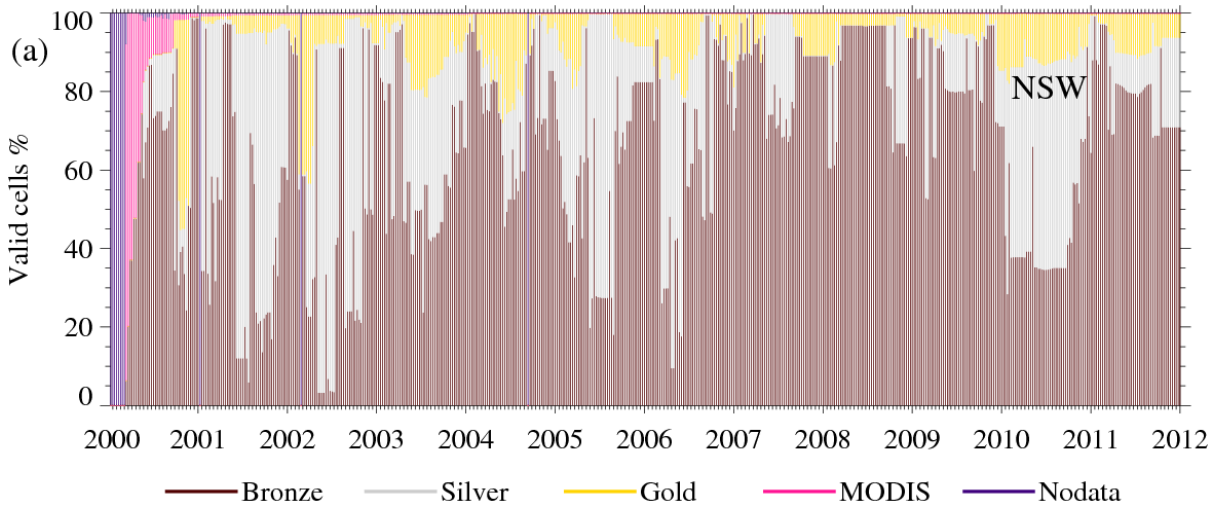

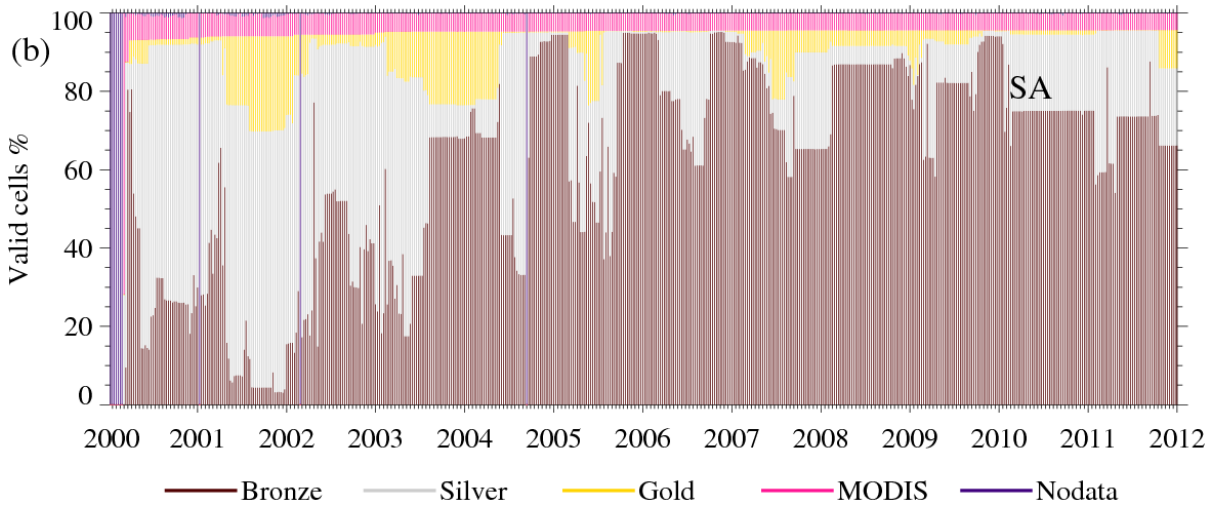

Figure 20. Percent valid cells by hierarchical type is shown for (a) NSW site and (b) SA site.

2.7 Validation and evaluation

The accuracy of the blended AET data were estimated from the three validation datasets described above by: (*i*) assessing closure of the catchment (reach) water balance in catchments (reaches) where precipitation and stream flow were well measured; (*ii*) comparison against independent 'point' observations of actual evaporation at an eddy covariance flux tower; and (*iii*) comparison against independent plot observations of site water use from sap-flow and site water balance measurements of plantation tree water use.

For the catchment water balance assessment, long-term stream flow values were calculated from stream flow gauge data, long-term precipitation was calculated from averaging the spatio-temporal precipitation data with the catchment contributing areas, and both were adjusted for catchment nesting if relevant (Table 5 and Table 7). The reach mass balance was determined by subtracting the sum of all upstream gauge streamflow from the downstream (outlet) gauge's streamflow, see Table 6. The reach precipitation was determined from the reach contributing areas, see Figure 17. These data allowed for a steady state estimate of AET being precipitation less stream flow for catchments and reaches. The steady state P-Q approach assumes the difference in storages (i.e., soil stores, groundwater and farm dams) is negligible from the start of the time series when compared to the end of the time series. This assumption adds uncertainty to the analysis, especially considering the period of record contains the millennium drought. The modelled AET was averaged over the same time and spatial extents, so a direct comparison could be made between the catchment and reach precipitation less stream flow.

The sub-daily Tumbarumba flux tower latent heat flux observations were integrated to average 8-day actual evapotranspiration. The AET model for these same 8-day periods were averaged over a 20 pixel window either side of the central flux tower location (41 by 41 pixels in total [~1 km by 1 km] for each 8-day period). The window around the flux tower was used to account for the expected 'footprint' of the flux tower instrumentation. Observations measured at a flux tower represent the latent heat flux from some variable surface area around the instrumentation, the size and location of which depends upon atmospheric conditions like wind speed and direction.

In our study, we used the site water balance estimates described above (Almeida & Sands, 2016; Benyon & Doody, 2015; Benyon et al., 2006). The site water balance data were

collected, roughly, on a fortnightly basis, but not systematically so. These site water balance estimates and the modelled AET data were aggregated to monthly values, so they could be compared (Table 9). The modelled AET data were assessed at each pixel representing the location of the site water balance plot centres. As the plots were on the order of a pixel in size, no spatial averaging was performed (compared to the 41 by 41 spatial averaging at the flux tower).

In addition to the LM blended AET dataset, three additional AET datasets were also assessed over the three validation datasets in order to perform a comparison with the blended product' accuracy: (*i*) the AET model run on the MODIS-only 8-day data; (*ii*) the AET model run on the Landsat-only data calculated for the isolated days that cloud-free Landsat data were available; and (*iii*) 'total evaporation' from the water balance model used by the BoM to perform their water resource assessments, the Australian Water Resource Assessment model (AWRA-L version 4.5, simply denoted AWRA herein). The daily AWRA data were averaged over the MODIS 8-day dates in order to match the other datasets.

The bias correction defined in Van Dijk et al. (2015) was performed when using MODIS-only data and done across all of Australia, resulting in $a_0 = 0.853$ and $a_1 = 0.293$, see Eq. (12). Since the overall objective of this project was to deliver an AET product that had both high spatial resolution and temporal density with no accuracy loss compared to the original MODIS-only product, we inspected the impact of defining a regional bias correction for the LM blended product. The accuracy of the Landsat-MODIS blended AET product was independently assessed using no bias correction ($a_0 = 1.0$ and $a_1 = 0.0$) and the original bias correction terms defined from MODIS-only ($a_0 = 0.853$ and $a_1 = 0.293$). We then defined an array of the three AET validation datasets of catchment and reach water balance, flux tower, and site water use data, described above, and an associated array of the no bias corrected version of the AET model for the same locations and times as the validation datasets were summarised over. From these two arrays, we determined the optimal a_0 and a_1 parameters required to minimise the RMSE of the three separate validation sets, without exceeding the RMSE value returned by the MODIS-only results for any of them. To do this optimisation, we used the Shuffled Complex Evolution (SCE) optimisation algorithm (Duan et al., 1994). The results of this regional optimisation is simply referred to as the 'regional' bias correction, herein. This allowed for three different versions of the LM blended AET model to be assessed against the validation data: (*i*) no bias correction; (*ii*) original bias correction; and (*iii*) regional bias correction. Both the 'no bias correction' and 'original bias correction' cases are commonly produced since the inception of the AET model. Comparing the validation of the no bias corrected version to that of the original and regional bias corrected versions also quantifies the sensitivity of the model to the bias correction step.

The vegetation plot data were assessed by comparing the total volumetric AET (kL) of all 8-day periods between the first and last field measurement dates (30/09/2009–03/08/2011) to the change in plot timber volume (m^3/ha) for that same time period from the field data. The ratio of these two values (AET/ΔV) (kL/(m^3/ha)) was then calculated as a metric of how much water over the plot was used to increase average timber volume by 1 m^3/ha across the plots . AET and ΔV were calculated for each plot and the overall average of all plots was determined. To estimate an 800 m^2 circular area from 25 m square cell AET data, we performed an inverse distance weighting of the centre pixel and its 8 neighbouring pixels around each plot. To account for loss of trees due to thinning, the total timber volume at each plot was calculated at the first and last field measurement times.

The 2003 fire over the NSW study site, started around 18 January, 2003 and progressed for about a month afterwards. To capture the dynamics of the fire, we calculated the z-score of each 8-day period in 2003 compared to the climatological average and standard deviation of each 8-day period over the 12 years:

$$\mathbf{z}_j = \frac{\mathbf{AET}_j - \boldsymbol{\mu}}{\boldsymbol{\sigma}}, \tag{13}$$

where $\mathbf{z}_j$ is the z-score of AET for time interval j, $\boldsymbol{\mu}$ is the climatological average AET for the associated 8-day period, and $\boldsymbol{\sigma}$ is the climatological standard deviation of AET for the associated 8-day period. The minimum z-score for the year 2003 was then recorded in a pixel-wise manner to identify the fire as the very low minimum z-scores.

2.8 Land-use-specific AET assessment

The 9 land-use classes were summarised using standard GIS techniques over the AET model outputs. These summaries were converted to different units to express AET in both relative and absolute terms. Since the following equations represent unit conversions, they don't necessitate different symbology. Rather the units are provided directly within the equations for clarity. The evaporation algorithm outputs the estimate of AET in units of mm/d. These units are useful for assessing the relative amounts of evaporation at any specific location and time-step, or for summarising evaporation rates of the various land-use classes. The land-use classes cover different proportions of the entire study areas, so it is also useful to convert the rates of AET values to volumes of AET to also understand the overall amounts of AET by land-use class. This was done by first converting the average AET rates for each land-use class, *i*, to daily volumes by:

$$\mathbf{AET}_i(m^3/d) = \frac{\mathbf{AET}_i(mm/d)}{1000(mm/m)} \cdot A_i(prop) \cdot A_T\left(m^2\right), \tag{14}$$

where $\mathbf{AET}_i$ is the estimated evaporation of land-use class, *i*, in some specified unit, A_i is the proportion of area of land-use class, *i*, and A_T is the total area of the study site in square metres. Since 1 m^3 of liquid water equals 1000 L (1 kL), then $\mathbf{AET}_i$ can be expressed in the following equivalent units:

$$\mathbf{AET}_i(m^3/d) = \mathbf{AET}_i(kL/d). \tag{15}$$

Considering Eq. (14) and (15), $\mathbf{AET}_i$ can be expressed in units of GL/d by simply dividing the volume of $\mathbf{AET}_i$ by one million:

$$\mathbf{AET}_i(GL/d) = \frac{\mathbf{AET}_i(kL/d)}{10^6(kL/GL)}. \tag{16}$$

We also defined a second relative measure of AET, based on volume, which provides a different insight into how the water use of the classes compare. First the proportion of the total study site volume of AET for each land-use class was determined:

$$\mathbf{AET}_i(prop) = \frac{\mathbf{AET}_i(GL/d)}{\mathbf{AET}_T(GL/d)}, \tag{17}$$

where $\mathbf{AET}_T$ is simply the total volume of evaporation over the entire study site, calculated as the sum of all 9 land-use class AET volumes:

$$\mathbf{AET}_T(GL/d) = \sum_{i=1}^{9} \mathbf{AET}_i(GL/d) \,. \tag{18}$$

This allowed for a meaningful relative metric of AET, being the proportion of AET of the land-use class per proportion of the area of that land-use class:

$$\frac{\mathbf{AET}_i(prop)}{A_i(prop)} \,. \tag{19}$$

Eq. (19) removes the area weighting that is intrinsic in the volume calculation, so that values above unity indicate above average water use relative to the whole study site, and volumes below unity indicate less than average water use relative to the whole study site. Eq. (19) simply provides another relative metric of the water use, but one that is normalised so that it is unitless and useful for making land-use class comparisons. Eq. (19) only considers the proportion of AET compared to the proportion of area. However, P and PET, the main covariates of evaporation that describe the nature of how much a site is either water-limited or energy-limited, vary over space and time. So, the analogous versions of Eq. (16) were also run on the precipitation and potential evapotranspiration datasets and summaries of the evaporative fractions of AET/P and AET/PET were also calculated. The ratio of AET/P provides critical hydrological context.

Summarising the land-use class AET in relative rates of mm/d does not consider that the land-uses may be biased based on how their spatial distribution coincides with environmental conditions like P or PET, for example. The summarised relative AET result could be mis-leading due to these environmental covariances. To attempt to account for such influences, we performed a paired analysis of selected land-use classes. Since the Softwood Plantation land-use class was the largest plantation class at both sites, we compared it to both the Native Vegetation and Grazing Modified Pasture land-use classes (the top two land-use classes by area at both study sites). We defined 20 paired points between Softwood and Native Vegetation and 20 paired points between Softwood and Grazing Modified Pasture at both sites (80 paired points in total, see Table 12 and Table 13). The overall average AET of a 1.5625 ha rectangle around each point (5-by-5 25m pixel window) was calculated. Points were located *ad hoc* using the land-use map, ensuring that each point was more than 2.5 pixels away from a land-use class boundary, that the full rectangle was within the land-use class, and that each point was, on average, less than 2 km away from its corresponding pair. The analysis should account for covariates such as P and PET, but would not account for management (*e.g.*, thinning) or natural disturbance (*e.g.*, fire). We performed a *t-test* to assess whether the Softwood Plantation mean AET's were significantly different to that of Natural Vegetation or Grazing Modified Pasture, and an *F-test* to assess whether the AET variances were significantly different. The results of the statistical tests were probabilities defining where the specified test becomes significant. Interpretation of results is: low probabilities (*e.g.*, < 0.01) would be more likely to demonstrate a significant difference than higher probabilities (*e.g.*, > 0.01).

Table 12. The locations of the points in the paired analyses at the NSW study site are provided in Map Grid of Australia 1994 (MGA94) zone 55 coordinates. See Figure 16a for the graphic representation of these points.

	Softwood *vs*. Native Vegetation				Softwood *vs*. Grazing Modified Pasture			
	Softwood		Native Veg.		Softwood		Graz. Mod. Past.	
No.	X	Y	X	Y	X	Y	X	Y
1	532737	6028517	534044	6028493	532127	6031743	532476	6032767
2	532785	6031397	533463	6032075	553778	6039976	553865	6040869
3	550646	6028808	549654	6028929	554475	6043243	555041	6042851
4	552437	6030841	552558	6031639	561467	6046075	561401	6045313
5	558003	6032390	557955	6031760	564320	6045639	564342	6044942
6	557761	6034205	557083	6034665	566477	6044834	566259	6044224
7	555922	6036964	555196	6037230	568981	6049212	568459	6048928
8	557906	6037206	558584	6037617	572314	6050039	573054	6050039
9	566304	6038319	565917	6037496	577193	6055506	577062	6054657
10	568289	6039190	567321	6039553	581201	6055506	581135	6054635
11	555535	6054655	555656	6055575	581179	6064175	581201	6064829
12	575307	6059883	575065	6059011	590240	6065961	589587	6066049
13	579470	6062206	578695	6061940	589064	6068902	588389	6068924
14	590046	6077477	589296	6077453	590022	6070405	589565	6070928
15	627437	6094079	627026	6093329	589979	6074848	589260	6074870
16	631527	6089965	630753	6090110	588977	6076133	588236	6076199
17	641837	6092845	642539	6092821	588694	6080206	587953	6080228
18	646339	6094345	645613	6094370	590436	6083082	590131	6083626
19	647379	6099888	648105	6099888	597733	6081034	597776	6081731
20	644983	6105914	645782	6105938	628989	6087721	628488	6087982

Table 13. The locations of the points in the paired analyses at the SA study site are provided in Map Grid of Australia 1994 (MGA94) zone 54 coordinates. See Figure 16b for the graphic representation of these points.

	Softwood *vs*. Native Vegetation				Softwood *vs*. Grazing Modified Pasture			
	Softwood		Native Veg.		Softwood		Graz. Mod. Past.	
No.	X	Y	X	Y	X	Y	X	Y
1	496238	5800324	498995	5800123	450318	5804214	451634	5803221
2	496238	5801756	498961	5801566	451485	5807342	450045	5806225
3	493630	5803078	498928	5803043	449276	5807441	447265	5807168
4	495834	5804731	498961	5804487	450368	5809551	448755	5810023
5	494732	5806494	498995	5806131	451684	5810594	450542	5811835
6	495834	5808111	499163	5807776	455829	5822707	454315	5822558
7	495687	5809690	499264	5809387	455084	5825884	453868	5827076
8	495540	5811196	499465	5810931	457939	5832686	459552	5831916
9	494916	5812592	499398	5812476	478145	5835143	480354	5835292
10	494989	5814171	499196	5813986	478740	5838593	475811	5838817
11	495981	5816081	499317	5815890	478566	5841225	476606	5842689
12	493814	5860855	499029	5860643	481446	5846909	478517	5847182
13	494585	5862802	498984	5862331	485318	5851253	483457	5852271
14	495944	5864528	498946	5864329	492467	5859668	489737	5859097
15	496385	5870773	498754	5869286	493783	5860884	490109	5861480
16	495504	5872536	498638	5871783	494577	5862820	491201	5863987
17	502262	5872095	504863	5871860	495942	5864558	491797	5866568
18	507478	5875841	505516	5876471	495495	5872551	491325	5873891
19	507735	5877311	505631	5877815	502247	5872129	498772	5874114
20	512767	5882196	516120	5881734	495322	5877044	497109	5878285

3 Results

3.1 Long-term average AET and proportions relative to key climate variables

The output of the model is provided in the form of long-term temporal average AET (Figure 21a-b), AET/P (Figure 21c-d), and AET/PET (Figure 21e-f) for the NSW site for both the LM blended dataset and the MODIS-only dataset, respectively. Figure 21c-d reveal that most of the site, over the long-term, evaporates less water than precipitation. Only 6.9% of the NSW site had AET > P, mainly along the Murrumbidgee and other river courses, water bodies, and a few forested areas (Figure 21c). Of note, few of the forestry plantation areas at the NSW site had modelled AET > P (13.9% of this AET > P area were forestry plantation classes). For an exception, see the rectangle in Figure 21c, where mostly softwood plantations had AET > P. The AET, AET/P, and AET/PET of this rectangular area is shown in Figure 22 and highlights the improved spatial characteristics of the LM blend when compared to the MODIS-only results. Results of a more complete summarisation of the land-uses with respect to AET/P is provided further below.

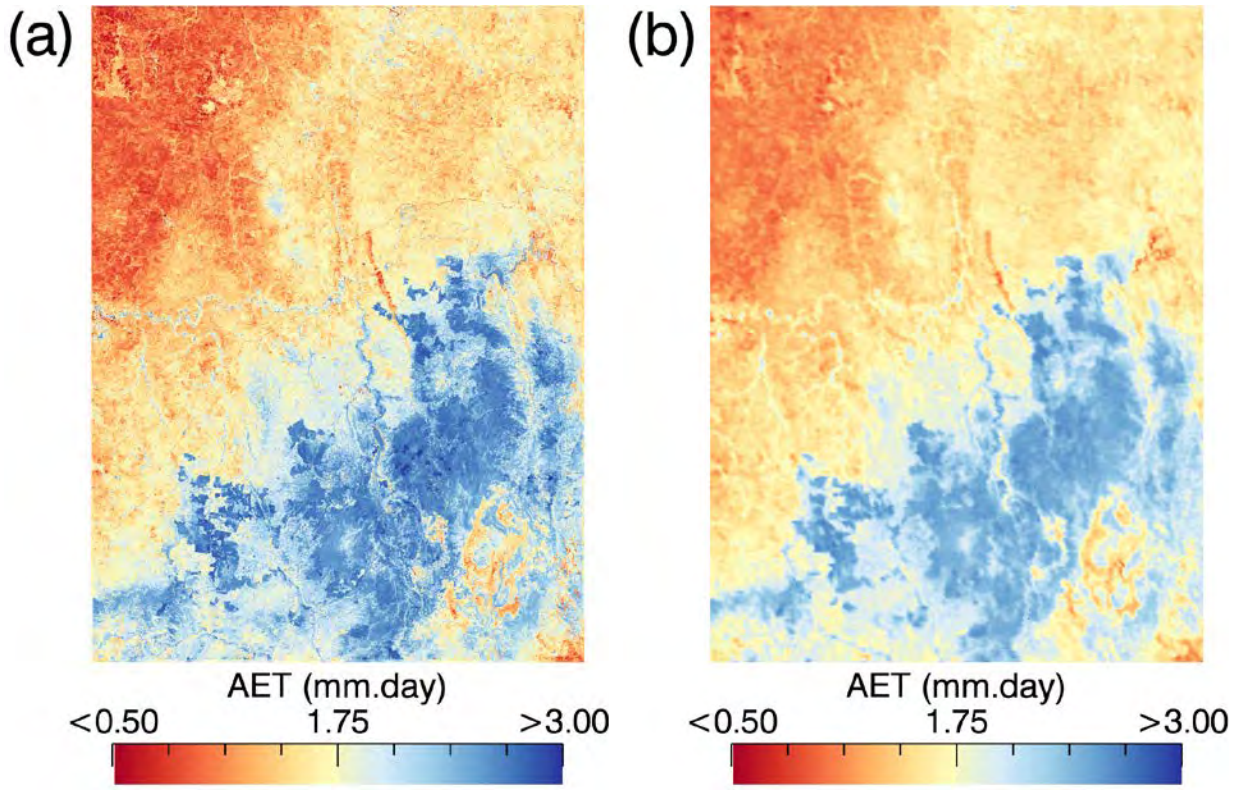

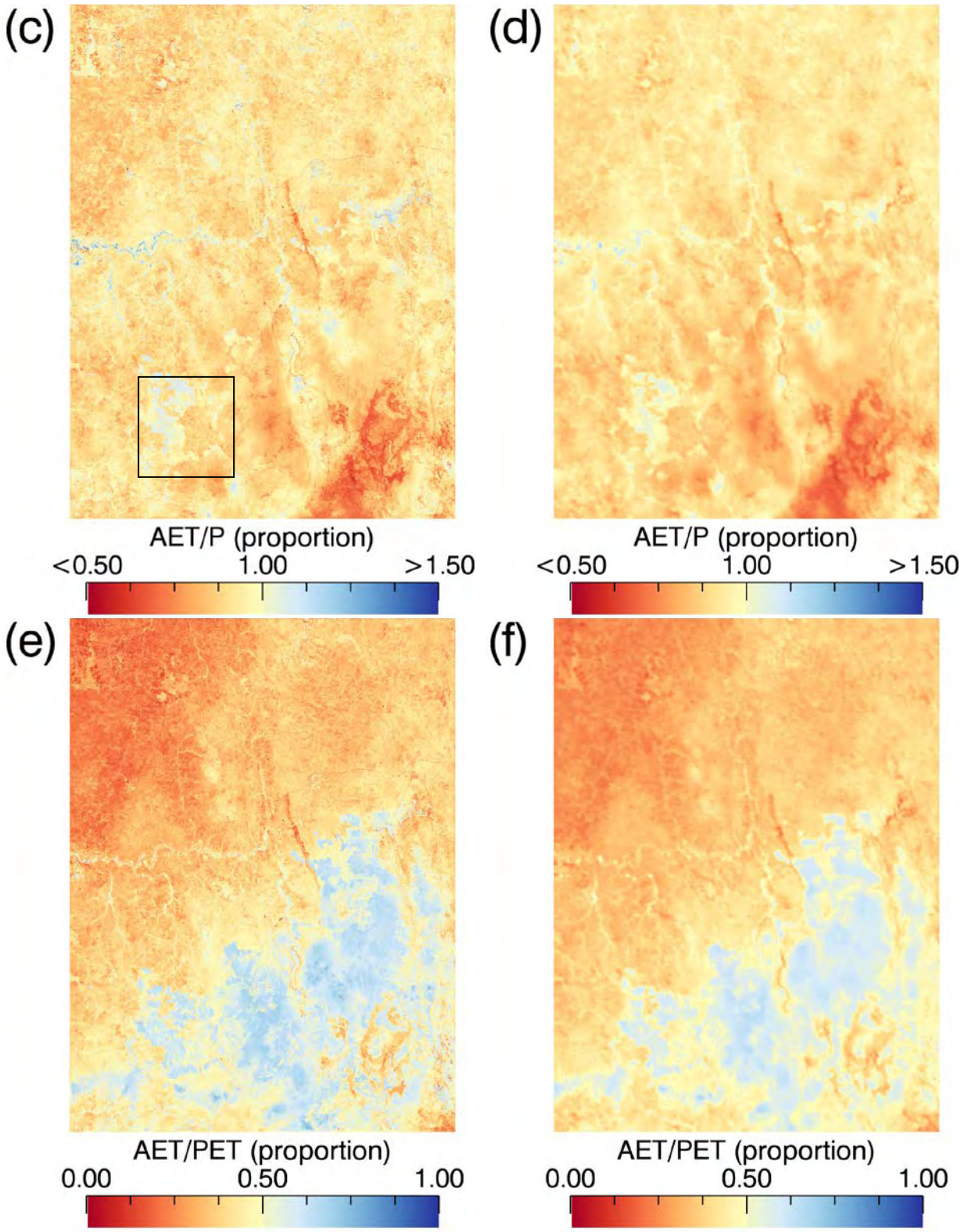

Figure 21. Long-term average (i.e., 1 Jan 2000 to 31 Dec 2011) AET and its proportions relative to key climatic controls for the NSW site at both the Landsat and MODIS resolutions. The Landsat resolution data are the output of the Landsat-MODIS blending to infill all gaps in the observed Landsat time series. Parts (a) and (b) show the AET grids at the Landsat and MODIS resolutions, respectively. Parts (c) and (d) show the AET/P proportions, and (e) and (f) are the AET/PET proportions; both at the Landsat and MODIS resolutions, respectively. The results for the black square in (c) are provided at full resolution in Figure 22.

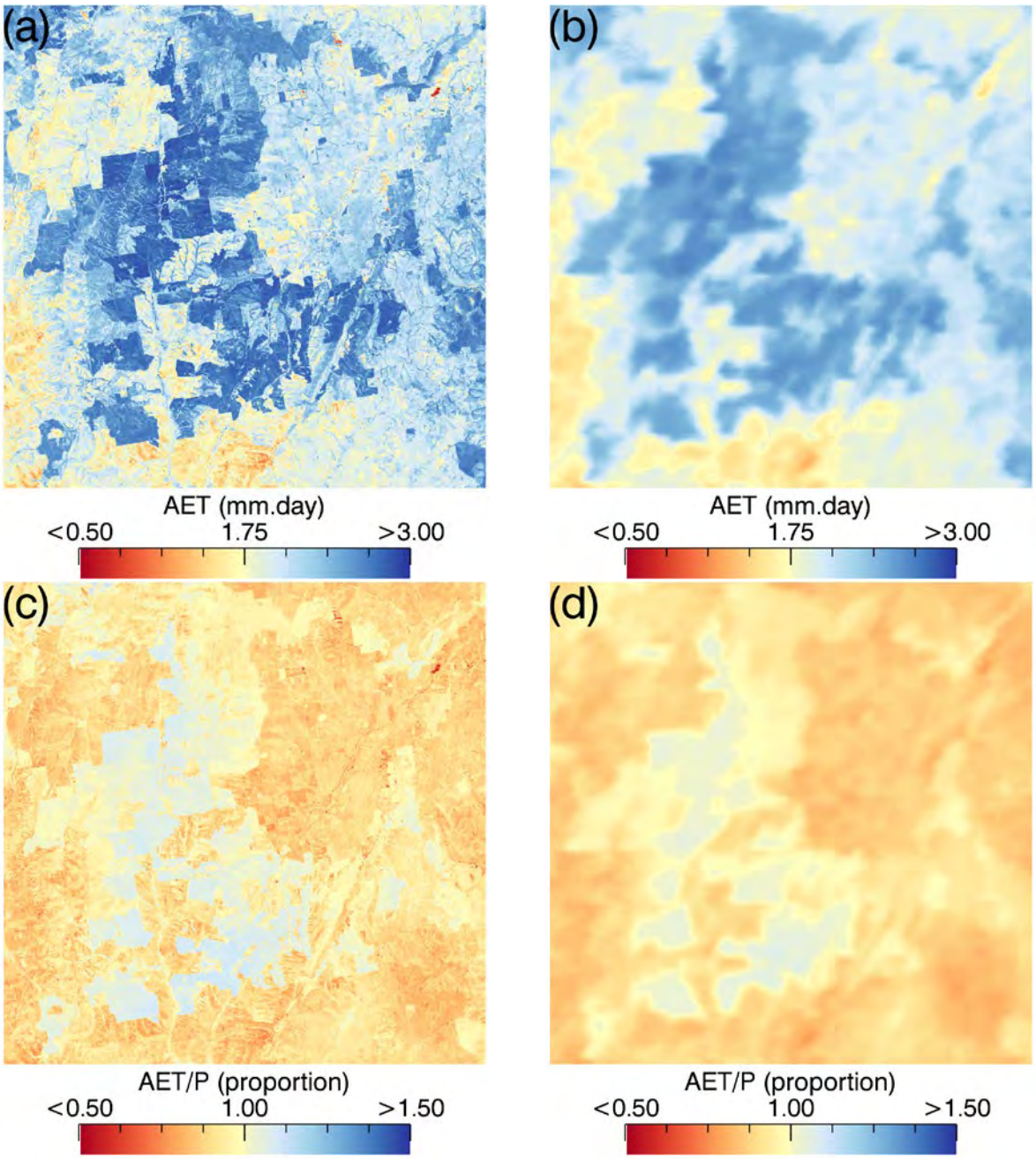
(a)
(b)
AET (mm.day)
<0.50
1.75
>3.00
AET (mm.day)
<0.50
1.75
>3.00
(c)
(d)
AET/P (proportion)
<0.50
1.00
>1.50
AET/P (proportion)
<0.50
1.00
>1.50

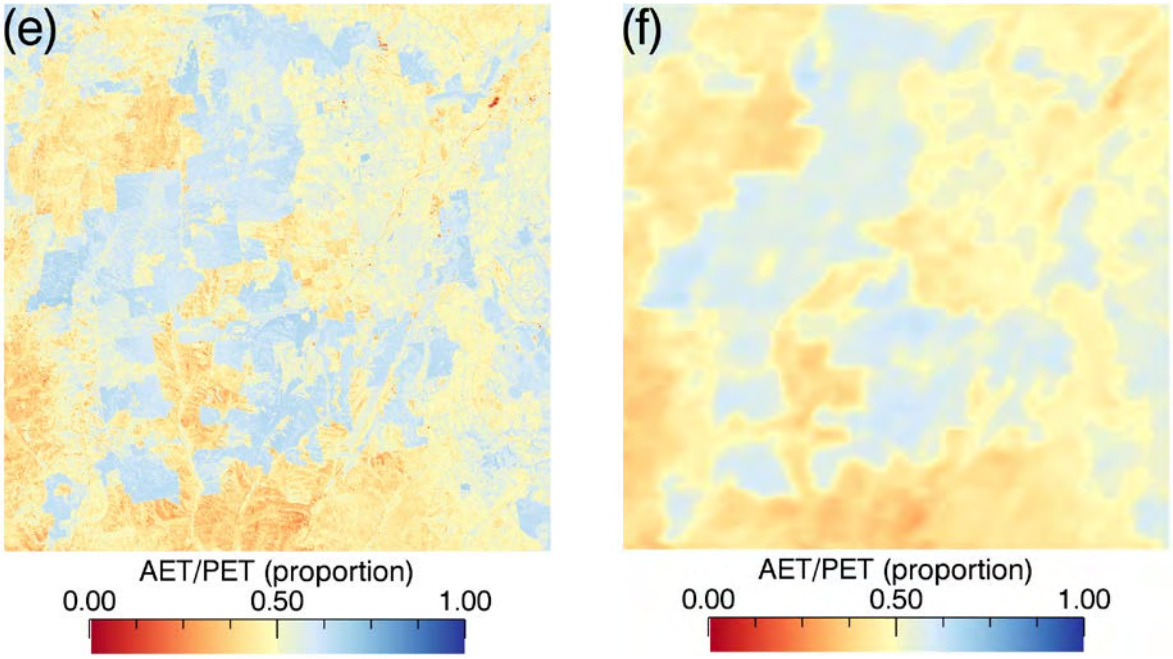

Figure 22. Long-term average (i.e., 1 Jan 2000 to 31 Dec 2011) AET and its proportions relative to key climatic controls for part of the NSW site (see Figure 21(c)) at both the Landsat and MODIS resolutions. The Landsat resolution data are the output of the Landsat-MODIS blending to infill all gaps in the observed Landsat time series. Parts (a) and (b) show the AET grids at the Landsat and MODIS resolutions, respectively. Parts (c) and (d) show the AET/P proportions, and (e) and (f) are the AET/PET proportions; both at the Landsat and MODIS resolutions, respectively.

Long-term temporal average AET (Figure 23a-b), AET/P (Figure 23c-d), and AET/PET (Figure 23e-f) for the SA site for both the LM blended dataset and the MODIS-only dataset were summarised. For SA, there was 37% of the site where AET > P, and this was more strongly associated with the forestry plantations than at the NSW site (24.4% of the AET > P area were forestry plantation classes). These land-use associations will be explored further in the land-use assessment, below.

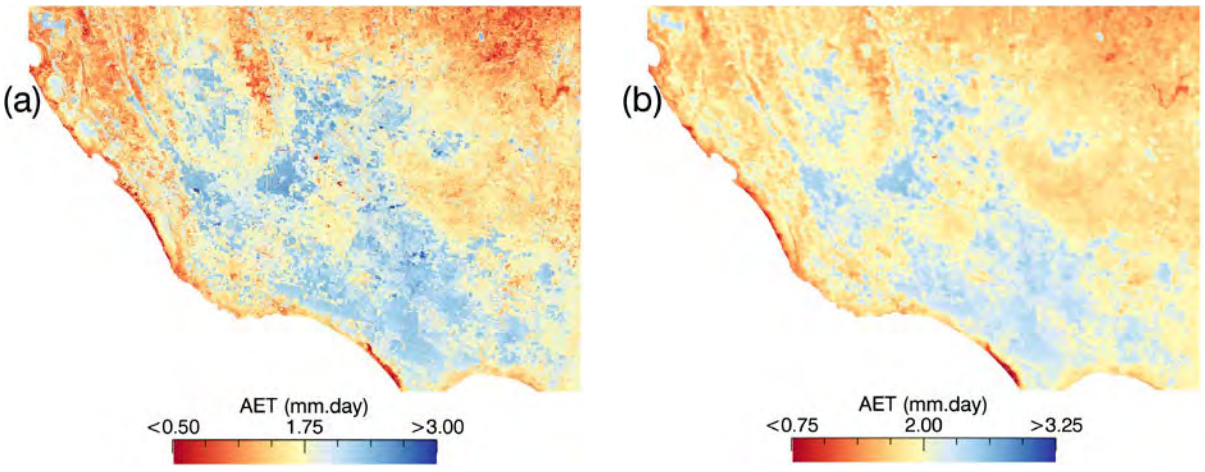

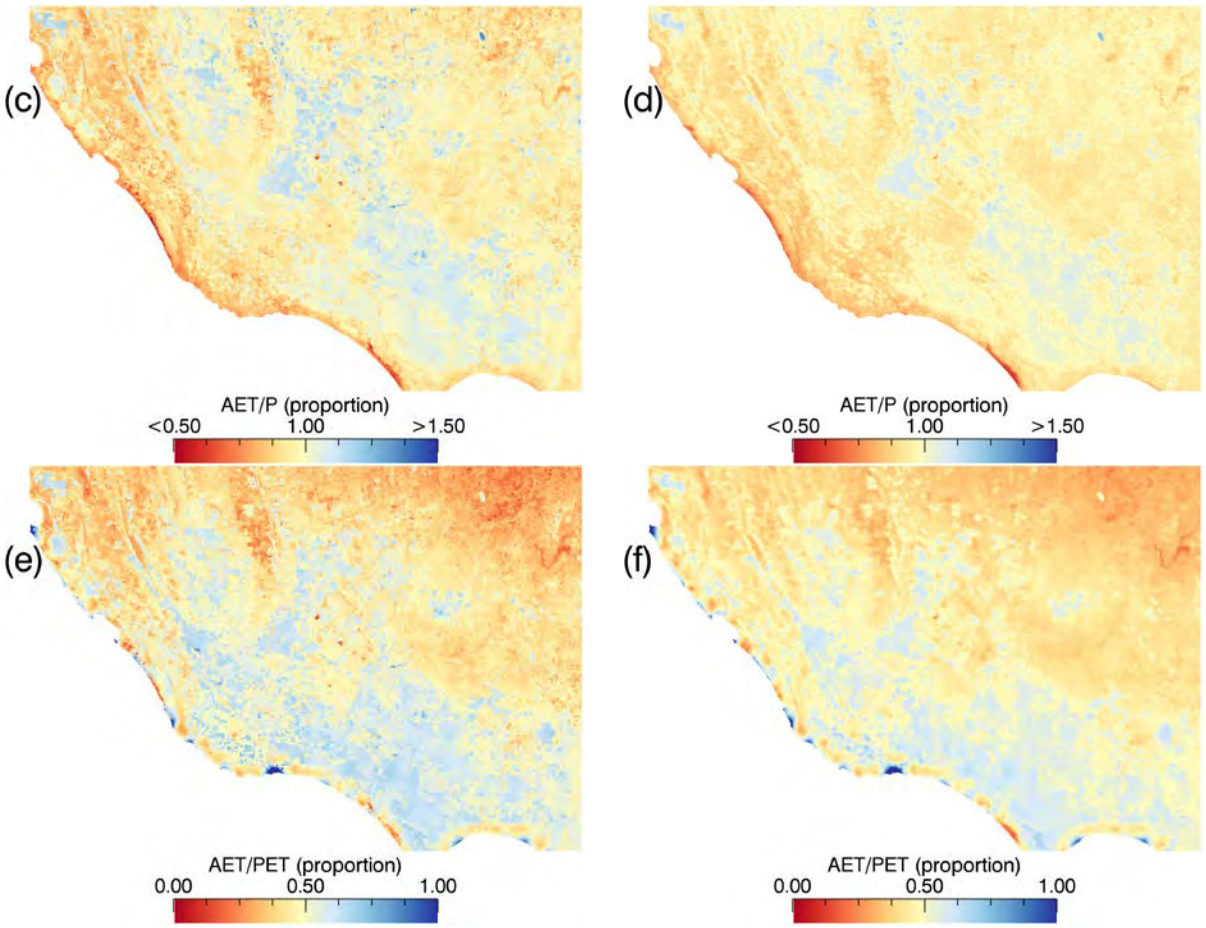

Figure 23. Long-term average (i.e., 1 Jan 2000 to 31 Dec 2011) AET and its proportions relative to key climatic controls for the SA site at both the Landsat and MODIS resolutions. The Landsat resolution data are the output of the Landsat-MODIS blending to infill all gaps in the observed Landsat time series. Parts (a) and (b) show the AET grids at the Landsat and MODIS resolutions, respectively. Parts (c) and (d) show the AET/P proportions, and (e) and (f) are the AET/PET proportions; both at the Landsat and MODIS resolutions, respectively.

The previous analysis shows the long-term temporal averages spatially (i.e., the time series are summarised as maps) and in Figure 24 we provide entire-study spatial averages temporally (i.e., the time series are summarised as time-series plots to highlight the temporal dynamics). For the NSW site Figure 24(a) shows the marked reduction in AET associated with lower P in the proceeding 6-12 months for several drought years, most notable for the 2006/07 summer. For the SA site slight more consistent P is received overall (when compared to the NSW site), with the lower AET associated with dry conditions in the 2006/07 spring-summer clearly visible Figure 24(b). Both these analyses of temporal averages (i.e., maps) and spatial averages of AET compared with P across and throughout the study extent reveal that resultant Landsat-MODIS blended AET responds to spatial and temporal variations of the main driver of the water-balance, P, in a logical and consistent manner.

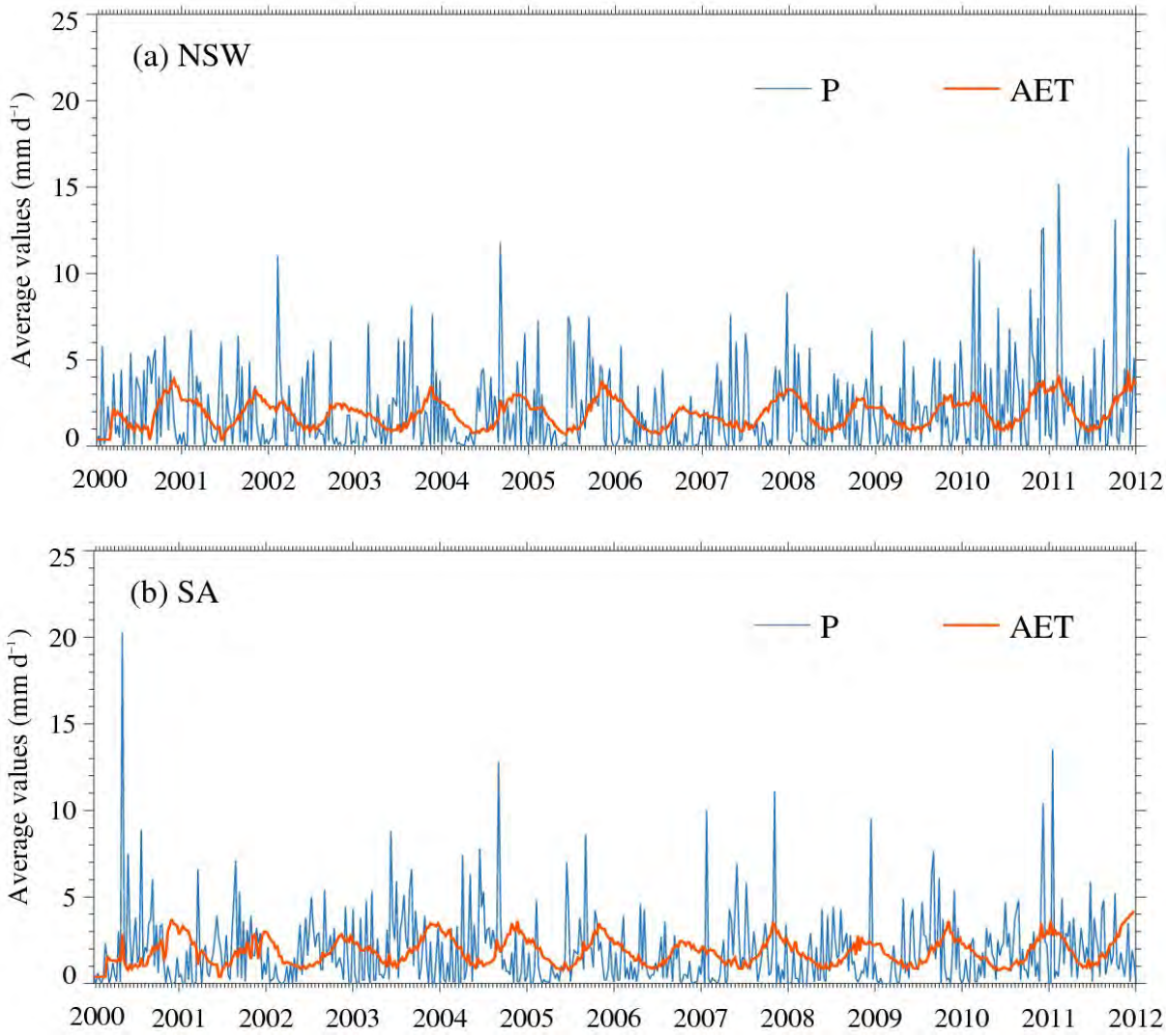

Figure 24. For the length of the study period, 8-day site-averaged AET and P across all land uses are shown for the (a) NSW site; and (b) SA site. In the first 9-12 months of the time series the AET values are less reliable due to the 'ramping up' of cloud-free Landsat blending images to perform the multi-hierarchical infilling; see Figure 20.

3.2 Topographic correction

The topographic correction was implemented by using the band and site specific *k* value for each individual epoch based on which 8-day period it fell within according to Figure 25 and Figure 26 for MODIS and Landsat, respectively. Due to the MCD43A4 data being modelled at solar noon, the solar azimuth angle for the MODIS data were always zero (Figure 25a and b). That combined with the coarser spatial resolution of MODIS resulted in climatological *k* values that were largely functions of solar zenith angle (Figure 25). The Landsat data retain their STOD nature, so they have variation in both solar zenith and azimuth angles (Figure 26). This, combined with the finer spatial resolution, resulted in climatological *k* values that were not so obviously linked to solar zenith angle alone for Landsat (Figure 26). The NSW site had considerably more variation in terrain relief (mean slope of 7.03°; see Figure 5) than did the SA site (mean slope of 2.57°; see Figure 9), so the *k* functions had different magnitude and shape between sites for both Landsat and MODIS (Figure 26). Because of the small variability in elevation at SA, the difference between *k* values for the 4 bands was not as large as at NSW, especially for MODIS data. At NSW, the main influence of performing the topographic correction was to alter the relationship between the NIR to the other bands (especially NIR to SWIR bands). For MODIS, this mainly happened in summer, whereas for Landsat, it was a fairly constant offset between NIR and SWIR bands throughout the year (Figure 26b). The large adjustment between NIR and SWIR bands for Landsat data at NSW (Figure 26b) would have an influence on the GVMI, which uses those two bands (see section 2.4). This change to GVMI, would in turn have an impact on the estimate of AET, which relies on the relative relationship between EVI and GVMI (section 2.4, Eq. (11)).

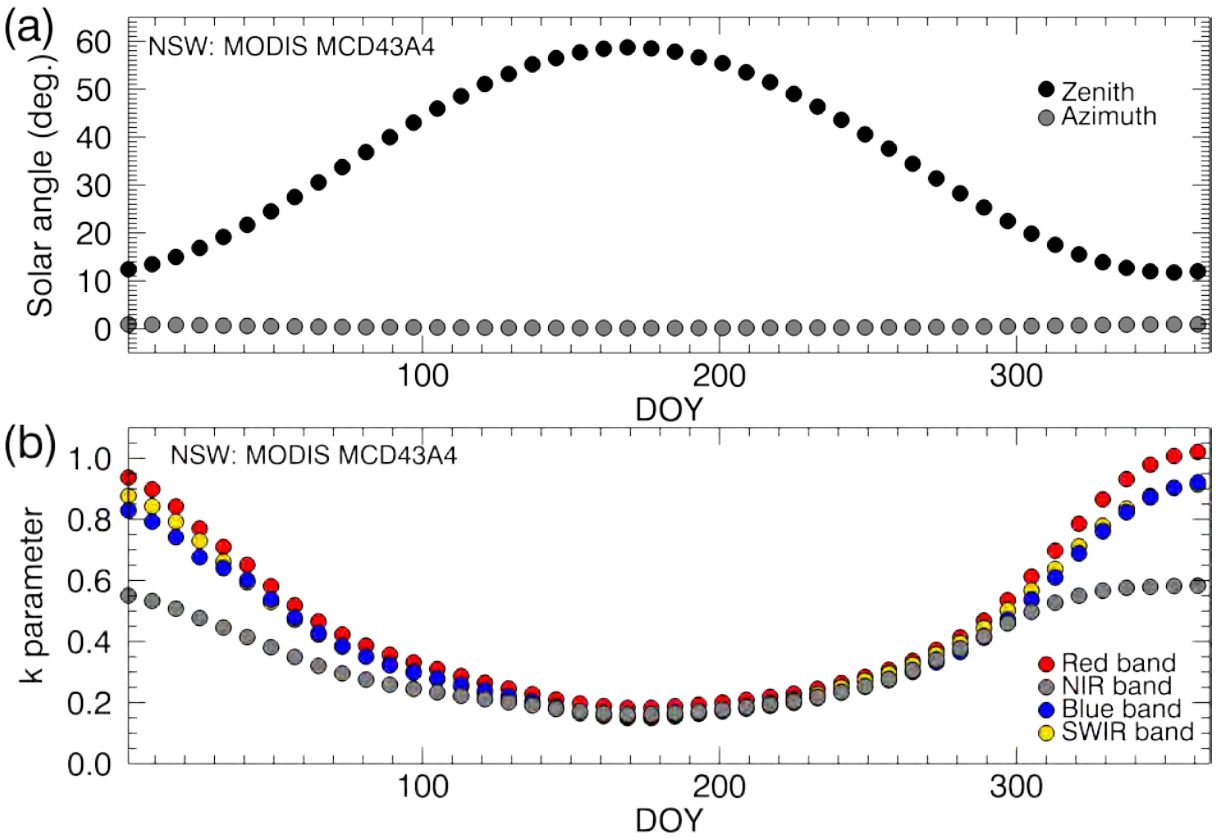

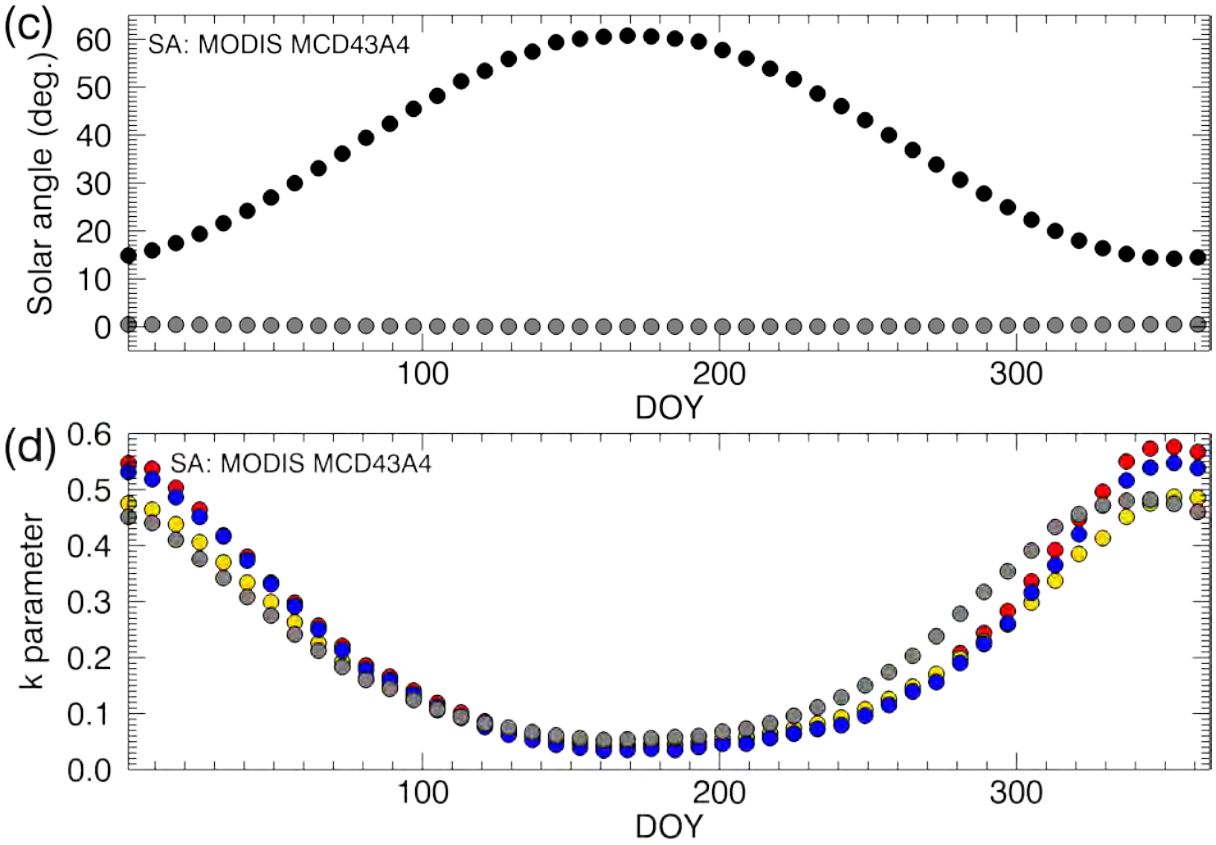

Figure 25. The solar angles and *k* parameters determined from the mean 8-day reflectances are shown for the 4 bands of interest for MODIS at both sites. The solar zenith and azimuth angles of the MODIS temporal mean 8-day composite periods at the NSW site are shown in (a). The *k* parameters determined from the mean 8-day reflectances for the 4 bands of interest for MODIS at NSW are shown in (b). The SA solar angles and *k* parameters are shown in (c) and (d), respectively. The legend in (a) applies to (c) and the legend in (b) applies to (d).

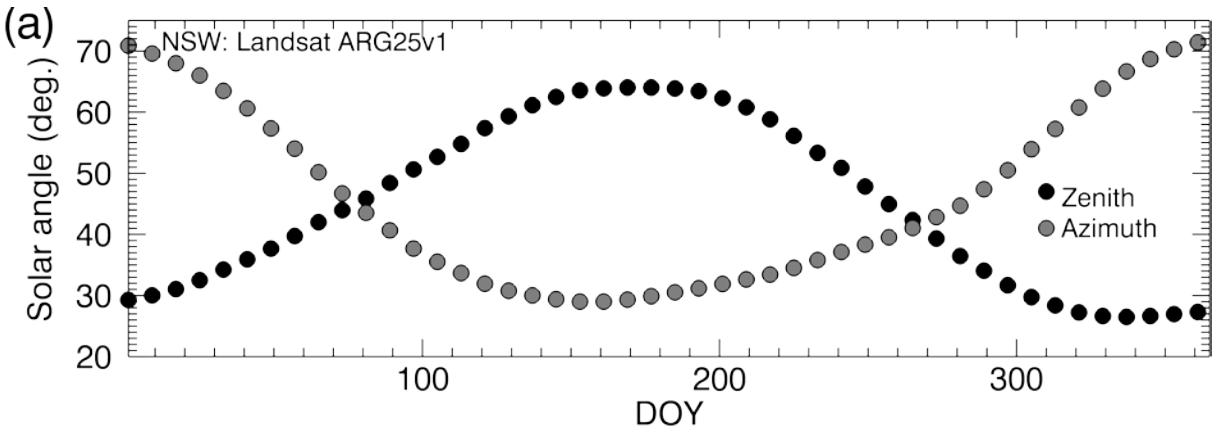

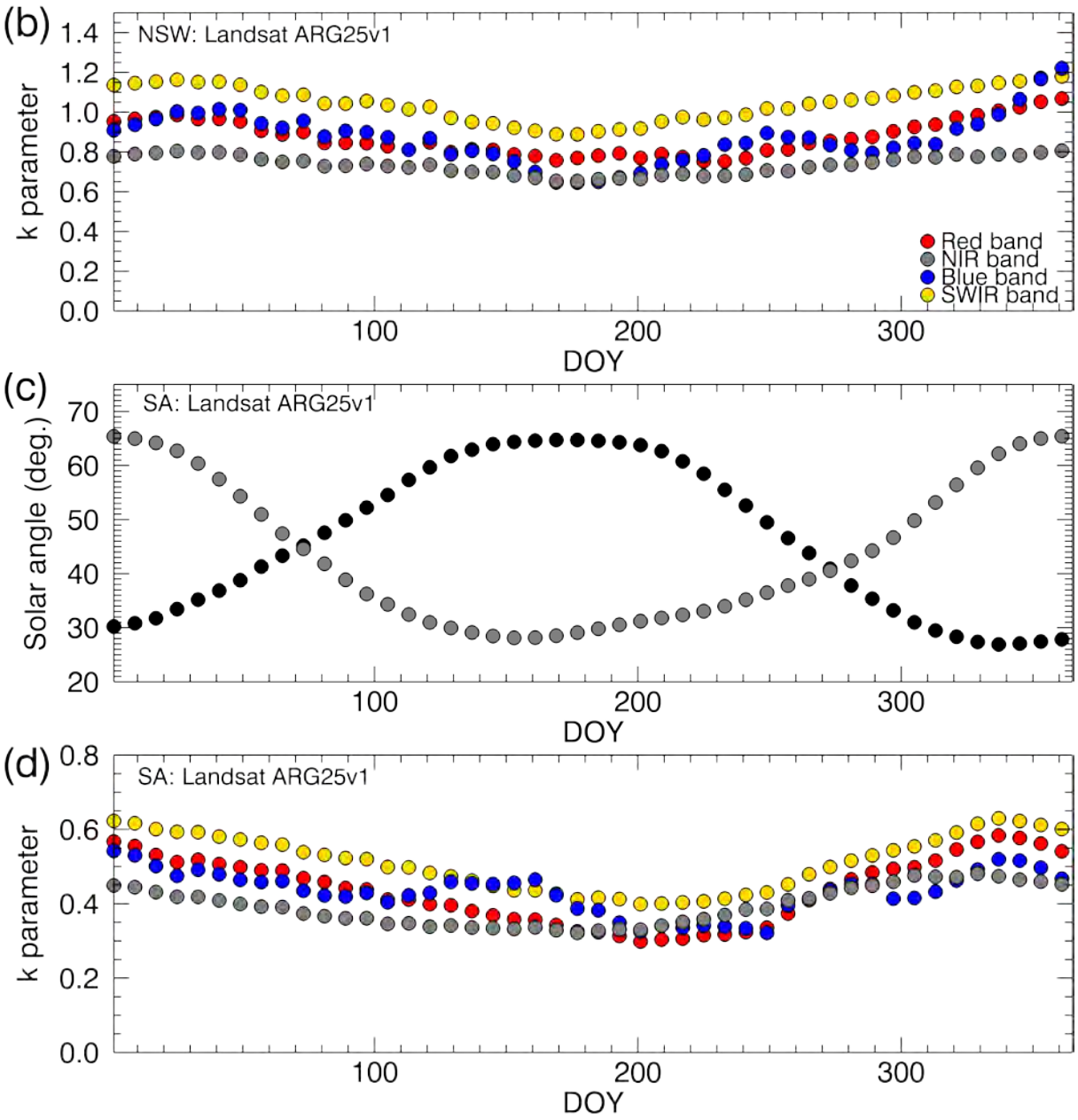

Figure 26. Solar angles and *k* parameters determined from the mean 8-day reflectances are shown for the 4 bands of interest for Landsat at both sites. The solar zenith and azimuth angles associated with Landsat mean 8-day composite periods at the NSW site are shown in (a). The *k* parameters determined from the mean 8-day reflectances for the 4 bands of interest for Landsat at NSW are shown in (b). The SA solar angles and *k* parameters are shown in (c) and (d), respectively. The legend in (a) applies to (c) and the legend in (b) applies to (d).

The influence of topographic correction on the AET algorithm was first qualitatively checked on observed Landsat imagery to assess how the illumination influence compared to major land cover change. As shown in Figure 27, the topographic effect was stronger than major land cover change for certain illumination angles as demonstrated by the January 2003 fire in NSW. The figure shows how sensitive the AET algorithm was to illumination angle. After topographic correction, the fire was clearly discernible. Further assessment of the 2003 fire at NSW is given below as evaluation in the next sub-section (i.e., section 3.3).

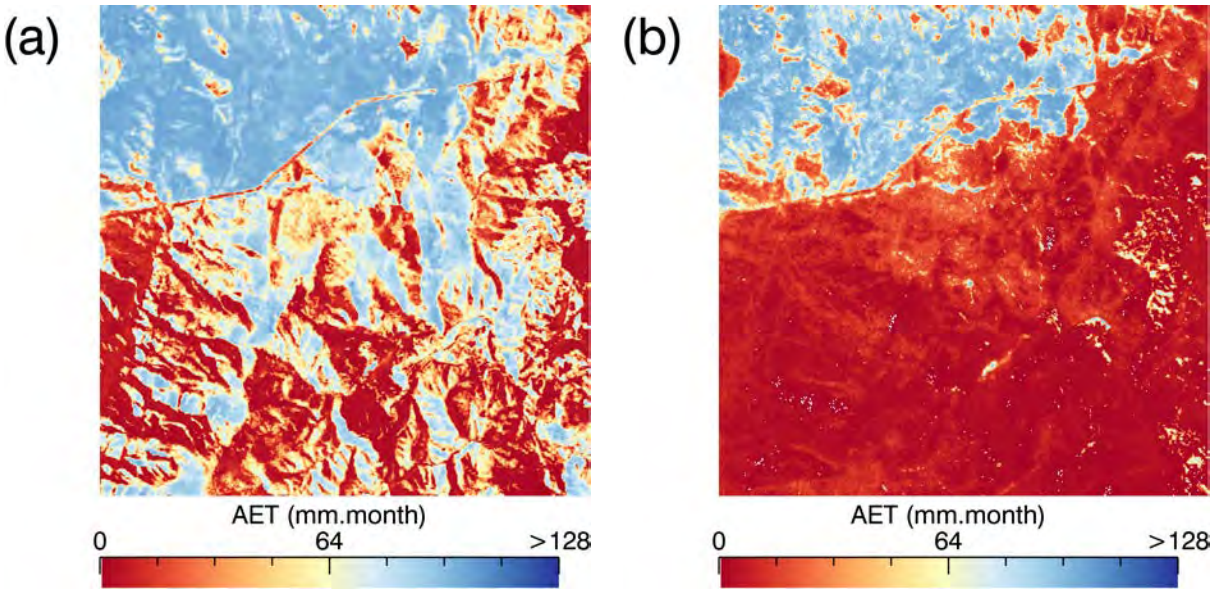

Figure 27. Effect of topographic correction on the estimation of AET is shown across a fire boundary at the NSW site. In (a) AET was estimated from an ARG25v1 Landsat NBAR image without topographic correction, and in (b) AET was estimated from the same image after topographic correction using the *k* values defined from Figure 26b for its specific 8-day composite period (8th 8-day period). The fire was not as clearly evident in the topographically uncorrected data (a), whereas after topographic correction, the fire could be clearly identified. This example used imagery from one Landsat 7 scene (P91R84) acquired on 06 March 2003. The fire occurred in January 2003. The area of this example is shown as the white rectangle in Figure 16a.

3.3 Validation and evaluation

The experimental design regarding validation of the AET model included assessment of the bias correction applied (Eq. (12)). The three bias corrections applied in this study are termed: (1) 'None'; (2) 'Original'; and (3) 'Regional', see Table 14. The original bias correction may not be optimal for our two study sites as it was performed: (i) from AET calculated from MODIS-only data (*i.e.*, having different spatial, spectral, and radiometric characteristics); (ii) over a different spatial extent (*i.e.*, over all-Australia); and (iii) over a different temporal extent. Because of these reasons, a regional bias correction was also performed, showing that when calculating AET from LM blended data over our two study sites, a slight decrease in the gain factor and a slight increase in the offset factor were helpful (Table 14). The validation performed over the no bias corrected and the original bias corrected LM blended dataset are considered independent. The regional bias correction was optimised using the validation data, so is not independent. However, due to the minor influence that the bias correction step has on the resultant model output, and how minor the difference was between the original and regional bias correction parameters (Table 14), the lack of total independence is deemed suitable for this applied study.

Table 14. The three bias corrections (Eq. (12)) used in this study are shown.

Bias Correction	a_0	a_1
None	1.000	0.000
Original	0.853	0.293
Regional	0.792	0.379

The RMSE of the three validation datasets (i.e., (i) catchment and reach area-based water balance; (ii) flux tower; and (iii) site plot-based water balance) are given for four AET datasets (i.e., (a) Landsat-only; (b) MODIS-only; (c) LM blended; and (d) AWRA)), see Table 15. Assessment of the Landsat-only and MODIS-only datasets provide a baseline for the accuracy expected from the two data sources used for the blending and AWRA provides a baseline for the accuracy of a water balance model currently used for national water assessment and accounts. The LM blended data were assessed for the three bias corrections ((i) None; (ii) Original; and (iii) Regional), Table 15. The regional LM blended, the MODIS-only, and the AWRA assessment are shown graphically in Figure 28 and the Landsat-only assessment is shown in Figure 29.

Table 15. The RMSE of the three validation datasets is provided for the Landsat-only, MODIS-only, three bias correction versions of the LM blend, and the AWRA water balance AET output.

Data source	Bias correction	RMSE (mm/d)		
		Area WB	Flux Tower	Site WB
Landsat-only	Original	0.50	0.50	1.02
MODIS-only	Original	0.27	0.52	0.98
LM Blended	None	0.36	0.60	1.13
LM Blended	Original	0.31	0.52	1.01
LM Blended	Regional	0.26	0.52	0.98
AWRA	—	0.13	0.63	1.21

The accuracy of the LM blended datasets was improved for each validation type progressively from no bias correction having the lowest accuracy, the original bias correction having higher accuracy, and the regional bias correction having the highest accuracy of these three LM datasets, Table 15. The regional bias correction LM dataset also had equal or better accuracy when compared to the MODIS-only or Landsat-only datasets for all three validation datasets (Table 15, Figure 28, and Figure 29). The AWRA dataset had highest overall accuracy for the area (catchment and reach) water balance, but had the lowest accuracies for the site-based assessments at the flux tower and the site water balance plots (Table 15 and Figure 28). This result is not unexpected, as AWRA is a water balance model, which are by design, good at modelling catchment-level processes and worse at modelling point-level processes.

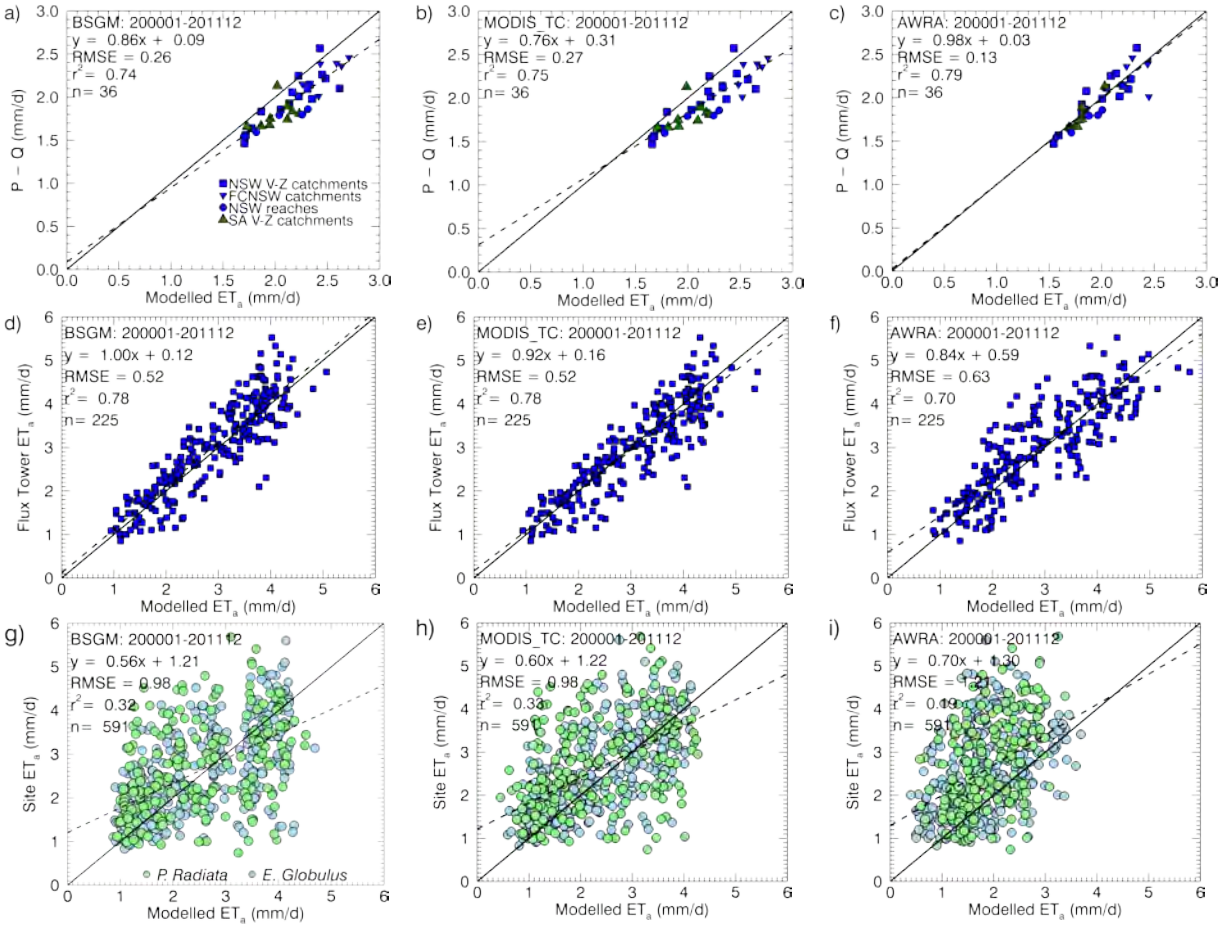

Figure 28. Comparison of modelled versus observed AET of the three validation datasets is shown for the regional bias correction versions of the LM blend, MODIS-only, and the AWRA water balance AET output. Parts (a), (b) and (c) use long-term catchment and reach water balance data (from both sites, see Table 5, Table 6 and Table 7) to validate the AET modelling. The legend in (a) also applies to (b) and (c). Parts (d), (e) and (f) use the 8-day Tumbarumba flux tower observations (its location is shown by the blue star in Figure 4(a)) to validate the AET modelling. Parts (g), (h) and (i) use monthly site water balance data for *P. Radiata* and *E. Globulus* from the SA site (see Table 9 and Figure 18) to validate the modelling. The legend in (g) also applies to (h) and (i). The left column (i.e., parts (a), (d) and (e)) shows the results when using the regional bias corrected versions of the LM blended AET output. The centre column (i.e., parts (b), (e) and (h)) show the MODIS-only output. The right column (i.e., parts (c), (f) and (i) show the AWRA water balance output.

The Landsat-only AET dataset performed well at the flux tower, reasonably well at the site water balance plots, and rather poorly over the area (catchment and reach) water balance

assessments compared to the LM blended datasets (Table 15, Figure 28, and Figure 29). The reduced accuracy of the Landsat-only AET dataset is seen primarily as a bias (Figure 29a), which is explained by the reduced temporal density of the Landsat data. The difference between the Landsat-only (Figure 29a) when compared to the MODIS-only (Figure 28b) or the LM blended dataset (Figure 28a) results for the area water balance assessment is indicative, then, of the error introduced by not having a high enough temporal density.

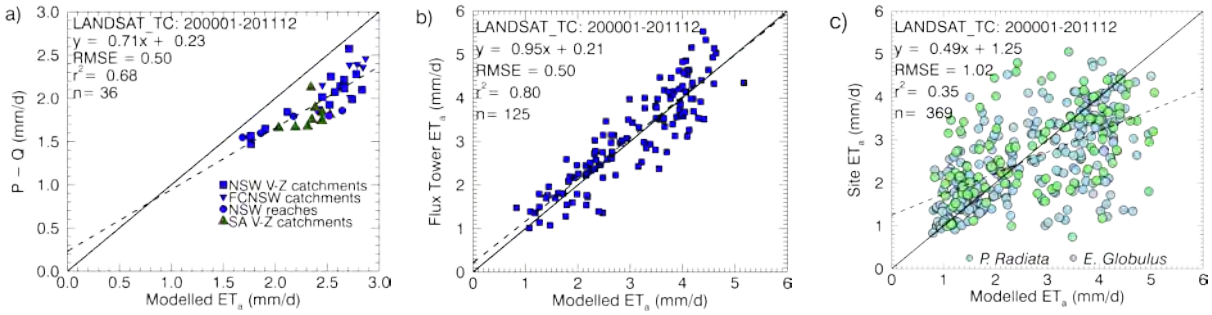

Figure 29. Comparison of modelled versus observed AET of the three validation datasets is shown for the Landsat-only AET output. Part (a) uses catchment and reach water balance data (from both sites, see Table 5, Table 6 and Table 7). To validate the AET modelling: (b) uses the Tumbarumba flux tower observations (its location is shown by the blue star in Figure 4(a)); and (c) uses the site water balance data for *P. Radiata* and *E. Globulus* from the SA site (see Table 9 and Figure 18).

The total volumetric AET (kL) of the plots and the change in plot timber volume (m^3/ha) between 30/09/2009–03/08/2011 are provided in for the three unthinned Red Hill catchment vegetation plots. The ratio of AET/ΔV shows how many kL of water were evaporated according to the AET model to increase average timber volume by 1 m^3/ha across the plots. The trees were planted in 1989, so were 20 and 22 years old at the times of field measurement. For the three unthinned plots, shows that on average, about 32 kL of water was evaporated to increase timber volume by 1 m^3/ha.

Table 16. The volumetric AET (kL) and the change in timber volume (ΔV, m^3/ha) are shown for the time period 30/09/2009–03/08/2011 (672 days) for the three unthinned Red Hill catchment vegetation plots. The ratio of AET/ΔV shows how much water was evaporated according to the AET model to increase timber volume by 1 m^3/ha. The trees were planted in 1989, so were 20 and 22 years old at the times of field measurement.

Plot No.	AET (kL)	ΔV (m^3/ha)	AET/ΔV (kL/(m^3/ha))
1	1513	48.7	31.0
2	1547	48.1	32.2
4	1574	48.4	32.5
Mean	**1544**	**48.4**	**31.9**

The minimum z-score for the year 2003 is shown in Figure 30a. The fire boundary includes contours describing the progression of the fire, so areas having wider spacing between contour lines are the areas that burned quicker than the areas where the lines are close together (Figure 30a). The minimum z-score analysis matches the fire well, especially for the areas of the fire having wide contour spacing, indicating a quicker and likely, more intense burn (Figure 30a). There are some ‘blue’ areas inside the fire boundary, usually in areas of close fire contours, indicating that in areas of slower burn (and likely less intense), either the AET model missed the areas, or the fire had incomplete coverage in these areas, or both (Figure 30a). There were also a few ‘red’ areas outside of the fire boundary, which had z-

scores approximately as low as within the fire, which may be due to isolated smaller fires or other disturbances. The annual average AET within the fire boundary demonstrates a low AET in 2003, followed by a generally increasing trend thereafter (Figure 30b). The PET data inside the fire boundary did not demonstrate this reduction and subsequent steady increase (Figure 30b). For such a major fire event, perhaps a stronger reduction in AET might be expected. However, the subjectivity of this expectation is hard to reconcile and the AET model does not discern the difference in AET from trees compared to undergrowth that might grow soon after a fire event. Regardless, Figure 30 shows that the model identifies the fire and that is a form of evaluation which bolsters the belief that the Landsat-MODIS blending and AET model are behaving sensibly.

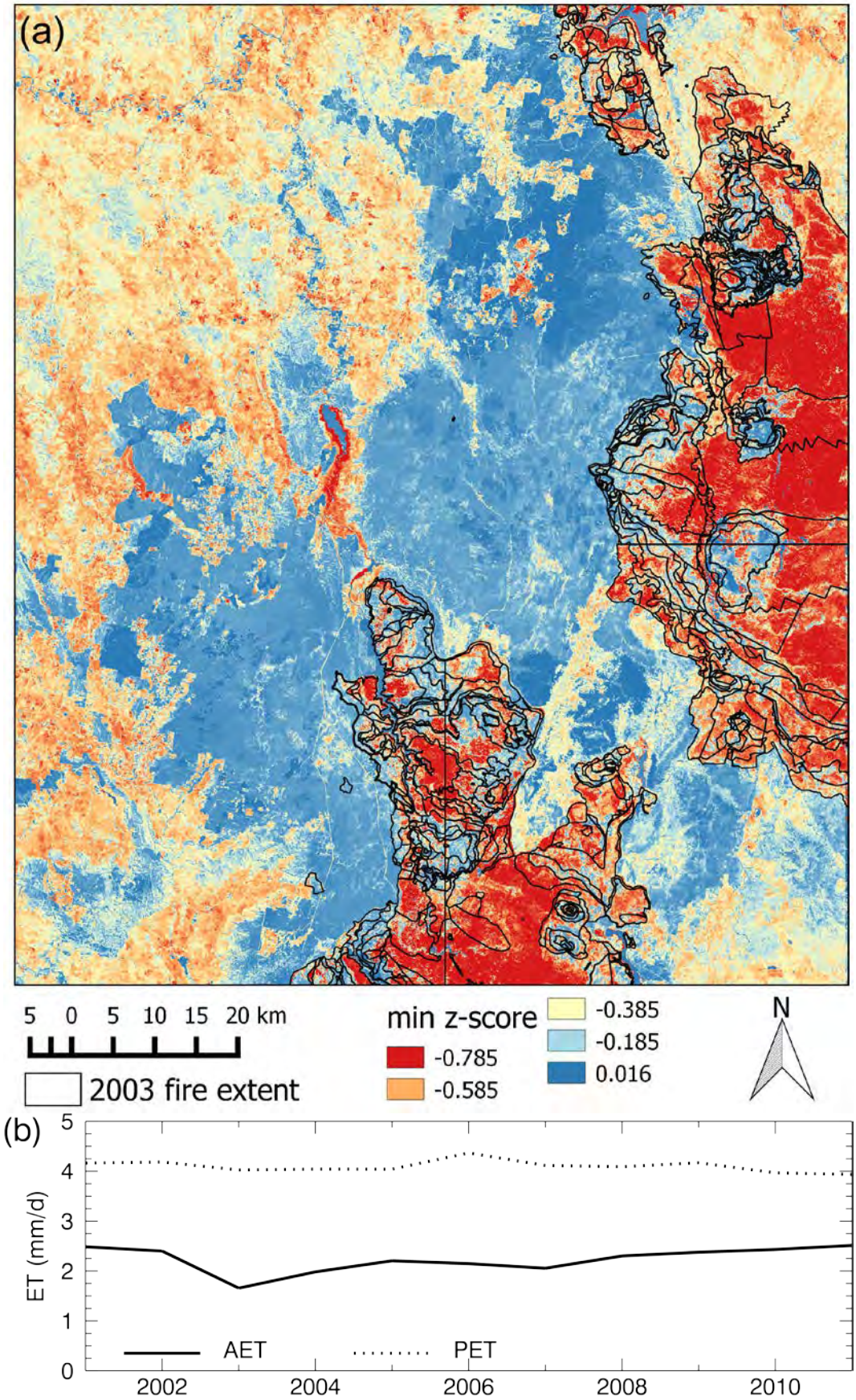

Figure 30. AET response to major fire in 2003 for the NSW site is shown. The minimum z-score recorded over the year is shown in (a) and the annual average AET and PET within the fire boundary is shown in (b). The spatial extent in (a) is defined by the GIS layer of the fire

boundary, so it is not the full extent of the NSW study site.

Over the SA study site, we had data on species, age, and thinning management of the forestry plantations, which allowed further evaluation of the average modelled output by species and age (Figure 31a). Figure 31a shows that on average, *E. globulus* AET was initially higher and increased more rapidly than *P. radiata*, suggesting that *E. globulus* is a faster growing species than *P. radiata*. *E. globulus* reached a plateau with respect to average AET after about 4 years, whereas *P. radiata* reached an average AET plateau after about 6 years (Figure 31a). The forestry management data included information on timing of multiple thinning operations. Figure 31b shows average AET of *P. radiata* of those stands that had been first thinned in 2000, the initial year of our study period. These thinned stands had an average age of about 15 years old. We then compared them to non-thinned stands of *P. radiata* that had an age of 15 in the year 2000 (Figure 31b). Although the non-thinned 15 yo *P. radiata* were noisier than the first thinned *P. radiata*, the reduction in AET of the thinned stands especially in years 0-2 after thinning was evident (Figure 31b). This also suggests that the model was behaving sensibly. After assessing the first thinning analysis, the decrease in *P. radiata* AET at age 15 and the subsequent increase in AET afterwards (Figure 31a) looks suspiciously like some of the data have been incorrectly labelled in the management database, and actually have had their first thinning at around year 15. Note, differences in species-level AET could be influenced by site quality, which has not been checked in this case.

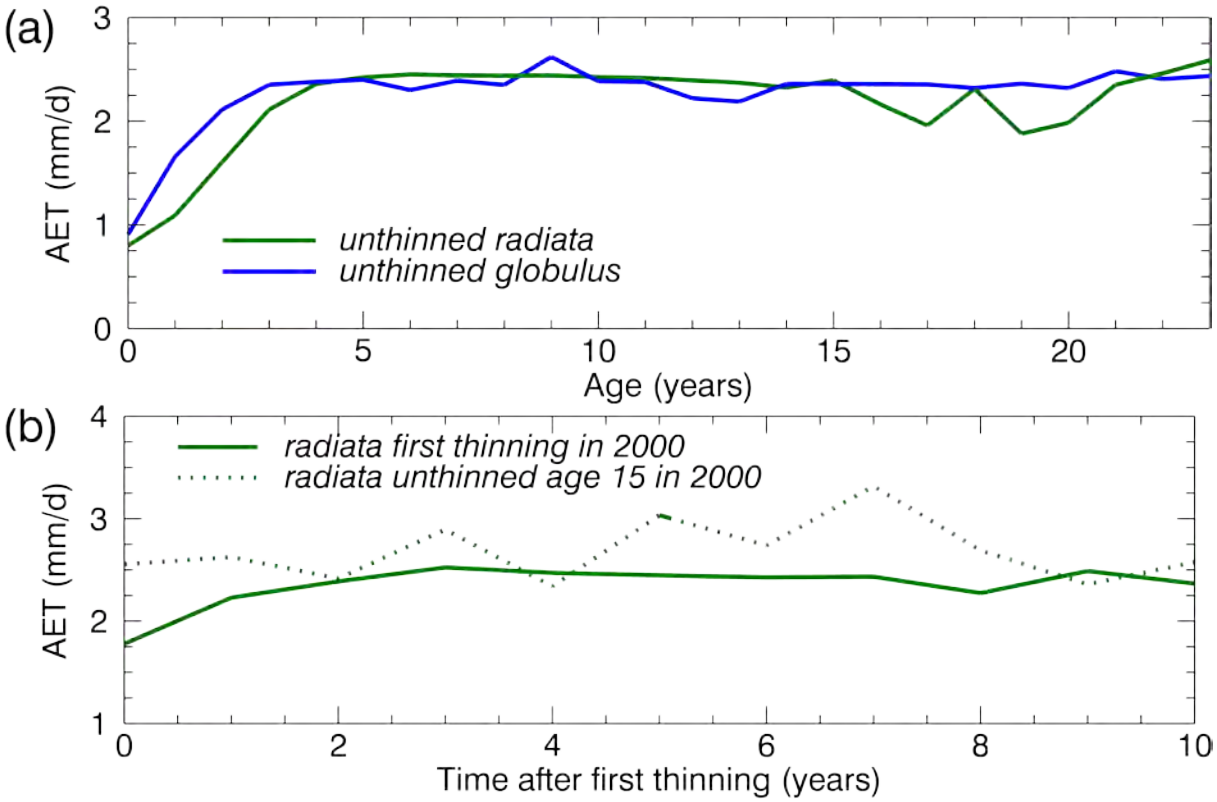

Figure 31. Average AET for unthinned *P. radiata* versus unthinned *E. globulus* at SA in (a) and average AET of *P. radiata* that had its first thining in 2000 compared to unthinned *P. radiata* having an age of 15 years old in 2000 is shown in (b).

Next we assess the ability of the Landsat-MODIS blended AET to detect forestry harvest operations. Several compartments in the vicinity of Burrungule in the SA site were harvested in 2004. Figure 32 clearly shows the reduction in the Landsat-MODIS blended AET due to the logging operations and the recovery following replanting. These changes are clearly seen in the time-series and the output images. The higher spatial resolution of the Landsat-MODIS

blended AET also highlight how forestry applications are better served by the higher resolution imagery. There is lower AET in the western portion of the logged compartments in Jan 2003, and in the Jan 2009 image the new planted canopy is yet to close and access roads are still visible (Figure 32).

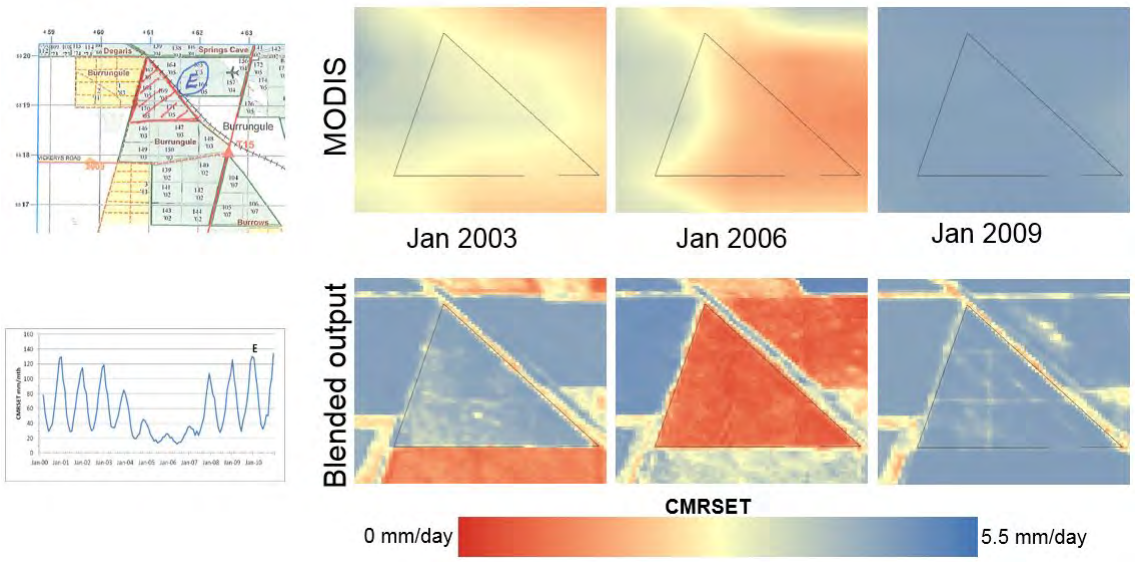

Figure 32. Changes in AET rates associated with forestry logging operations in the vicinity of Burrungule in the SA site. The compartments were logged in 2004, with MODIS AET images provided in the top row and Landsat-MODIS blended AET images in the bottom row.

3.4 Land-use specific AET assessment

The land-use specific AET assessment is the main summarisation of the report in which the two objectives are addressed. That is, to assess: (*i*) the magnitudes and dynamics of land-use-specific water use for entire catchments containing plantations; and (*ii*) whether there are other high-water use activities in the selected catchments/regions that use as much, or possibly even more, water as plantation forestry. Due to the importance of this analysis, multiple summaries were made over all 9 land-use type, including volumetric totals of AET, relative rates of AET, normalised AET relative to P, normalised AET relative to PET, as well as a paired analysis of selected land-use types. All summaries of AET in this section use the regional bias corrected version of the LM blended model output.

Table 17. Proportional areas are provided for the 9 land-use classes for each study site. Rank of area is given in parentheses, and *i* refers to the land-use class index as introduced in the equations in section 2.8 above.

Land-use number (*i*)	Land-use name	NSW $A_i(prop)$	SA $A_i(prop)$
1	Native Vegetation	0.23 (2)	0.18 (2)
2	Unknown Plantation	0.04 (5)	<0.01 (9)
3	Hardwood Plantation	<0.01 (9)	0.02 (7)
4	Softwood Plantation	0.05 (4)	0.10 (3)
5	Dryland Cropping	0.12 (3)	0.04 (5)
6	Irrigation	<0.01 (8)	0.02 (8)
7	Urban	0.02 (6)	0.04 (4)
8	Water	0.01 (7)	0.03 (6)
9	Grazing Modified Pasture	0.53 (1)	0.57 (1)

The areas of the land-use classes are given as proportions in Table 17. At both sites, the Grazing Modified Pasture class was the highest land-use by area, accounting for over 50 percent of the study areas, with Native Vegetation being the second highest at both sites (Table 17). At both sites, the highest Plantation land-use class was Softwood Plantation, accounting for 5% of the overall area at NSW, and 10% at SA, see Table 17. Total forestry plantation area was < 10% at NSW and < 13% at the SA site (Table 17), showing that forestry plantations cover a relatively small area of the study sites.

Average volumetric AET, P, and PET and the evaporative fractions AET/P and AET/PET are provided in Table 18 and Table 19 for NSW and SA, respectively. In particular, the AET/P metric provides important hydrological context; if over the long-term AET/P ≤1, then it is expected to use minimal groundwater resources. Average volumetric AET of the two main plantation classes (Softwood and Unknown) ranked 4th and 5th highest at NSW, meaning that from a total amount of water use standpoint, there were three land-uses that exceeded plantations (Table 18). When summarising AET/P at NSW, the two main plantation land-uses ranked 6th and 8th highest, meaning most other land-use classes had higher water use compared to their input precipitation (Table 18). At SA, the two main plantation land-use classes (Softwood and Hardwood) ranked 3rd and 7th when summarised from a volumetric standpoint, and were 2nd and 1st ranked when summarised by AET/P (Table 19). These metrics point to a contrast between the two study sites, highlighted by the AET/P summaries of the model, where at NSW the plantation land-use class averages were below unity (AET < P, Table 18) and at SA where the plantation land-use class averages were above unity (AET > P, Table 19).

Table 18. Average volumetric AET (GL/d), P (GL/d), PET (GL/d), AET/P, and AET/PET are provided for the NSW site. Rank of land-use class metrics are given in parentheses. Associated area proportions are given in Table 17.

Land-use name	$\mathbf{AET}_i(GL/d)$	$\mathbf{P}_i(GL/d)$	$\mathbf{PET}_i(GL/d)$	$\frac{\mathbf{AET}_i(GL/d)}{\mathbf{P}_i(GL/d)}$	$\frac{\mathbf{AET}_i(GL/d)}{\mathbf{PET}_i(GL/d)}$
Native Vegetation	14.33 (2)	16.68 (2)	26.02 (2)	0.86 (9)	0.55 (3)
Unknown Plantation	2.83 (5)	3.18 (5)	4.69 (5)	0.89 (8)	0.60 (2)
Hardwood Plantation	0.00 (9)	0.00 (9)	0.00 (9)	0.91 (7)	0.36 (8)
Softwood Plantation	3.40 (4)	3.46 (4)	5.49 (4)	0.98 (6)	0.62 (1)
Dryland Cropping	4.52 (3)	4.60 (3)	13.18 (3)	0.98 (5)	0.34 (9)
Irrigation	0.24 (8)	0.22 (8)	0.47 (8)	1.11 (1)	0.52 (4)
Urban	1.01 (6)	1.00 (6)	2.44 (6)	1.01 (3)	0.41 (7)
Water	0.72 (7)	0.68 (7)	1.43 (7)	1.06 (2)	0.50 (5)
Grazing Modified Pasture	25.29 (1)	25.57 (1)	60.04 (1)	0.99 (4)	0.42 (6)
Total	52.35	55.34	113.76	0.95	0.46

Table 19. Average volumetric AET (GL/d), P (GL/d), PET (GL/d), AET/P, and AET/PET are provided for the SA site. Rank of land-use class metrics are given in parentheses. Associated area proportions are given in Table 17.

Land-use name	$\mathbf{AET}_i(GL/d)$	$\mathbf{P}_i(GL/d)$	$\mathbf{PET}_i(GL/d)$	$\frac{\mathbf{AET}_i(GL/d)}{\mathbf{P}_i(GL/d)}$	$\frac{\mathbf{AET}_i(GL/d)}{\mathbf{PET}_i(GL/d)}$
Native Vegetation	12.12 (2)	11.16 (2)	22.43 (2)	1.09 (4)	0.54 (4)
Unknown Plantation	0.44 (9)	0.40 (9)	0.87 (9)	1.09 (5)	0.50 (7)
Hardwood Plantation	1.51 (7)	1.26 (7)	2.55 (7)	1.19 (1)	0.59 (2)
Softwood Plantation	7.33 (3)	6.46 (3)	12.08 (3)	1.14 (2)	0.61 (1)
Dryland Cropping	2.11 (5)	2.28 (5)	4.79 (4)	0.93 (9)	0.44 (9)
Irrigation	1.24 (8)	1.13 (8)	2.16 (8)	1.10 (3)	0.57 (3)
Urban	2.31 (4)	2.32 (4)	4.58 (5)	1.00 (6)	0.50 (6)
Water	1.53 (6)	1.60 (6)	3.00 (6)	0.96 (8)	0.51 (5)
Grazing Modified Pasture	32.93 (1)	33.55 (1)	68.61 (1)	0.98 (7)	0.48 (8)
Total	61.52	60.17	121.07	1.02	0.51

The climatological mean volumetric AET of the major land-use classes is also provided in Figure 33. All three plantation classes were combined to assess the overall plantation water use for NSW in Figure 33(a) and for SA in Figure 33(b). At both sites, the Grazing Modified Pasture class and the Native Vegetation classes had higher volumetric AET than the combined plantation AET (Figure 33a-b). When the plantation land-use classes were assessed separately, the Dryland Cropping class had higher AET than the Unknown or Softwood Plantation classes at NSW, primarily due to high AET in the Dryland Cropping class in Spring (Figure 33c). At SA, the Softwood Plantation class volumetric AET exceeded all the next few ranked classes (Figure 33d) and the Hardwood Plantation class volumetric AET was lower than Dryland Cropping class, which also peaked in Spring in SA (Figure 33e). The peak in Dryland Cropping AET was emphasised by graphing the 8-day time-series of its volumetric AET compared to that of a minor plantation class at NSW and SA (Figure 34a and b, respectively).

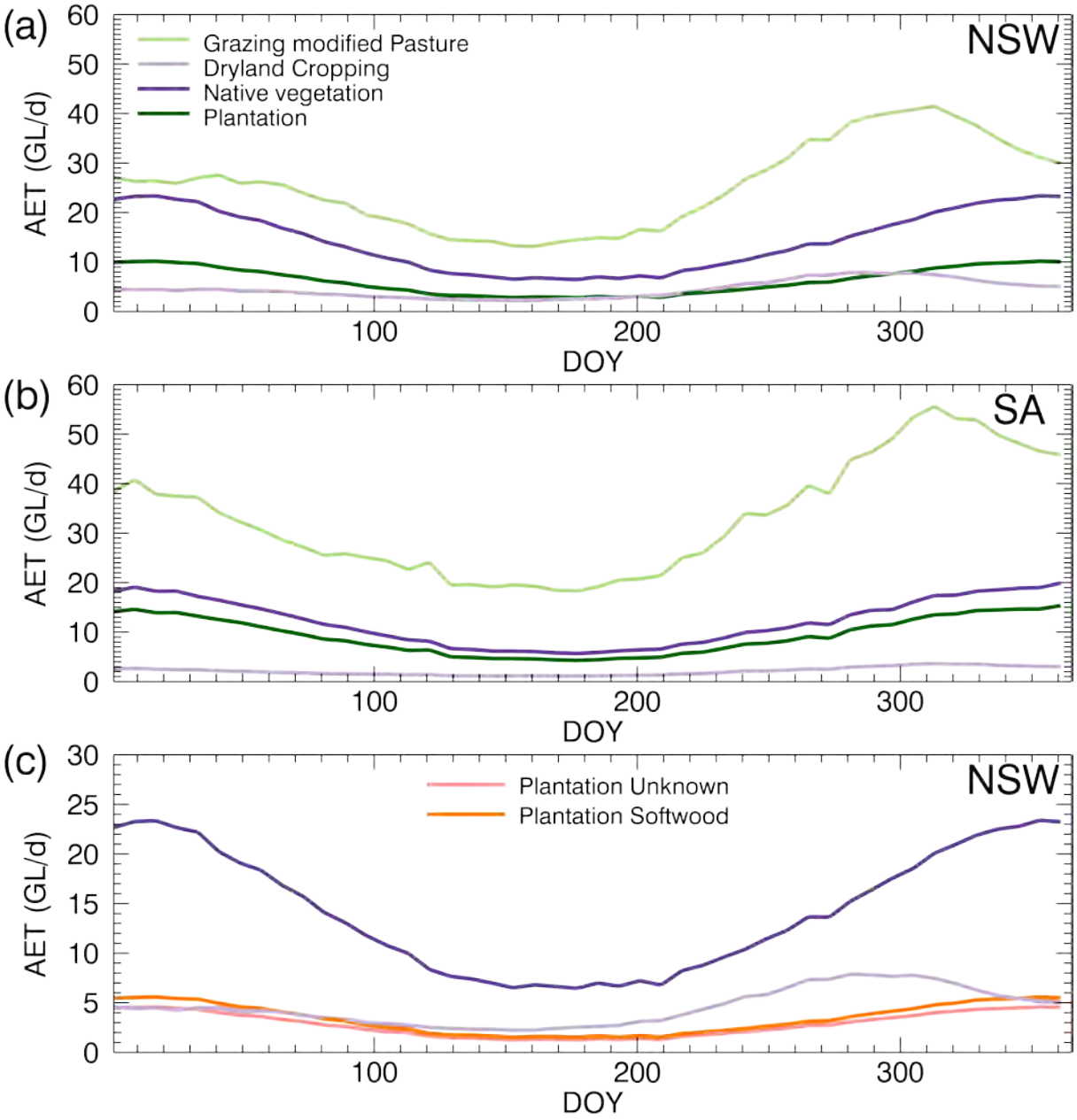

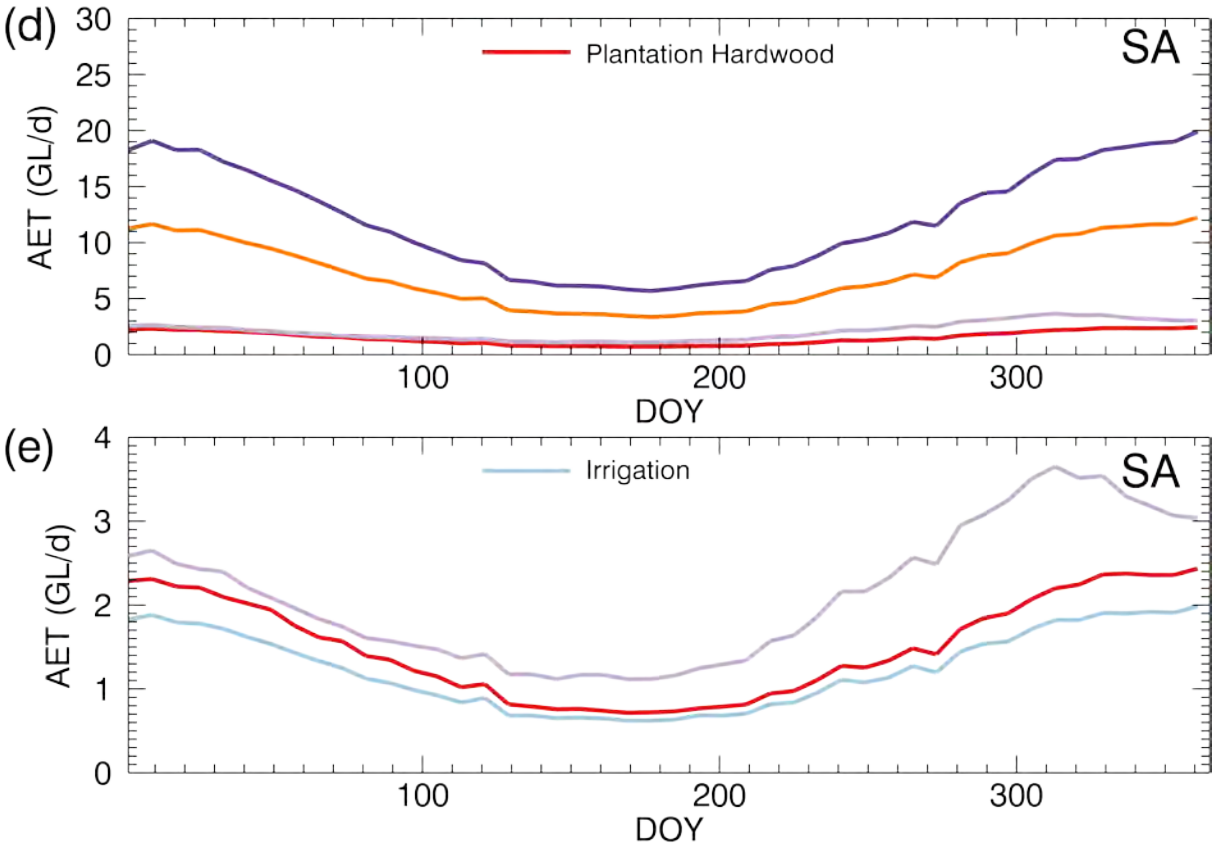

Figure 33. Climatological AET (GL/d) is shown for the major land use classes as determined by area for NSW in (a) and (c) and for SA in (b), (d), and (e). Legend elements are provided on the figure part where they are first introduced, but the colours apply for any subsequent instances and they match those of Figure 16.

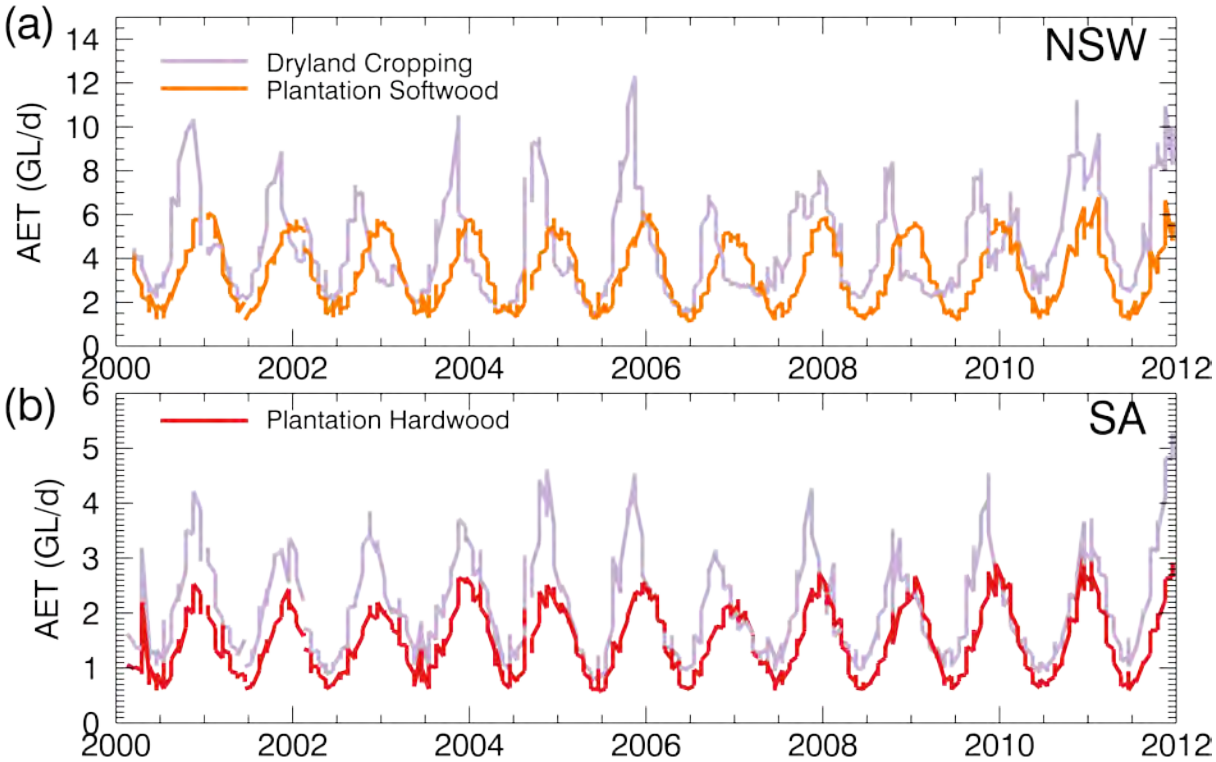

Figure 34. Time-series AET (GL/d) is shown for specified land-use classes for (a) the NSW site and (b) the SA site. Legend elements are provided on the figure part where they are first introduced, but the colours apply for any subsequent instances and they match those of Figure

16.

At NSW, the classes with the highest AET/P were Irrigation, Water, and Urban classes; and these were the only three classes where AET exceeded P at NSW (Table 18). These three high AET/P classes have exceedingly small proportional areas, which reduces the certainty that they are hydrologically meaningful (Table 17). Since none of the plantation classes, on average, have AET that exceeds P in NSW, the model indicates that it is unlikely much net ground water is being used by plantation forestry there. This is supported by Figure 35a, which shows the pixel-based temporal average AET/P for the forestry plantation classes (all other classes are grey) being primarily below unity. The climatological AET/P is shown for the combined forestry plantation land-use classes compared to the other major land-use classes by area in Figure 36, which shows, generally, a high AET/P in summer and a low AET/P in winter with the Grazing Modified Pasture and Dryland Cropping classes also being high in Spring for NSW, but not for SA.

At SA, the comparison of AET to P showed 5 land-use classes where AET exceeded P, and in fact, that the overall total AET of all 9 classes exceeded that of P for the whole area (Table 19). The top five land-use AET/P included the three forestry plantation classes, the native vegetation class, and the irrigation class (Table 19). Of these, the native vegetation and softwood plantation classes had proportional areas ≥0.1 and thus imbued higher certainty (Table 17). While overall volumetric AET exceeded P for the forestry plantations at SA, this was highly variable (Figure 35b). There were large proportions of plantation where AET was equal to or less than P, especially in the lower AI band nearer to the coastline (Figure 35b and Figure 10).

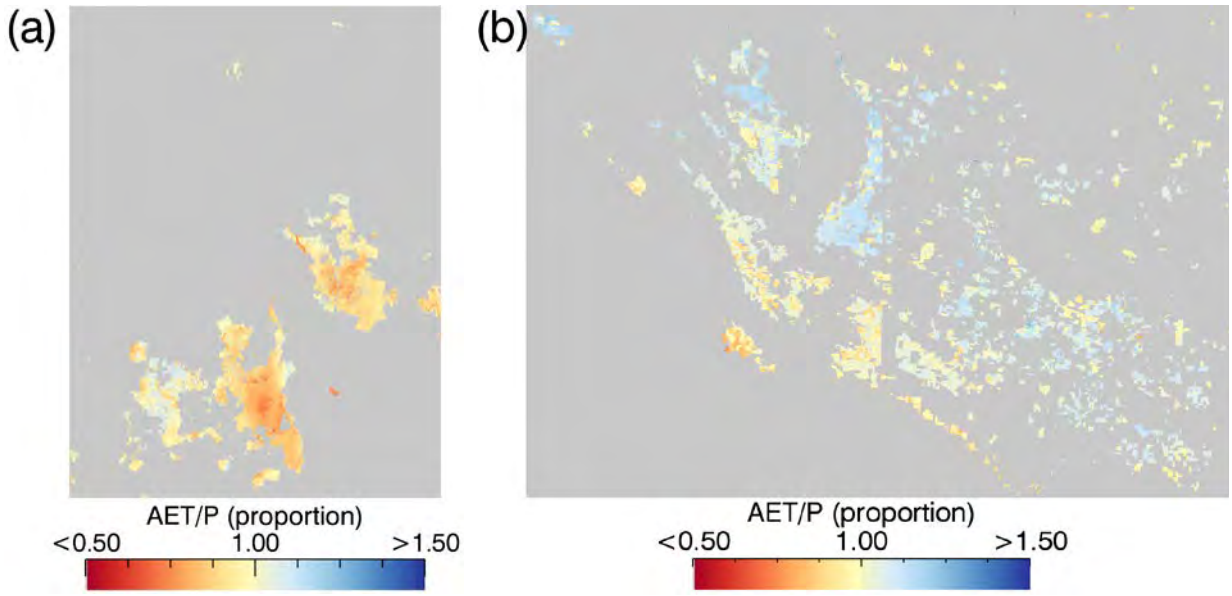

Figure 35. The pixel-wise temporal average rates of AET/P for the (a) NSW site and (b) SA site. For (a) only State Forest for NSW is shown with all other land-uses coloured grey. For (b) all plantations for the SA site are shown with all other land-uses coloured grey.

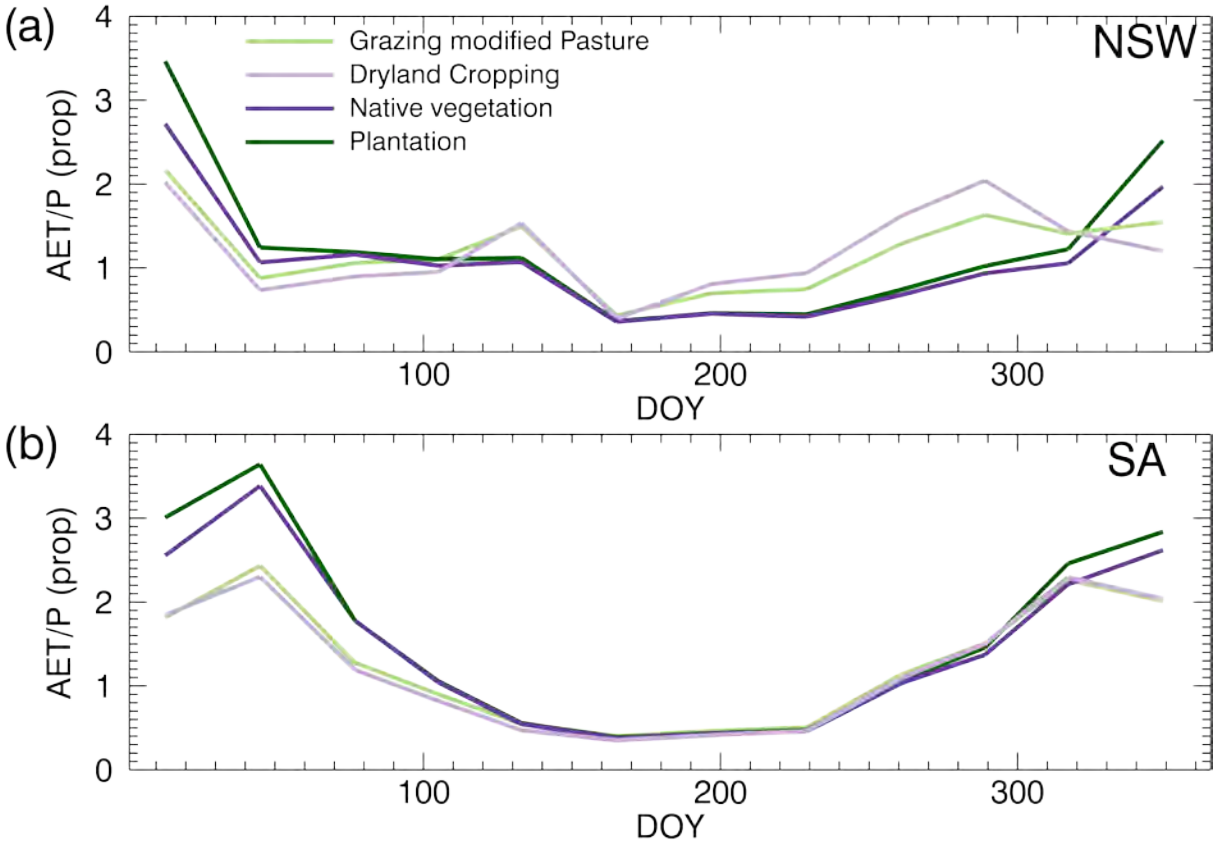

Figure 36. Climatological AET/P (proportion) is shown for the major land use classes as determined by area for NSW in (a) and for SA in (b). Legend elements are provided on the figure part where they are first introduced, but the colours apply for any subsequent instances and they match those of Figure 16. Climatologies were calculated on months rather than 8-day periods.

The mean relative rates of AET per land-use class (mm/d) for both study sites are also provided in Table 20 and Table 21. The relative assessment of AET, obviously, removes the influence of any particular land-use class' areal proportion (not including any indirect effects due to potential errors for those classes which are inordinately small). For both sites, the two highest AET rates in mm/d were forestry plantation land use classes (Softwood and 'Unknown' plantation sites, respectively at NSW and Softwood and Hardwood plantations, respectively at SA), see Table 20 and Table 21. The third highest AET rate was native vegetation at NSW and irrigation at SA (Table 20 and Table 21). It should be noted that the Native Vegetation class includes native grassland vegetation and so should not be considered to be native forest, see section 2.2.2. Also of note, is the water class having relatively low AET rates at both sites (and being 5th and 7th highest AET out of 9 classes for NSW and SA, respectively). This is addressed in more detail below, in the discussion section. Table 20 and Table 21 also show the proportion of AET (Eq. (17)) over the proportion of area (*A*), which allowed for a quick understanding of what classes had higher than average AET (those above unity) compared to classes which had lower than average AET (those below unity).

Table 20. Average land-use class relative rates of AET (mm/d), proportional AET, proportion of area, and the ratio of proportional AET to proportion of area are provided for the NSW site. Rank of land-use class metric is given in parentheses.

Land-use name	$\mathbf{AET}_i(mm/d)$	$\mathbf{AET}_i(prop)$	$A_i(prop)$	$\frac{\mathbf{AET}_i(prop)}{A_i(prop)}$
Native Vegetation	2.28 (3)	0.27 (2)	0.23 (2)	1.18 (3)
Unknown Plantation	2.48 (2)	0.05 (5)	0.04 (5)	1.29 (2)
Hardwood Plantation	1.48 (8)	<0.01 (9)	<0.01 (9)	0.77 (8)
Softwood Plantation	2.59 (1)	0.07 (4)	0.05 (4)	1.35 (1)
Dryland Cropping	1.45 (9)	0.09 (3)	0.12 (3)	0.75 (9)
Irrigation	2.17 (4)	<0.01 (8)	<0.01 (8)	1.13 (4)
Urban	1.75 (7)	0.02 (6)	0.02 (6)	0.91 (7)
Water	2.14 (5)	0.01 (7)	0.01 (7)	1.11 (5)
Grazing Modified Pasture	1.77 (6)	0.48 (1)	0.53 (1)	0.92 (6)
Total	2.28 (3)	1.00	1.00	1.00

Table 21. Average land-use class relative rates of AET (mm/d), proportional AET, proportion of area, and the ratio of proportional AET to proportion of area are provided for the SA site. Rank of land-use class metric is given in parentheses.

Land-use name	$\mathbf{AET}_i(mm/d)$	$\mathbf{AET}_i(prop)$	$A_i(prop)$	$\frac{\mathbf{AET}_i(prop)}{A_i(prop)}$
Native Vegetation	2.02 (4)	0.20 (2)	0.18 (2)	1.08 (4)
Unknown Plantation	1.92 (5)	0.01 (9)	<0.01 (9)	1.02 (5)
Hardwood Plantation	2.22 (2)	0.02 (7)	0.02 (7)	1.18 (2)
Softwood Plantation	2.23 (1)	0.12 (3)	0.10 (3)	1.19 (1)
Dryland Cropping	1.65 (9)	0.03 (5)	0.04 (5)	0.88 (9)
Irrigation	2.08 (3)	0.02 (8)	0.02 (8)	1.11 (3)
Urban	1.84 (6)	0.04 (4)	0.04 (4)	0.98 (6)
Water	1.80 (7)	0.02 (6)	0.03 (6)	0.96 (7)
Grazing Modified Pasture	1.77 (8)	0.54 (1)	0.57 (1)	0.94 (8)
Total	2.02 (4)	1.00	1.00	1.00

While the relative assessment of AET removes the influence of any particular land-use class' areal proportion, it does not consider that the land-uses may be biased based on how their spatial distribution coincides with environmental conditions. For example, a forested land-use may exist in a higher rainfall zone than a grassland class, on average. The previous summarisations in Table 18 and Table 19 show just this. To quantify this influence, we performed a paired analysis of the Softwood Plantation land-use class to both the Native Vegetation and Grazing Modified Pasture land-use classes. This paired analysis allowed for covariates such as P and PET to be accounted for and thus a way to statistically test whether the means and variances of these selected land-use classes were significantly different. The scatter plots of the mean AET for the two study sites are shown in Figure 37 and the statistical assessment is given in Table 22.

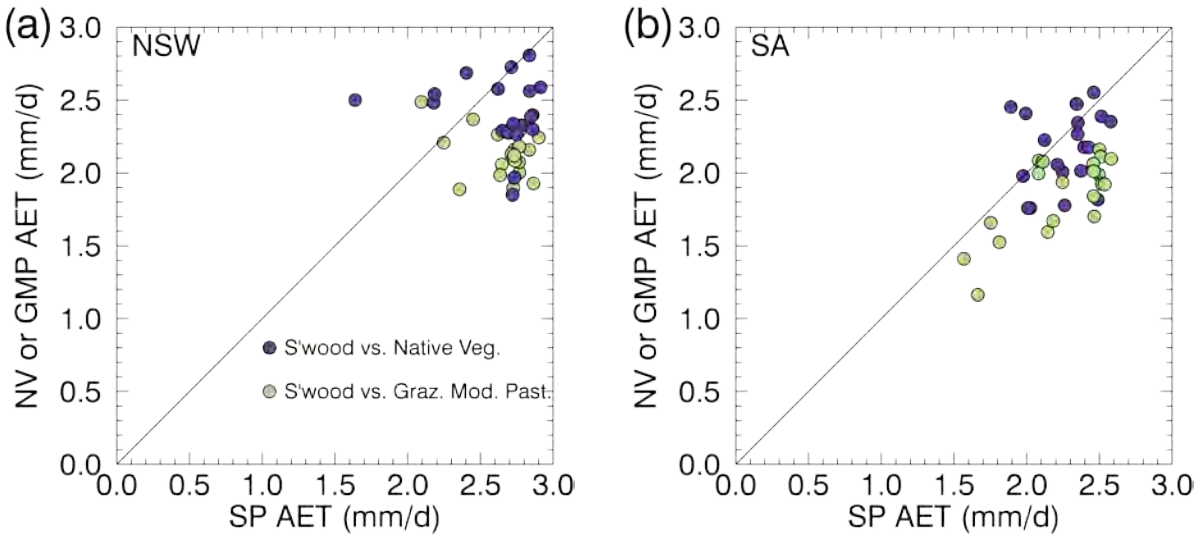

Figure 37. Softwood Plantation (SP) mean AET vs Native Vegetation (NV) or Grazing Modified Pasture (GMP) mean AET is shown for the paired analysis points for NSW in (a) and for SA in (b). The legend in (a) applies to (b).

In Figure 37, points falling below the one-to-one line represent those where Softwood Plantation had a higher mean AET than the other land-use that it was paired with (whether it be Native Vegetation or Grazing Modified Pasture). The points falling above the one-to-one line, conversely were those where either the Native Vegetation or the Grazing Modified Pasture AET was higher than that from the corresponding Softwood Plantation point. At both sites, there were on the order of 6 of the 20 points where Native Vegetation had a higher or roughly equivalent mean to that of Softwood Plantation, whereas only one or two Grazing Modified Pasture points had higher mean AET than their corresponding Softwood Plantation points (Figure 37). That is, the Softwood Plantation AET had a higher mean than the other two land-use classes for most of the point-pairs, especially when compared to the Grazing Modified Pasture class. The results of the statistical analysis showed that at the P=0.01 level, only Softwood Plantation vs. Grazing Modified Pasture had significantly different means, and this was found at both sites (Table 22). Neither site showed significant difference between means for Softwood Plantation vs. Native Vegetation at the P = 0.01 level and neither site showed significantly different variances for either comparison (Table 22). The difference between the Softwood Plantation and the Native Vegetation AET means was 'more significant' at NSW as this comparison would be significant at the P = 0.05 level (Table 22).

Table 22. Statistical summary of the paired analysis shows whether the mean or variance of Softwood points was significantly different to the mean or variance of either Native Vegetation or Grazing Modified Pasture at both study sites. For each assessment, the number of samples was n = 20. The values presented in the table define the probability that the mean analysis (t-test) or the variance analysis (F-test) was significant. Low probabilities (*e.g.*, < 0.01) would be more likely to demonstrate a significant difference than higher probabilities (*e.g.*, > 0.01).

Land-use comparison	Significance (probability)			
	NSW		SA	
	Means	Variances	Means	Variances
Softwood Plantation vs. Native Vegetation	0.0272290	0.235830	0.1541094	0.2618181
Softwood Plantation vs. Grazing Modified Pasture	0.0000004	0.237479	0.0000002	0.4573940

4 Discussion

Our study showed the importance of topographic correction when performing LM blending, especially for the NSW site, which had considerably more variation in topographic relief than the SA site (Figure 5 and Figure 9). At NSW, the illumination effect was stronger than the influence of the 2003 fire for much of the burned area (Figure 27). That is, illumination effect was a stronger influence on the AET algorithm than major land use change. This was an unanticipated result. Specifically, we found that the influence of illumination mainly altered the relationship between the NIR to the other bands, especially NIR to SWIR bands, and especially for Landsat data (as seen by the large and fairly constant difference in *k* parameters required to correct them, Figure 26b). The illumination influence between the NIR and SWIR bands mainly changed the GVMI, which uses those two bands (Eq. (6)). This change to GVMI, in turn impacted the estimate of AET, which heavily relies on the relative relationship between EVI and GVMI (Eq. (11)). So, while there may be other applications of blending remote sensing that may be less affected by the illumination influence, we suggest that these interactions be carefully checked due to the severity of the impact found in this current study. Also, for future studies using the CMRSET algorithm, we strongly suggest performing topographic correction first, especially if Landsat data are used and if the site has a good deal of topographic relief.

Blending Landsat and MODIS data results in optimal domain characteristics, (i.e., high spatial resolution and temporal density, see Table 1 and Figure 1 and for an example of the spatial resolution improvement, see Figure 22). It is important to note, however, that the domain characteristics of Table 1 and Figure 1 are not the same as accuracy. Accuracy is calculated by comparing model output to some reference, or validation dataset(s). So, while performing LM blending will improved domain characteristics, this improvement may be achieved at the cost of decreasing accuracy. To assess any potential accuracy loss, the blended AET models were compared to the Landsat-only AET model and the MODIS-only AET model (all assessed against validation datasets). LM blended data accuracy was slightly worse than that of using MODIS-only when either no bias correction or the original bias correction parameters were used. The Landsat-only AET dataset also slightly out-performed the non-bias corrected and the original bias corrected LM blended output at the flux tower and at the site water balance plots, but not over the area (catchment and reach) water balance (Table 15, Figure 28, and Figure 29). The reduced accuracy of the Landsat-only AET dataset was primarily a bias (Figure 29a), which was likely explained by the reduced temporal density of the Landsat data; that is, having fewer images to calculate a mean over can easily cause a biased result. A regional bias correction was defined, then, that allowed for the LM blended data to retain the high spatial resolution of Landsat and the high temporal density of MODIS without accuracy loss. The regional bias correction parameters were only a slight adjustment from the original parameters (Table 14). It is not known whether the need for bias correction parameter adjustment was due to the blending process or whether it was due to geographic specifics of the study sites, or due to both of these considerations.

In addition to the more formal validation, which provided accuracy assessment, evaluation was performed. Evaluation data were those not acquired in the same physical units as AET, yet were able to be related to (or allow for the summarisation of) the process of AET and provide a means of assessing AET from a catchment management and/or forestry perspective. These were semi-quantitative in nature and simply assessed whether summarisations of AET seemed reasonable, thus bolstering confidence in the model output. Evaluation of the LM blended AET dataset showed that the model was able to: (*i*) delineate the 2003 fire at the NSW site well by calculating the minimum z-score for the year on a pixel-wise basis and demonstrated a reduced yearly average AET within the fire boundary (Figure 30); (*ii*)

differentiate between *E. globulus* and *P. radiata* growth rates, and differentiate between thinned and unthinned *P. radiata* at the SA study site (Figure 31); and (*iii*) define the amount of water used to increase the volume of unthinned *P. radiata* plots at the NSW site (). *P. radiata* at the SA site reached an average AET maximum plateau after about 6 years (Figure 31a), which is consistent with the findings of Webb and Kathuria (2012), who found that the Red Hill *P. radiata* plantation reached full canopy closure at 6 years old after which stream flow declined. Overall, the evaluation of the LM blended data bolstered confidence that the model was behaving sensibly.

The land-use specific AET assessment included volumetric totals of AET in units of GL/d, relative measures of AET to P and AET to PET (which provided important hydrological and surface energy context, respectively), and also relative measures of AET in units of mm/d. The relative assessment of AET (mm/d) removed the influence of area (not including any indirect effects due to potential errors for those classes which are inordinately small). The volumetric summary of AET considers the total area of each land-use class when calculating the mean AET and so for both sites, the Grazing Modified Pasture and the Native Vegetation land-use classes had the highest two average volumetric AET, respectively, due to their inordinately large areal proportions (Table 18 and Table 19). Dryland Cropping volumetric AET (GL/d) was higher than Softwood plantation in NSW and higher than Hardwood plantation in SA (Table 18 and Table 19). Of note, the water land-use class did not come out at the highest relative rate of AET (mm/d) for either site, but rather fifth at NSW and seventh at SA (Table 20 and Table 21). This is likely largely due to water having such a small proportion of area at both sites (see Table 17), making any spatial error in co-registration between the land-use map and the AET output potentially problematic when calculating class averages. Also the water land-use class would not be 100% covered with water through the entire temporal extent of the study (this is the difference between land-use and land cover), meaning that AET from a water land-use class should not be interpreted to mean that this is evaporation from water. To help understand our point, we provide the following forestry example. If a softwood plantation is harvested, it would still fall within the softwood plantation land-use class even though it no longer has any tree cover. In that case, assessing AET from the component of harvested softwood plantation should not be interpreted as the evaporation from some species of softwood tree. So, while the evaporation is coming from the softwood plantation land-use class, in that case, the evaporation is not coming from a stand of softwood trees. Notwithstanding, at 1.80 mm/d, the average rate of water land-use class AET at the SA site, in particular, seems lower than expected (Table 21). When the land-use specific assessment summarised AET/P the classes with the highest AET/P were Irrigation and Water at NSW (Table 18) and Hardwood and Softwood plantation at SA (Table 19). The high AET/P land-use classes at NSW had exceedingly small proportional areas, which reduces the certainty that they were hydrologically meaningful, however (Table 17). Regardless, the metric of AET/P was important to summarise and warrants further discussion.

As described in the introduction, the ability for a surface to evaporate is often described by the energy and moisture available (the so-called, water and energy-limits frameworks). To first order, these two covariates (water and energy) are the most generically important covariates to AET. Over the long-term and/or over spatial averages, these are well described by P and PET. The ratio of AET/P or AET/PET are both referred to as the evaporative fraction and these provide important hydrological and surface energy context, respectively. Therefore, these two evaporative fractions were used as part of the land-use assessment. AET/P, in particular, provided vital hydrological context with respect to that assessment as over the long-term when AET/P > 1, then (ignoring any potential errors) extra water than precipitation from directly above would need to be accessed. This extra water could come from irrigation or lateral inflow either above or below ground. Above ground later inflow

would be due to overland flow of precipitation due to topographic considerations, which could either be evaporated at the surface (if it resulted in standing water) or could infiltrate (if the soil was not saturated) where it could be accessed as long as it remained in the root zone. Regardless, of whether it was above or below ground, the important thing is that lateral inflow was originally precipitation that fell at a different location than where it eventually evaporated from. Likewise, AET/P > 1 could also indicate that the extra water stored in the soil profile or groundwater could be from precipitation that fell at the same location, but at a different time (before the study period began). So, there are spatial and temporal considerations and surface and ground water hydrologic considerations that make the source of this extra water hard to determine. Also, model error (especially bias) makes reliance upon such precise calculation of the evaporative fractions tenuous. So, we have not defined a simple rule that any land-use class that had a long-term average AET/P > 1 was accessing ground water. It would be naïve to assume so. With that said, for land-use classes having AET/P > 1 in the long-term, it indicates that some extra water source is being accessed. One likely source is ground water. To do so with more confidence, however, a sensitivity analysis of the impact of error (*e.g.* bias) on AET/P would need to be done.

Considering the qualifying remarks made above, there were some interesting overall statements that can be made with a certain higher degree of confidence about the AET/P results. These can be made with higher certainty because they rely primarily on the relative rather than on the absolute comparisons between AET and P at both sites and also because they mainly rely on long-term and large-area averages, which reduces the influence of errors (excepting bias). Firstly, the mean total AET/P was higher at SA (1.02) than NSW (0.95), Table 18 and Table 19. This suggests that the SA site is more likely accessing groundwater than the NSW site. This generally matches a hydrological understanding of the two sites as the NSW site is more likely driven by surface hydrology given its steep terrain and further distance to water table and the SA site is more characterised by flat terrain and shallower distances to the water table. Secondly, both sites had a great deal of spatial variability in AET/P across the plantation land-use classes and both had areas within the plantation class where AET/P was well below 1 and where AET/P was well above 1 (Figure 35). At both sites, the summarisation of AET/P seems to effectively identify areas within the forestry plantations where there is higher likelihood of trees accessing groundwater compared to areas where there is lower likelihood of trees accessing groundwater (Figure 35). When considered this way, the AET/P summarisation could be a very useful management tool to identify areas where groundwater use is likely and vice-versa, areas where groundwater use is unlikely. At SA, in particular, the overall aridity index gradient being lower aridity from the southwest coastline to higher inland aridity towards the northeast of the study site seems to explain the overall pattern of likelihood of groundwater use (Figure 10c and b). There is also a great deal of variability above this overall pattern, though, that would be critical for management and forming policy decisions (Figure 35). Finally, the period of record of our study covered the so-called Millennium drought, which could impact the AET and evaporative fraction results of our study in at least two ways: it could potentially (1) cause an underestimation of land use water use due to the water limitation caused by an extended drought; and (2) alter the proportion of AET/P and or AET/PET compared to a time period that is more representative of long term mean climatic conditions. The overall backdrop of the Millennium drought on the interactions between AET and the energy and water balances should be kept in mind when interpreting the results of this study.

5 Conclusions

Landsat-MODIS blending using the ESTARFM algorithm, implemented in a hierarchical approach to infill cloud effected pixels, can generate a time-series of imagery with both high-spatial resolution (25 m) and high-temporal frequency (8-day) that are suitable for input into the CMRSET algorithm. The output of this algorithm were AET estimates across all land-uses contained in the two study sites. Validation with all available in situ measurements from both study sites (including catchment and reach water balances, flux tower and site water balances) revealed that the resultant AET grids were highly accurate. Evaluation with forestry management and 'environmental variability' datasets confirmed that the resultant AET grids were fit-for-purpose to calculate land-use-specific AET summaries.

Stratifying the AET time series grids by nine land-uses revealed that volumetrically, both agricultural and native vegetation areas used more water than forestry plantation at both study sites. At both sites, Grazing Modified Pasture, Native Vegetation, and Dryland Cropping used more total water than any of the forestry plantation land-use classes. Even when all forestry plantation land-use types were combined, they still used less total water than the Grazing Modified Pasture and Native Vegetation classes. We found that the main forestry plantation land-use classes had the highest relative rates of AET (mm/d) at both sites, but that this assessment was biased due to the plantations being planted in high precipitation (P) areas. Paired analysis of Softwood Plantation vs. Native Vegetation at both sites showed no significant difference between means at the $p = 0.01$ level (n = 20).

Summarisation of AET/P within the assessment of land-use specific-AET provided critical hydrological context that was absent when AET was summarised simply based on rate of AET (mm/d) or based on volume (GL/d). At NSW, the main forestry plantation land-use classes by area were low water users when normalised by precipitation; Softwood and Unknown Plantations ranked 6th and 8th out of 9 classes when water use was summarised by AET/P and both of these classes' average AET/P was below unity (being 0.98 and 0.89, respectively). In contrast, for the SA site, the two main forestry plantation land-use classes by area were high water users when normalised by precipitation; Softwood and Hardwood Plantations ranked 1st and 2nd out of 9 when water use was summarised by AET/P and both of these classes' average AET/P was above unity (being 1.19 and 1.14). This indicated that forestry plantation water use needs to be considered on a site-by-site basis.

Further, we found that there was high variability of AET/P across the forestry plantations, so forestry water use should not be treated uniformly even over a single study site. For the NSW site, only 6.9% of the area had AET > P, located mainly along the Murrumbidgee and other river courses, water bodies, and a few forested areas. At SA, 37% of the site had AET > P, and this was more strongly associated with the forestry plantations than at the NSW site. While these findings suggest greater probability of groundwater usage in the SA site, it is important to interpret these long-term AET/P summaries within the context of the data used to estimate AET (and P), the model framework and assumptions, and in terms of the hydrology. With that understood, it was indicated that the AET/P data might be useful for assessment of identifying those plantations that use higher than expected water in regions where AET/P is generally lower than unity (e.g., NSW) or those plantations that use lower than expected water in regions where AET/P is generally above unity (e.g., SA), thus being directly useful for informing management and policy decisions.

Importantly for the objectives of this project the Landsat-MODIS blended AET/P and MODIS AET/P had similar spatial pattern and values. This meant that we were able to generate high-resolution and high-frequency AET grids without sacrificing AET accuracy. This is important when needing to monitor AET rates across environments and management systems where AET can be highly spatially and temporally variable.

This project developed an in-house software system to perform Landsat-MODIS blending on a magnitude (across time and space) never before attempted globally elsewhere; compare our study sites spatial and temporal extents with those reported in Table 2. These ETa datasets were validated with all available independent datasets and by assessing suitable landscape patterns, both spatially and temporally. They were then use to provide land-use-specific summaries of AET, including: (i) volumetric totals of AET; (ii) relative rates of AET; (iii) normalised AET relative to P; (iv) normalised AET relative to PET; and (v) paired analysis of adjacent equal-sized selected land-use types. With agreement of FWPA and our FWPA Project Steering Committee it is has been decided that the Landsat-MODIS blending ETa datasets developed in this project will be made freely available on the CSIRO Data Access Portal (DAP) once the journal paper from this research is officially accepted by the target journal. Currently the skills and 'know-how' to do this massive processing task solely rests with the project team. This means they would need to be engaged to perform this processing over new areas or to extend the temporal domain at each of the two study sites developed herein. However, the project team would prefer to assist working with software engineers / system architects to progress the development of the current research-focused Landsat-MODIS blending system into a more operational and accessible blending system housed on the National Computing Infrastructure (NCI). Discussions are currently underway within CSIRO regarding the potential of this. Developing a more operational and accessible blending system would build on this project, and would additionally build upon the more 'fundamental' investments made by: (i) CSIRO to parallelise the blending algorithm and to develop the MODIS 'data-cube'; (ii) Geoscience Australia to develop the Landsat 'data-cube' (including its geometric, atmospheric and topographic corrections); and (iii) the NCI to develop and maintain a computing facility that allows these types of processing jobs with demanding computational requirements, being data access, storage, memory and processing power.

6 Recommendations and Future Work

The following recommendations and suggestions for future work can be made following this project. Noting that the primary project aim was to develop a long-term dataset of remotely sensed AET estimates at suitable spatial resolution and temporal frequency. While there are many ways such a dataset can be used to address issues of water allocation, water accounting and land-use-specific water management, both within and between forestry, agriculture and other sectors, implementing these is future work beyond the scope of this project.

1) Current measurements of water-use for irrigation areas are performed and such data would have been a valuable source of validation data for land-uses other than forestry. While such water-use data are measured as part of operational irrigation water supply, the project team was unable to access any land-holder data due to privacy concerns. While these data need to be spatially-explicit to perform validation of the Landsat-MODIS 25 m resolution AET grids, to negate the concerns about privacy, we suggested that these results can be visualised as a 'X-Y' plot so that the locations and amounts of water used are not spatially revealed. This was explained to irrigators yet none were willing to share their data for this scientific project. To resolve this issue likely requires a concerted effort from relevant State Government agencies to facilitate a data access agreement, thereby allowing land-use-specific AET estimates to be validated for a wider range of land-uses.

2) Topographic correction of Landsat data prior in areas of high relative relief needs to be implemented before running the AET algorithm. Not performing the topographic correction means that the results from the CMRSET AET algorithm could not effectively delineate major land-cover change (i.e., fire) in our study, as the illumination effects dominated the signal. In the Geoscience Australia Landsat 'data-cube', which is the primary Landsat data source now being used in Australia, this correction is currently being performed and will available in the next update. The Landsat-MODIS blending system developed in this FWPA has the potential to become an operational system. This follows much investment by CSIRO to parallelise the blending algorithm and to develop the MODIS 'data-cube' and by Geoscience Australia developing the Landsat 'data-cube'. Discussions are currently underway within CSIRO regarding how to progress the development of the current research-focused Landsat-MODIS blending system into a more operational and accessible system housed on the National Computing Infrastructure (NCI).

3) To strengthen the confidence in the AET results generated here it would be possible (yet is non-trivial and beyond to scope of contracted project) to generate associate gridded error surface estimates for the remotely sensed based AET algorithms at the Landsat resolution and the 8-day time step produced here. Where and when we have independent validation data (e.g., flux tower and stream flow data) we have used these to characterise the AET errors. To develop the proposed associate error surface grids there are two main sources of error that would need to be accounted for: (i) error from the Landsat-MODIS blending algorithm which are used to blend the indices required by the CMRSET algorithm; and (ii) error and uncertainty from the input precipitation grids and meteorological grids used as input to calculate the PET grids which the remote sensing indices scale to estimate AET. Implementing (i) is a major undertaking (1-2 years of work) as none of the international groups involved in developing remote sensing blending algorithms has done this. These international groups (CSIRO included) have performed 'sensitivity type' analysis to characterise the errors. This is done by having three sequential Landsat images, simulating the middle one and comparing it against the observations for the middle Landsat image. To date, there is no routine way to estimate blending error as part of the blending process and considerable effort developing an approach and an algorithm (with associated debugging and

testing) would be needed. Propagating error associated with the PET grids is a moderate undertaking and would take in the vicinity of 3-6 months.

4) To further strengthen the confidence in the AET results generated here it would be possible to implement remote sensing AET algorithms using: (i) resistance based models (which use remotely sensed land surface temperature to solve the surface energy balance) and/or (ii) conductance based models (which use remotely sensed reflective data to provide key vegetation biophysical parameterisations). If one method were implemented over a similar time-frame at a similar spatial resolution, as performed here, this provides the means to cross-check the two products. However, only have two estimates essentially provides information on the differences between them, and to increase the utility and to allow the opportunity for implementing sophisticated techniques if both approaches were used this would allow the triple collocation approach to be applied to rigorously assess the error and uncertainty both spatially and temporally. If only one approach was to be funded we advocate the use of the land surface temperature / surface energy balance approach as reflective bands are used in the model here, and decoupling of the atmosphere and forest canopy will result in increases of surface temperature that are more transient than changes in vegetation biophysical parameters.

5) Land-use specific water-use needs to be viewed in the broader catchment water balance assessment. The time-series of (i.e., high-resolution) 25-m 8-day AET grids represents the longest / largest spatial-temporal domain that MODIS-Landsat blended data have been used to estimate AET anywhere globally. Given this it would seem judicious for this resource to be further used to understand the dynamics of numerous ecohydrological processes in the study sites including: (i) assessing forestry water-use efficiency; (ii) understanding shallow water-table dynamics and AET rates (more relevant for the SA site); (iii) assessing groundwater usage by forested landscapes; and (iv) allowing forestry agencies to assess the impact of their management options in terms of water-use. These four items are briefly discussed, in turn, below.

6) The high-resolution AET grids generated here can be combined with forestry biomass data, including both growth field surveys and LiDAR (Light Detection And Ranging) measurements, to assess the water-use efficiency of the forestry plantations. This would likely reveal very relevant information regarding the efficiencies of management decisions and how they are implemented.

7) The SA site experiences a Mediterranean climate with numerous ephemeral water-logged areas appearing across the landscape over winter which persist to mid-Spring (depending on the climate variability). These ephemeral areas likely constitute a relatively large water-use across the region, and for many it is unknown how large an area they effectively drain and what volume of water (and proportion of the regional water balance) they return to the atmosphere via AET. To complement this analysis it would be best if very high resolution (i.e., in the order of 1-5 m) digital surface model (DSM i.e., with the effect of vegetation and other above-ground structures removed) were available regionally. Such a DSM would likely best be acquired using LiDAR imagery.

8) The spatial patterns of the long-term AET/P output suggests there is information on groundwater usage between land-uses and within the forestry land-use class. This information can be used to inform conceptual models of the subsurface hydrology, and also can constrain numerical models of the coupled groundwater-surface water systems (including their degree of connectivity and interactions) at both sites. The spatial variability in the vegetation water-usage (in excess of P) within the forested landscapes can be integrated with forestry management to possibly reveal new information across both sites about forested

groundwater usage. This AET/P grid could be classified into groups of likely groundwater usage, for example, if ETa/P > 1.4 that part of the landscape could be identified as 'very likely' to be using groundwater, if 1.4 > ETa/P > 1.3 then 'highly likely', if 1.3 > ETa/P > 1.2 then 'moderately likely', if 1.2 > ETa/P > 1.1 then 'possible' and if 1.1 > ETa/P > 1.0 then 'within the bounds of data uncertainty'. Obviously closer examination of the thresholds would be needed; these are examples only to provide clarity for the Project Steering Committee.

9) In both sites there exists the ability to integrate these high-spatial resolution (25 m) and high temporal frequency (8-day) AET estimates to better understand how forestry management practices have impacted the site water-usage. For example, the AET of paired sites (that are adjacent to minimise precipitation differences and the same size) with different planting density and/or thinning regimes can be tracked in the AET dataset. This unique dataset, when combined with forestry agencies historic management systems, may allow forestry management agencies to better consider water-usage when planning and implementing their operations. Noting that forestry management needs to account for numerous time-scales in the decision making process, and that multiple criteria encompassing the 'triple-bottom-line' need to be considered when implementing daily to decadal forestry management.

10) Finally, if finer resolution management and growth dynamics and water use are required, then scale appropriate field measurement of actual water use data need to be collected and made available to support this. Also, remote sensing currently does not provide structurally specific AET rates in forestry. Therefore, field measurement that partitions stand-level AET into structurally specific components would be particularly crucial for both calibration and validation of future spatio-temporal modelling using remote sensing.

7 Acknowledgements

This project was funded by Forest and Wood Products Australia (FWPA), ForestrySA, and CSIRO Land and Water. We thank all members of the project steering committee for valuable comments and assistance, they include: (i) Dr Chris Lafferty (FWPA, R&D Manager); (ii) Dr Mike Sutton (Manager, Forest Information and Planning, Forestry Corporation of NSW); (iii) Dr Ashley Webb (formerly Forests NSW, Research Scientist - Water and Forests, currently Leader, Soils North, Agriculture NSW, Senior Research Scientist, NSW Department of Primary Industries); (iv) Dr Jim O'Hehir (General Manager, Ranges & Research, ForestrySA); (v) Dr Mike Powell (ForestrySA, Manager Research); and (vi) Dr Don McGuire (formerly ForestrySA, Principal Scientist Research, currently Executive Environmental Consultant). Special thanks to Dr Mike Sutton and Dr Don McGuire for each spending time with the project team providing full and interesting / informative three day sessions of site familiarisation for the NSW site and SA site, respectively.

Dr Duncan Watt (Planning Manager, Snowy Region, Forestry Corporation of NSW) for speedy provision and responding to all questions quickly regarding forestry management and planning data for the Tumut area. Thanks to Dr Mike Sutton for raising the profile of our project with the Tumut office.

Mr Brad Jarrett (Technical Officer, Forestry Corporation of NSW) for providing the Red Hill catchment vegetation plots of observed productivity in the Tumut area. Plus thanks for showing us 'Smiley-the-Tree' when walking to the last stream flow gauge for the day during our field-visit to the Tumbarumba area.

Dr Lisa Turner (Project Officer, Forestry Corporation of NSW) for provision of stream flow data in the Tumut area.

Dr Glen Rivers (One-Forty-One) and Dr Dionisio Battad (Manager GIS, ForestrySA) for approval and provision, respectively, of forestry management data in the One-Forty-One / ForestrySA operated estate. Thanks to both Dr Jim O'Hehir and Dr Mike Powell for raising the profile of our project with One-Forty-One.

Dr Tanya Doody, CSIRO Land and Water, Adelaide, for: (i) travelling back to the 'Green Triangle' and locating the water balance field sites with an accuracy of about 5 m for use with the high resolution (i.e., 25 m) AET estimates generated here; and (ii) for answering numerous questions about how the data were measured and processed.

Dr Irina Emelyanova, formerly with CSIRO Land and Water and now with CSIRO Energy, who provided the project team with a much greater understanding of the blending algorithms used in this research.

Dr Jane Stewart and Dr Lucy Randall (both from Natural Resources Branch, ABARES (Australian Bureau of Agricultural and Resource Economics and Sciences), Department of Agriculture) for answering questions about the best nationally-consistent land-use datasets available.

Dr Alex Ip and Dr Leo Lymburner (both with the National Earth Observation Group, Environmental Geoscience Division, Geoscience Australia) for making the Landsat data available on the National Computing Infrastructure (NCI) facility.

Dr Luke Domanski (formerly with CSIRO Advanced Scientific Computing, CSIRO Information Management and Technology) for parallelisation of the ESTARM code and linking this with GDL to optimally run on the NCI or any other parallel computing facility. The continued support of Dr Sam Moskwa (Novel Technology Manager, CSIRO Advanced Scientific Computing, CSIRO Information Management & Technology) was essential.

Dr Robert Bell (High Performance Computing National Partnerships, Scientific Computing, CSIRO Information Management and Technology) for ensuring that our project always had the disk space and CPU requirements needed (sometimes at short notice) for run the ESTARFM blending on the NCI.

National Computing Infrastructure staff responded to all emails very quickly and sought to minimise any down-time to ensure that the ESTARFM processing occurred with minimal disruption.

Dr Matt Paget (CSIRO Land and Water) and Dr Edward King (CSIRO Oceans and Atmosphere) for maintaining the MODIS pipeline and quickly responding to any questions we had about the MODIS data used here.

Dr Jorge Peña-Arancibia and Dr Yongqiang Zhang (both Surface Water, Research Scientists, CSIRO Land and Water) for access to river reach data and gap-filled stream flow datasets, respectively.

Associate Professor Patrick Lane, School of Ecosystem and Forest Sciences, The University of Melbourne, a FWPA-appointed independent reviewer of this report, made many valuable suggestions that help improve this research.

Thanks for support from relevant CSIRO managers, being Dr Glen Walker and Dr Lu Zhang at the proposal stage through to Dr Warwick McDonald / Dr Peter Stone and Dr Francis Chiew / Dr Glenn Newnham at the completion stage.

8 References

ABARES. (2011) Part 2-The Australian Land Use and Management Classification' in Guidelines for land use mapping in Australia: principles, procedures and definitions. *fourth edition, Australian Bureau of Agricultural and Resource Economics and Sciences, Canberra*: data.daff.gov.au/anrdl/metadata_files/pe_abares99001806.xml.

Almeida, A. C. and Sands, P. J. (2016) Improving the ability of 3-PG to model the water balance of forest plantations in contrasting environments. *Ecohydrology 9*: 610-630.

Anderson, M. C., Kustas, W. P., Alfieri, J. G., Gao, F., Hain, C., Prueger, J. H., Evett, S., Colaizzi, P., Howell, T. and Chavez, J. L. (2012) Mapping daily evapotranspiration at Landsat spatial scales during the BEAREX'08 field campaign. *Advances in Water Resources 50*: 162-177. doi:10.1016/j.advwatres.2012.06.005

Anderson, M. C., Kustas, W. P. and Norman, J. M. (2007) Upscaling flux observations from local to continental scales using thermal remote sensing. *Agronomy Journal 99*(1): 240-254. doi:10.2134/agronj2005.0096S

Anderson, M. C., Kustas, W. P., Norman, J. M., Hain, C. R., Mecikalski, J. R., Schultz, L., Gonzalez-Dugo, M. P., Cammalleri, C., d'Urso, G., Pimstein, A. and Gao, F. (2011) Mapping daily evapotranspiration at field to continental scales using geostationary and polar orbiting satellite imagery. *Hydrology and Earth System Sciences 15*(1): 223-239. doi:10.5194/hess-15-223-2011

Bastiaanssen, W. G. M., Menenti, M., Feddes, R. A. and Holtslag, A. A. M. (1998) A remote sensing surface energy balance algorithm for land (SEBAL) - 1. Formulation. *Journal of Hydrology 213*(1-4): 198-212.

Benyon, R. G. and Doody, T. M. (2015) Comparison of interception, forest floor evaporation and transpiration in Pinus radiata and Eucalyptus globulus plantations. *Hydrological Processes 29*(6): 1173-1187. doi:10.1002/hyp.10237

Benyon, R. G., Theiveyanathan, S. and Doody, T. M. (2006) Impacts of tree plantations on groundwater in south-eastern Australia. *Australian Journal of Botany 54*(2): 181-192. doi:10.1071/bt05046

Budyko, M. I. (1974). Climate and life. Academic, New York. pp.

Calder, I. R. (1986) Water-Use of Eucalypts - A Review With Special Refernce to South-India. *Agricultural Water Management 11*(3-4): 333-342. doi:10.1016/0378-3774(86)90049-1

Calder, I. R., Hall, R. L. and Prasanna, K. T. (1993) Hydrological Impact of Eucalyputs Plantation in India. *Journal of Hydrology 150*(2-4): 635-648. doi:10.1016/0022-1694(93)90129-w

Cammalleri, C., Anderson, M. C., Gao, F., Hain, C. R. and Kustas, W. P. (2013) A data fusion approach for mapping daily evapotranspiration at field scale. *Water Resources Research 49*(8): 4672-4686. doi:10.1002/wrcr.20349

Cammalleri, C., Anderson, M. C., Gao, F., Hain, C. R. and Kustas, W. P. (2014) Mapping daily evapotranspiration at field scales over rainfed and irrigated agricultural areas using remote sensing data fusion. *Agricultural and Forest Meteorology 186*: 1-11. doi:10.1016/j.agrformet.2013.11.001

Ceccato, P., Flasse, S. and Gregoire, J. M. (2002a) Designing a spectral index to estimate vegetation water content from remote sensing data - Part 2. Validation and applications. *Remote Sensing of Environment 82*(2-3): 198-207. doi:10.1016/s0034-4257(02)00036-6

Ceccato, P., Gobron, N., Flasse, S., Pinty, B. and Tarantola, S. (2002b) Designing a spectral index to estimate vegetation water content from remote sensing data: Part 1 - Theoretical approach. *Remote Sensing of Environment 82*(2-3): 188-197.

Chen, B., Ge, Q., Fu, D., Yu, G., Sun, X., Wang, S. and Wang, H. (2010) A data-model fusion approach for upscaling gross ecosystem productivity to the landscape scale based on remote sensing and flux footprint modelling. *Biogeosciences 7*(9): 2943-2958. doi:10.5194/bg-7-2943-2010

Dong, T., Liu, J., Qian, B., Zhao, T., Jing, Q., Geng, X., Wang, J., Huffman, T. and Shang, J. (2016) Estimating winter wheat biomass by assimilating leaf area index derived from fusion of Landsat-8 and MODIS data. *International Journal of Applied Earth Observation and Geoinformation 49*: 63-74. doi:http://dx.doi.org/10.1016/j.jag.2016.02.001

Donohue, R. J., McVicar, T. R. and Roderick, M. L. (2009) Climate-related trends in Australian vegetation cover as inferred from satellite observations, 1981–2006. *Global Change Biology 15*(4): 1025-1039.

Donohue, R. J., McVicar, T. R. and Roderick, M. L. (2010) Assessing the ability of potential evaporation formulations to capture the dynamics in evaporative demand within a changing climate. *Journal of Hydrology 386*(1-4): 186–197. doi:doi:10.1016/j.jhydrol.2010.03.020

Donohue, R. J., Roderick, M. L. and McVicar, T. R. (2007) On the importance of including vegetation dynamics in Budyko's hydrological model. *Hydrology and Earth System Sciences 11*(2): 983-995.

Donohue, R. J., Roderick, M. L. and McVicar, T. R. (2008) Deriving consistent long-term vegetation information from AVHRR reflectance data using a cover-triangle-based framework. *Remote Sensing of Environment 112*(6): 2938-2949.

Duan, Q. Y., Sorooshian, S. and Gupta, V. K. (1994) Optimal Use of the SCE-UA Global Optimization Method for Calibrating Watershed Models. *Journal of Hydrology 158*(3-4): 265-284. doi:10.1016/0022-1694(94)90057-4

Dutta, D., Kim, S., Hughes, J., Vaze, J. and Yang, A. (2015) AWRA-R v5.0 Technical Report. *CSIRO Land and Water, Australia*: 92.

Dye, P. (2013) A review of changing perspectives on Eucalyptus water-use in South Africa. *Forest Ecology and Management 301*: 51-57. doi:10.1016/j.foreco.2012.08.027

Dye, P. and Versfeld, D. (2007) Managing the hydrological impacts of South African plantation forests: An overview. *Forest Ecology and Management 251*(1-2): 121-128. doi:10.1016/j.foreco.2007.06.013

Emelyanova, I. V., McVicar, T. R., Van Niel, T. G., Li, L. T. and Van Dijk, A. I. J. M. (2012) On blending Landsat-MODIS surface reflectances in two landscapes with contrasting spectral, spatial and temporal dynamics. *WIRADA Project 3.4: Technical Report. CSIRO: Water for a Healthy Country Flagship, Canberra, Australia.*: 72 https://publications.csiro.au/rpr/pub?list=SEA&pid=csiro:EP128838.

Emelyanova, I. V., McVicar, T. R., Van Niel, T. G., Li, L. T. and Van Dijk, A. I. J. M. (2013) Assessing the accuracy of blending Landsat–MODIS surface reflectances in two landscapes with contrasting spatial and temporal dynamics: A framework for algorithm selection. *Remote Sensing of Environment 133*: 193-209.

Everson, C. S., Dye, P. J., Gush, M. B. and Everson, T. M. (2011) Water use of grasslands, agroforestry systems and indigenous forests. *Water Sa 37*(5): 781-788. doi:10.4314/wsa.v37i5.15

Ferraz, S. F. B., Lima, W. D. and Rodrigues, C. B. (2013) Managing forest plantation landscapes for water conservation. *Forest Ecology and Management 301*: 58-66. doi:10.1016/j.foreco.2012.10.015

Fu, D., Chen, B., Zhang, H., Wang, J., Black, T. A., Amiro, B. D., Bohrer, G., Bolstad, P., Coulter, R., Rahman, A. F., Dunn, A., McCaughey, J. H., Meyers, T. and Verma, S. (2014) Estimating landscape net ecosystem exchange at high spatial–temporal resolution based on Landsat data, an improved upscaling model framework, and eddy

covariance flux measurements. *Remote Sensing of Environment 141*: 90-104. doi:http://dx.doi.org/10.1016/j.rse.2013.10.029

Fu, D., Zhang, L., Chen, H., Wang, J., Sun, X. and Wu, T. (2015) Assessing the Effect of Temporal Interval Length on the Blending of Landsat-MODIS Surface Reflectance for Different Land Cover Types in Southwestern Continental United States. *ISPRS International Journal of Geo-Information 4*(4): 2542-2560; doi:2510.3390/ijgi4042542.

Gallant, J. C., Dowling, T. I., Read, A. M., Wilson, N., Tickle, P. and Inskeep, C. (2011) 1 second SRTM Derived Digital Elevation Models User Guide. *Geoscience Australia*: 106, www.ga.gov.au/topographic-mapping/digital-elevation-data.html.

Gao, F., Masek, J., Schwaller, M. and Hall, F. (2006) On the blending of the Landsat and MODIS surface reflectance: Predicting daily Landsat surface reflectance. *IEEE Transactions on Geoscience and Remote Sensing 44*(8): 2207-2218.

Glenn, E. P., Doody, T. M., Guerschman, J. P., Huete, A. R., King, E. A., McVicar, T. R., Van Dijk, A., Van Niel, T. G., Yebra, M. and Zhang, Y. Q. (2011) Actual evapotranspiration estimation by ground and remote sensing methods: the Australian experience. *Hydrological Processes 25*(26): 4103-4116.

Glenn, E. P., Nagler, P. L. and Huete, A. R. (2010) Vegetation Index Methods for Estimating Evapotranspiration by Remote Sensing. *Surveys in Geophysics 31*(6): 531-555.

Guerschman, J. P., Van Dijk, A. I. J. M., Mattersdorf, G., Beringer, J., Hutley, L. B., Leuning, R., Pipunic, R. C. and Sherman, B. S. (2009) Scaling of potential evapotranspiration with MODIS data reproduces flux observations and catchment water balance observations across Australia. *Journal of Hydrology 369*(1-2): 107-119.

Huete, A., Didan, K., Miura, T., Rodriguez, E. P., Gao, X. and Ferreira, L. G. (2002) Overview of the radiometric and biophysical performance of the MODIS vegetation indices. *Remote Sensing of Environment 83*(1-2): 195-213.

Jarihani, A. A., McVicar, T. R., Van Niel, T. G., Emelyanova, I. V., Callow, J. N. and Johansen, K. (2014) Blending Landsat and MODIS Data to Generate Multispectral Indices: A Comparison of "Index-then-Blend" and "Blend-then-Index" Approaches. *Remote Sensing 6*(10): 9213-9238. doi:10.3390/rs6109213

Jia, Z., Liu, S., Xu, Z., Chen, Y. and Zhu, M. (2012) Validation of remotely sensed evapotranspiration over the Hai River Basin, China. *Journal of Geophysical Research - Atmospheres 117*: D13113, doi:13110.11029/12011JD017037.

Jones, D. A., Wang, W. and Fawcett, R. (2009) High-quality spatial climate data-sets for Australia. *Australian Meteorological and Oceanographic Journal 58*(4): 233-248.

Kalma, J. D., McVicar, T. R. and McCabe, M. F. (2008) Estimating Land Surface Evaporation: A Review of Methods Using Remotely Sensed Surface Temperature Data. *Surveys in Geophysics 29*(4-5): 421-469.

King, E. A., Van Niel, T. G., van Dijk, A. I. J. M., Wang, Z., Paget, M. J., Raupach, T., Guerschman, J. P., Haverd, V., McVicar, T. R., Miltenburg, I., Raupach, M. R., Renzullo, L. J. and Zhang, Y. Q. (2011) Actual evapotranspiration estimates for Australia: Inter-comparison and evaluation. *CSIRO: Water for a Healthy Country Flagship Technical Report, Canberra, Australia.*: 150, https://publications.csiro.au/rpr/download?pid=csiro:EP132275&dsid=DS132278.

Lerat, J., Dutta, D., Kim, S., Hughes, J., Vaze, J. and Dawes, W. (2013) Refinement and extension of the AWRA-R model. *CSIRO: Water for a Healthy Country National Research Flagship, Australia*: 64 pp. Viewed 17 December 2015, https://publications.csiro.au/rpr/download?pid=csiro:EP136859&dsid=DS136856.

Leuning, R., Cleugh, H. A., Zegelin, S. J. and Hughes, D. (2005) Carbon and water fluxes over a temperate Eucalyptus forest and a tropical wet/dry savanna in Australia: measurements and comparison with MODIS remote sensing estimates. *Agricultural*

and Forest Meteorology 129(3–4): 151-173. doi:http://dx.doi.org/10.1016/j.agrformet.2004.12.004

Leuning, R., van Gorsel, E., Massman, W. J. and Isaac, P. R. (2012) Reflections on the surface energy imbalance problem. *Agricultural and Forest Meteorology 156*: 65-74. doi:10.1016/j.agrformet.2011.12.002

Li, F., Jupp, D. L. B., Thankappan, M., Lymburner, L., Mueller, N., Lewis, A. and Held, A. (2012) A physics-based atmospheric and BRDF correction for Landsat data over mountainous terrain. *Remote Sensing of Environment 124*: 756-770. doi:http://dx.doi.org/10.1016/j.rse.2012.06.018

Liu, S. F., Xiong, J. and Wu, B. F. (2011) ETWatch: a method of multi-resolution ET data fusion. *Journal of Remote Sensing 15*(2): 255–269.

Lu, D., Ge, H., He, S., Xu, A., Zhou, G. and Du, H. (2008) Pixel-based Minnaert Correction Method for Reducing Topographic Effects on a Landsat 7 ETM+ Image. *Photographic Engineering and Remote Sensing 74*(11): 1343-1350.

Ludwig, J. A., Bastin, G. N., Wallace, J. F. and McVicar, T. R. (2007) Assessing landscape health by scaling with remote sensing: when is it not enough? *Landscape Ecology 22*(2): 163-169.

Major, E. J., Cornish, P. M. and Whiting, J. K. (1998) Red Hill hydrology project establishment report including a preliminary water yield analysis. *Research Paper No. 36. State Forests of New South Wales, Forest Research and Development Division, Sydney*: 24.

McMahon, T. A., Peel, M. C., Lowe, L., Srikanthan, R. and McVicar, T. R. (2013) Estimating actual, potential, reference crop and pan evaporation using standard meteorological data: a pragmatic synthesis. *Hydrology and Earth System Sciences 17*(4): 1331-1363. doi:10.5194/hess-17-1331-2013

McVicar, T. R., Davies, P. J., Qinke, Y. and Zhang, G. (2002). An Introduction to Temporal-Geographic Information Systems (TGIS) for Assessing, Monitoring and Modelling Regional Water and Soil Processes. ACIAR, Canberra. pp. 205-223.

McVicar, T. R., Li, L. T., Van Niel, T. G., Zhang, L., Li, R., Yang, Q. K., Zhang, X. P., Mu, X. M., Wen, Z. M., Liu, W. Z., Zhao, Y. A., Liu, Z. H. and Gao, P. (2007a) Developing a decision support tool for China's re-vegetation program: Simulating regional impacts of afforestation on average annual streamflow in the Loess Plateau. *Forest Ecology and Management 251*(1-2): 65-81.

McVicar, T. R., Roderick, M. L., Donohue, R. J., Li, L. T., Van Niel, T. G., Thomas, A., Grieser, J., Jhajharia, D., Himri, Y., Mahowald, N. M., Mescherskaya, A. V., Kruger, A. C., Rehman, S. and Dinpashoh, Y. (2012a) Global review and synthesis of trends in observed terrestrial near-surface wind speeds: Implications for evaporation. *Journal of Hydrology 416-417*: 182-205.

McVicar, T. R., Roderick, M. L., Donohue, R. J. and Van Niel, T. G. (2012b) Less bluster ahead? Ecohydrological implications of global trends of terrestrial near-surface wind speeds. *Ecohydrology 5*(4): 381-388.

McVicar, T. R., Van Niel, T. G., Li, L., Hutchinson, M. F., Mu, X. and Liu, Z. (2007b) Spatially distributing monthly reference evapotranspiration and pan evaporation considering topographic influences. *Journal of Hydrology 338*(3-4): 196-220.

Nelder, J. A. and Mead, R. (1965) A Simplex Method for Function Minimization. *The Computer Journal 7*(4): 308-313. doi:10.1093/comjnl/7.4.308

Norman, J. M., Anderson, M. C., Kustas, W. P., French, A. N., Mecikalski, J., Torn, R., Diak, G. R., Schmugge, T. J. and Tanner, B. C. W. (2003) Remote sensing of surface energy fluxes at 10^1-m pixel resolutions. *Water Resources Research 39*(8): 18. doi:10.1029/2002wr001775

Penman, H. L. (1948) Natural Evaporation from Open Water, Bare Soil and Grass. *Proceedings of the Royal Society, London A193*: 120-145.

Philip, J. R. (1957) Evaporation, and Moisture and Heat Fields in the Soil. *Journal of Meteorology 14*(4): 354-366.
Phinn, S. R. (1998) A framework for selecting appropriate remotely sensed data dimensions for environmental monitoring and management. *International Journal of Remote Sensing 19*(17): 3457-3463.
Ring, T. (2014). *A Comparison of Modeling Schemes for Mapping Daily Evapotranspiration at High Resolution using Remote Sensing.* (Master of Science), Oregon State University.
Ritchie, J. T. (1972) Model for Predicting Evaporation from a Row Crop with Incomplete Cover. *Water Resources Research 8*(5): 1204-1213.
Rodell, M., Velicogna, I. and Famiglietti, J. S. (2009) Satellite-based estimates of groundwater depletion in India. *Nature 460*(7258): 999-U980. doi:10.1038/nature08238
Roderick, M. L., Hobbins, M. T. and Farquhar, G. D. (2009a) Pan Evaporation Trends and the Terrestrial Water Balance I. Principles and Observations. *Geography Compass 3*(2): 746-760.
Roderick, M. L., Hobbins, M. T. and Farquhar, G. D. (2009b) Pan Evaporation Trends and the Terrestrial Water Balance II. Energy Balance and Interpretation. *Geography Compass 3*(2): 761-780.
Rodriguez-Suarez, J. A., Soto, B., Perez, R. and Diaz-Fierros, F. (2011) Influence of Eucalyptus globulus plantation growth on water table levels and low flows in a small catchment. *Journal of Hydrology 396*(3-4): 321-326. doi:10.1016/j.jhydrol.2010.11.027
Semmens, K. A., Anderson, M. C., Kustas, W. P., Gao, F., Alfieri, J. G., McKee, L., Prueger, J. H., Hain, C. R., Cammalleri, C., Yang, Y., Xia, T., Sanchez, L., Mar Alsina, M. and Vélez, M. (2016) Monitoring daily evapotranspiration over two California vineyards using Landsat 8 in a multi-sensor data fusion approach. *Remote Sensing of Environment*: (In Press) doi:http://dx.doi.org/10.1016/j.rse.2015.10.025
Sinclair Knight Merz, CSIRO and and the Bureau of Rural Sciences. (2010). *Surface and/or groundwater interception activities: initial estimates*. Retrieved from Canberra:
Su, Z. (2002) The Surface Energy Balance System (SEBS) for estimation of turbulent heat fluxes. *Hydrology and Earth System Sciences 6*(1): 85-99.
Sun, F., Roderick, M. L., Farquhar, G. D., Lim, W. H., Zhang, Y., Bennett, N. and Roxburgh, S. H. (2010) Partitioning the variance between space and time. *Geophysical Research Letters 37*: L12704, doi:12710.11029/12010GL043323.
Tapley, B. D., Bettadpur, S., Ries, J. C., Thompson, P. F. and Watkins, M. M. (2004a) GRACE measurements of mass variability in the Earth system. *Science 305*(5683): 503-505. doi:10.1126/science.1099192
Tapley, B. D., Bettadpur, S., Watkins, M. and Reigber, C. (2004b) The gravity recovery and climate experiment: Mission overview and early results. *Geophysical Research Letters 31*(9): 4. doi:10.1029/2004gl019920
Van Dijk, A., Warren, G., Van Niel, T., Byrne, G., Pollock, D. and Doody, T. (2015) Derivation of data layers from medium resolution remote sensing to support mapping of groundwater dependent ecosystems. A draft report for the National Water Commission. *CSIRO Land and Water, Australia*: 28.
van Dijk, A. I. J. M. and Keenan, R. J. (2007) Planted forests and water in perspective. *Forest Ecology and Management 251*(1-2): 1-9. doi:10.1016/j.foreco.2007.06.010
Van Gorsel, E. V. A., Leuning, R. A. Y., Cleugh, H. A., Keith, H. and Suni, T. (2007) Nocturnal carbon efflux: reconciliation of eddy covariance and chamber measurements using an alternative to the u*-threshold filtering technique. *Tellus B 59*(3): 397-403. doi:10.1111/j.1600-0889.2007.00252.x

Van Niel, T. G., Li, L. T. and McVicar, T. R. (2016) Workflow of Landsat-MODIS image blending to estimate land-use-specific actual evapotranspiration of entire catchments containing plantations. *Forest & Wood Products Australia*: 29.

Webb, A. A. (2012) Can timber and water resources be sustainably co-developed in south-eastern New South Wales, Australia? *Environment, Development and Sustainability 14*(2): 233-252. doi:10.1007/s10668-011-9319-3

Webb, A. A. and Kathuria, A. (2012) Response of streamflow to afforestation and thinning at Red Hill, Murray Darling Basin, Australia. *Journal of Hydrology 412*: 133-140. doi:10.1016/j.jhydrol.2011.05.033

Wu, B., Yan, N., Xiong, J., Bastiaanssen, W. G. M., Zhu, W. and Stein, A. (2012) Validation of ETWatch using field measurements at diverse landscapes: A case study in Hai Basin of China. *Journal of Hydrology 436–437*: 67-80. doi:http://dx.doi.org/10.1016/j.jhydrol.2012.02.043

Wu, M. Q., Niu, Z. and Wang, C. Y. (2014) Asessing the accuracy of spatial and temporal image fusion model in a complex area in south China. *Journal of Geo-Information Science 16*(5): 776-783 (In Chinese with an English Abstract).

Yang, Y., Anderson, M. C., Gao, F., Hain, C. R., Semmens, K. A., Kustas, W. P., Noormets, A., Wynne, R. H., Thomas, V. A. and Sun, G. (2016) Daily Landsat-scale evapotranspiration estimation over a forested landscape in North Carolina, USA using multi-satellite data fusion. *Hydrology and Earth System Sciences: Discussion*: doi:10.5194/hess-2016-5198.

Zhang, X. P., Zhang, L., McVicar, T. R., Van Niel, T. G., Li, L. T., Li R., Yang, Q. K. and Liang, W. (2008) Modeling the impact of afforestation on mean annual streamflow in the Loess Plateau, China. *Hydrological Processes 22*: 1996-2004.

Zhang, Y., Peña-Arancibia, J. L., McVicar, T. R., Chiew, F. H. S., Vaze, J., Liu, C., Lu, X., Zheng, H., Wang, Y., Liu, Y. Y., Miralles, D. G. and Pan, M. (2016) Multi-decadal trends in global terrestrial evapotranspiration and its components. *Scientific Reports 6*: 19124. doi:10.1038/srep19124

Zhang, Y., Viney, N., Frost, A., Oke, A., Brooks, M., Chen, Y. and Campbell, N. (2013) Collation of Australian modeller's streamflow dataset for 780 unregulated Australian catchments. *CSIRO: Water for a Healthy Country National Research Flagship*: 117.

Zhu, X. L., Chen, J., Gao, F., Chen, X. H. and Masek, J. G. (2010) An enhanced spatial and temporal adaptive reflectance fusion model for complex heterogeneous regions. *Remote Sensing of Environment 114*(11): 2610-2623.